NEW INVESTIGATION OF NITROGEN LASER INDUCED FLUORESCENCE IN FORMALDEHYDE: SPECTRA AND SPECTRALLY RESOLVED LIFETIMES.

Ralph Ernest Chatham

New Investigation of Nitrogen Laser Induced Flourescence in Formaldehyde: Spectra and Spectrally Resolved Lifetimes

by

Ralph E. Chatham

SECURITY CLASSIFICATION OF THIS PAGE (When Data Entered)

REPORT DOCUMENTATION PAGE

READ INSTRUCTIONS BEFORE COMPLETING FORM

1. REPORT NUMBER	2. GOVT ACCESSION NO. / 3. RECIPIENT'S CATALOG NUMBER
4. TITLE (and Subtitle): New Investigation of Nitrogen Laser Induced Flourescence in Formaldehyde: Spectra and Spectrally Resolved Lifetimes	5. TYPE OF REPORT & PERIOD COVERED: Thesis
	6. PERFORMING ORG. REPORT NUMBER
7. AUTHOR(s): CHATHAM, Ralph E.	8. CONTRACT OR GRANT NUMBER(s)
9. PERFORMING ORGANIZATION NAME AND ADDRESS: State University of New York at Stony Brook	10. PROGRAM ELEMENT, PROJECT, TASK AREA & WORK UNIT NUMBERS
11. CONTROLLING OFFICE NAME AND ADDRESS: Naval Postgraduate School, Monterey, CA 93940	12. REPORT DATE: DEC 1977
	13. NUMBER OF PAGES: 218
14. MONITORING AGENCY NAME & ADDRESS(if different from Controlling Office)	15. SECURITY CLASS. (of this report): Unclass
	15a. DECLASSIFICATION/DOWNGRADING SCHEDULE

16. DISTRIBUTION STATEMENT (of this Report)

A. Approved for public release; distribution unlimited.

17. DISTRIBUTION STATEMENT (of the abstract entered in Block 20, if different from Report)

18. SUPPLEMENTARY NOTES

19. KEY WORDS (Continue on reverse side if necessary and identify by block number)

Laser, Nitrogen Laser, Flourescence

20. ABSTRACT (Continue on reverse side if necessary and identify by block number)

Measurements were made of the flourescence resulting from N_2 laser excitation of H_2CO vapor at pressures between one and 760 torr. Higher pressure spectral measurements show vibrationally emission bands originating in the 4^1 and 0^0 levels. These data supplement Brand's (1956) spectra studies and extend the identification of these band systems beyond 5000Å. 10Å bandwidth spectra data taken at pressures below 100 torr revealed over 25 new bands which appear to originate from either the $4^2 6^1$ or $4^1 6^1$ levels.

DD FORM 1 JAN 73 1473 EDITION OF 1 NOV 65 IS OBSOLETE
S/N 0102-014-6601 |
(Page 1)

SECURITY CLASSIFICATION OF THIS PAGE (When Data Entered)

NEW INVESTIGATIONS OF NITROGEN LASER INDUCED FLUORESCENCE IN FORMALDEHYDE:

Spectra and Spectrally Resolved Lifetimes

by

Ralph Ernest Chatham
Lieutenant United States Navy

to

The Graduate School

in partial fulfillment of the requirements

for the degree of

Doctor of Philosophy

in

Physics

State University of New York

at

Stony Brook

December, 1977

STATE UNIVERSITY OF NEW YORK

AT STONY BROOK

THE GRADUATE SCHOOL

We, the dissertation committee for the above candidate for the Ph.D. degree, hereby recommend acceptance of the dissertation.

Abstract of the Dissertation

NEW INVESTIGATIONS OF NITROGEN LASER INDUCED
FLUORESCENCE IN FORMALDEHYDE:
Spectra and Spectrally Resolved Lifetimes

by

Ralph Ernest Chatham

Doctor of Philosophy

in

Physics

State University of New York at Stony Brook

1977

Measurements were made of the fluorescence resulting from N_2 laser excitation of H_2CO vapor at pressures between one and 760 torr. Higher pressure spectral measurements show vibrationally relaxed emission bands originating in the 4^1 and 0^0 levels. These data supplement Brand's (1956) spectra studies and extend the identification of these band systems beyond 5000Å. 10Å bandwidth spectra data taken at pressures below 100 torr revealed over 25 new bands which appear to originate from either the $4^2 6^1$ or $4^1 6^1$ levels. The variation of band intensity with pressure indicates a strong collision-dependent coupling between these levels.

Fluorescence decay curves for these bands observed with 10Å resolution exhibit two decay rates, and the initial, more

rapid, rate becomes independent of pressure above about 60 torr. Linear extrapolation of the fast decay rate to zero pressure yields $\tau(4^2 6^1) = 19\pm2$ns and $\tau(4^1 6^1) = 29\pm2$ns. The second, slower decay rate is the same for both levels (50±5ns). The self quenching cross section for the fast decay is $10\pm2\times10^{-17}$cm^2 for the $4^2 6^1$ bands and $20\pm4\times10^{-17}$cm^2 for the $4^1 6^1$ levels. Similar behavior is observed for argon quenching.

This lifetime data is compatible with that of Aoki et al. and Sakurai et al. both of whom used observation bandwidths in excess of 800Å. The data cannot, however, be joined smoothly with that taken by Baronavski below one torr with a 200Å bandwidth. New measurements at pressures between 0.5 and 10 torr are needed, but they must have an observational bandwidth of 10Å or less to differentiate between bands originating in the $4^2 6^1$ and $4^1 6^1$ levels.

TABLE OF CONTENTS

LIST OF FIGURES

LIST OF TABLES

LIST OF TABLES

ACKNOWLEDGEMENTS

During the time these investigations were made I have been an officer on active duty in the United States Navy. My tuition and dissertation expenses have been paid by a U.S. Navy BURKE Fellowship. I am extremely grateful to the Navy for providing me this opportunity.

There is a host of individuals without whom this work could never have been completed. Foremost among them is my adviser Dr. Robert deZafra. Although his advice has not always been accorded the acceptance it deserved, it has almost invariably been correct. The advice and instruction of Dr. Harold Metcalf has also been of great value. Messrs. L. Lenzi, J. Spigonardo and J. Curran of the Physics Machine Shop provided invaluable assistance and instruction in all phases of the construction of the apparatus. T. Mattone and S. Sousa assisted and advised during the photographic spectroscopic phase of this work. Dr. Barry Lutz was kind enough to let me use his 1M and 3.5M spectrometers and showed considerable patience with my inexperience.

I must also thank Mark Feldman, Paul Lebow and Fred Raab for the friendly interchange of equipment and many helpful discussions concerning nitrogen lasers. In addition my thanks to Jim Barrett for helpful discussions about almost anything.

Finally, I must acknowledge my deep indebtedness to my parents (who did not have to pay for this dissertation), and my wife who, although she did not have to type it, did recopy one section so that the typist could read it.

CHAPTER I

INTRODUCTION

I. INTRODUCTION

There is a considerable interest in the lifetimes and predissociation mechanisms of the excited formaldehyde molecule, H_2CO. Active research is being conducted in the use of this predissociation via selective laser excitation to separate various isotopes of the three atomic species which make up the molecule[1-5]. In addition, the molecule's comparatively simple structure and a large body of experimental data concerning that structure make it a useful test case for theoretical models[1,5]. There are also astrophysical applications. The fact that light in the near ultraviolet causes dissociation of formaldehyde with a quantum yield which is close to one makes the molecule a sensitive detector of the radiation environment in the dense interstellar molecular clouds in which it has been observed by radio astronomy[7].

Although a good deal of data has been collected recently for the isotopic species D_2CO, there have been few measurements of the many H_2CO excited state lifetimes[1,8-14]. The principal problem has been that the predissociation mechanism is much more effective in H_2CO than in D_2CO[1,14]. This produces dissociation lifetimes for some vibrational levels of the order of fifteen to thirty nanoseconds. Since

the radiative lifetime is several orders of magnitude greater than this[10], few of the excited state molecules of H_2CO radiate before they dissociate. Fluorescence detection methods, therefore, observe only a small fraction of the excited molecules, resulting in difficult detection under high spectral resolution. Since the dissociation rate varies strongly with the vibrational energy and mode of the excited state[1,14,15], good resolution is needed to monitor specific excited states which may be of interest.

In order to overcome some of these problems laser excitation may be used. The laser must be capable of exciting a single vibronic level, have a very short pulse duration, and a high peak intensity. An accidental overlap in wavelengths, pulse lengths shorter than ten nanoseconds, and intensities approaching one megawatt make the nitrogen laser an excellent tool for the observation of lifetimes of several excited vibrational levels in both H_2CO[11-13] and D_2CO[8,9].

This dissertation concerns a series of measurements I have made of nitrogen laser excited fluorescence in H_2CO. The experiments were conducted by focusing the output of a home-built nitrogen laser into a heated cell containing formaldehyde vapor at various pressures. The fluorescence

produced was focused onto the slit of a spectrometer, and either photographed or detected by a photomultiplier, the output of which was electronically processed to provide wavelength or lifetime information.

The data can be broken down into four general classes. There are photographic and photoelectric spectra of fluorescence where the pressure of the vapor was close to atmospheric. These data supplement and extend to the red the analysis of the band systems studied by Brand[16-18]. An additional series of spectra of the fluorescence at pressures below about sixty torr showed a sequence of about twenty new bands originating either from the electronic-vibrational level directly excited by the nitrogen laser, or from excited levels lying close to it which are populated by collisional transfer. The fourth class of data concerns the lifetimes of the individual states as a function of pressure from a few torr to a few hundred. These data are complicated by the appearance of two exponentials in the decay curve and by a pressure dependence which deviates from the simple theoretical models of collision quenching.

In following sections I will discuss the known molecular structure and spectra, the existent data on predissociation and lifetimes, and the theories of pressure dependence of observed lifetimes. Then the experimental procedures will be discussed, and data presented, followed

by a summary. An appendix discusses the construction of the nitrogen laser used.

CHAPTER II

BACKGROUND

II. A. INTRODUCTION TO FORMALDEHYDE

Understanding any polyatomic molecule takes a certain amount of specialized knowledge. In this section I will assume that the reader is acquainted with the behavior of diatomic molecules and will try to summarize the additional molecular physics applicable to formaldehyde. This information is widely scattered in the literature and is not readily available from a single source. Each author has his own favorite notation, which he assumes the reader already understands. In addition, as knowledge of the molecule developed, notations changed, and mode numbers were altered. I will spend some time on this background to assist the reader to understand not only this dissertation, but the general literature on formaldehyde.

The section is organized as follows. First some physical properties are mentioned. Then a discussion of the symmetry properties of the molecule is presented, followed by a description of the electronic, vibrational, and rotational structure of interest. Next the transitions and selection rules applicable to formaldehyde are considered. The section concludes with a discussion of the characteristics of the observed spectra.

1. Physical Properties and Quantum Structure

At standard temperature and pressure formaldehyde (oxymethylene, H_2CO) polymerizes as a white powder. At room temperature the vapor pressure of the monomer over the polymer is a few torr[19]. Higher pressures may be obtained by heating, but care must be taken to insure that the apparatus is uniformly heated or polymer will form on the cooler surfaces. Formaldehyde is soluble both in alcohol and water, but loses its chemical identity in solution.

In the electronic ground state the molecule has the planar structure shown in figure (1)[20]. The wave functions of formaldehyde are eigenfunctions of certain symmetry operators. H_2CO belongs to the C_{2v} point group by virtue of its two planes of symmetry [$\sigma_v(xz)$, and $\sigma_v(yz)$] and an axis of symmetry through the C-O bond[21,22]. The molecule is not affected by a reflection through either the x-z or y-z planes or by a rotation, $C_2(z)$, of π radians about the z axis. The possible eigenvalues of the symmetry operators acting on the wave functions must be either plus or minus one, but the three operations are not independent; any one operation can be produced by a product of the other two. All wave functions of C_{2v} molecules thus belong to one of four different classes or symmetry species:

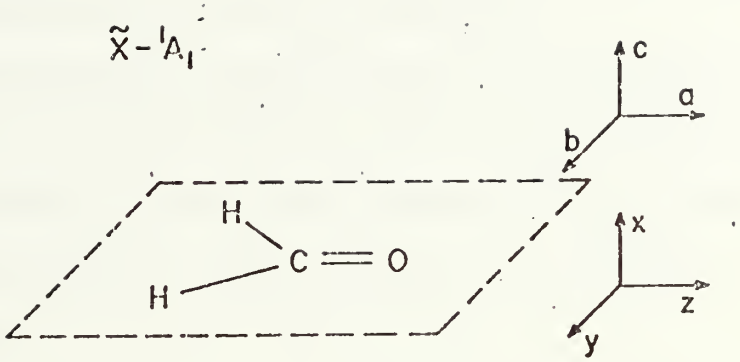

FIGURE (1): Formaldehyde Ground State Geometry.

The conventional body-fixed coordinate systems are indicated. The z axis is oriented along the direction of greatest symmetry (C_2) and a, b, and c are the principal axes of inertia where $I_a<I_b<I_c$. The H-C-H bond angle is 125°. The C-H bond length is 1.17Å and the C-O length is 1.27Å.

$A_1(+\ +)$: symmetric under $C_2(z)$, symmetric under $\sigma_v(xz)$,

$A_2(+\ -)$: symmetric under $C_2(z)$, anti-symmetric under $\sigma_v(xz)$,

$B_1(-\ +)$: anti-symmetric under $C_2(z)$, symmetric under $\sigma_v(xz)$,

$B_2(-\ -)$: anti-symmetric under both operations.

These are the irreducible representations of the C_{2v} point group. Dipole transition selection rules between states can be calculated knowing only these group theoretical representations of the wave functions[23]. These rules will be discussed in section II.A.6.

2. Electronic States

If one makes the usual Born-Oppenheimer approximation of separating the total wave function into electronic, vibrational, and rotational parts, the symmetry of the complete function will have the product of the symmetries of the individual parts. Electronic states are identified by the symmetry symbol of the electronic wave function with the usual spin multiplicity as a pre-superscript, e.g. $^1A_2$. In addition, as in diatomic molecules, another letter is used to indicate the energy sequence of electronic states above the ground state, i.e. $\tilde{X}$ is the ground state, $\tilde{A}$ is the first excited state, $\tilde{B}$ is the second excited state and so forth. The tilda avoids confusion with the group theoretical

designators. The energy sequence of electronic states with a multiplicity different from the ground state is designated by a lower case letter, e.g. $\tilde{a} - {}^3A_2$. As an example of this notation, this dissertation is concerned with transitions from the ground $\tilde{X} - {}^1A_1$ state to the $\tilde{A} - {}^1A_2$ excited electronic state and subsequent fluorescence returning the molecule to a number of vibrational levels of the $\tilde{X} - {}^1A_1$ state. The electronic angular momentum projection about an axis that gives rise to the Σ, π, Δ, ... designations of linear molecules is not useful here because the projection about any axis in a polyatomic molecule is in general not a good quantum number.

An additional notation is used by C. Bradley Moore and collaborators in a series of papers concerning photochemistry and isotope separation in formaldehyde[1-4,15]. In these, the ground state is labeled S_o, the "S" standing for singlet. The $\tilde{A} - {}^1A_2$ state is S_1 and the $\tilde{a} - {}^3A_2$ is labeled T_1, for triplet. For brevity in designating these states, I will adopt the same notation here.

3. Vibrational States

Formaldehyde may vibrate in any of six normal modes. Each mode has a symmetry designation similar to that given in

the preceeding section, but now labeled with a lower case letter. Figure (2)shows the approximate atomic motions of these vibrations, their ground state fundamental frequencies, and the symmetry designation. The overall vibrational symmetry depends upon the number of quanta in each mode. For example, one quantum of the fourth vibrational mode (out of plane bending) has b_1 (- +) symmetry, two quanta in mode four gives $b_1 \times b_1$ or a_1 (+ +) symmetry. An even number of quanta in any mode in the ground state gives an a_1 species, while an odd number of quanta in any mode produces the symmetry listed in figure (2).

The modern notation for a particular vibrational state of the ground electronic state of the formaldehyde molecule consists of a string of digits which indicate the active modes, each one followed by a subscript indicating the number of quanta in that mode. For example, $2_1 4_3$ means a state which has one quantum of vibration in the second mode and three quanta of vibration in the fourth mode. The unexcited modes are omitted. This notation and the numbering of modes in figure (2) came into general use in the early 1960's. Before that a different numbering scheme was used due to a different labeling of molecular coordinates[25]:

The pre-1960 mode ν_6 is now ν_4.

The pre-1960 mode ν_4 is now ν_5.

The pre-1960 mode ν_5 is now ν_6.

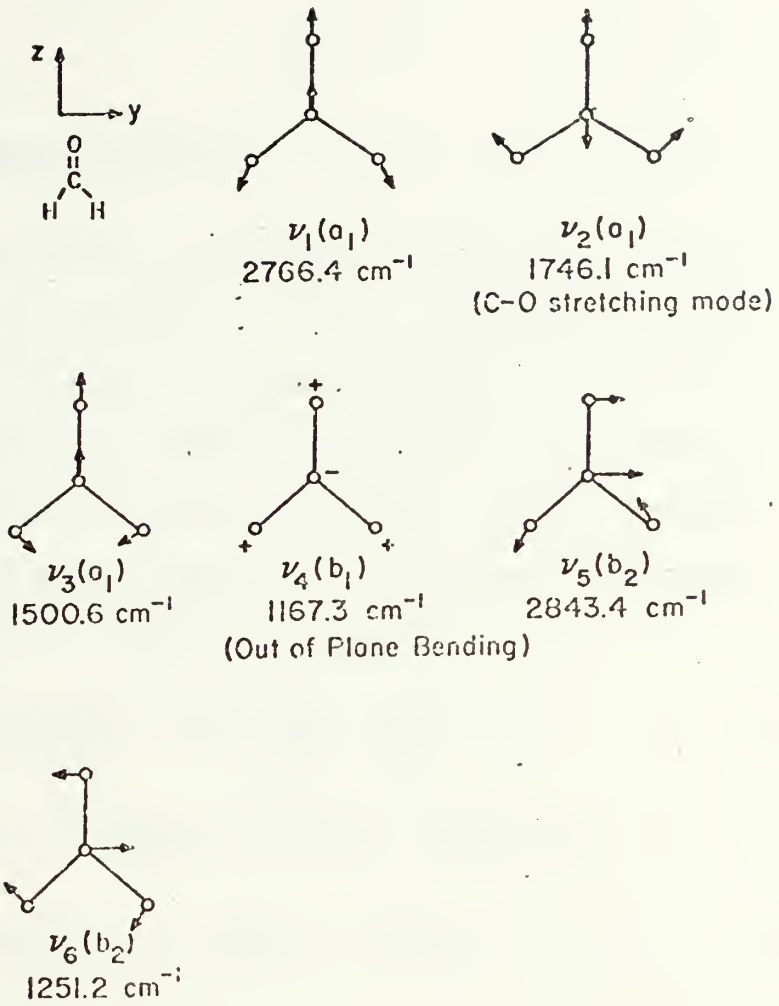

FIGURE (2): Normal Vibrational Modes of Formaldehyde. (after Job, Sethuraman, and Innes[24]) The modern mode labeling, ground state fundamental frequencies, and symmetry species are indicated.

4. Rotational States

Formaldehyde is an asymmetric top rotor, but since the two larger moments of inertia, I_b and I_c, are almost equal, its rotational structure can, for many purposes, be approximated with a symmetric top model[26]. Because this model contains one more degree of freedom than diatomic molecular rotation, an additional quantum number, K, is introduced. The energy eigenvalues of the symmetric top are[27]:

$$E = \frac{J(J+1)\hbar^2}{2I_b} + K^2\hbar^2 \left(\frac{1}{2I_a} - \frac{1}{2I_b}\right). \tag{1}$$

In terms of the rotational constants, defined as

$$A \equiv \frac{h}{8\pi^2 I_a} > B \equiv \frac{h}{8\pi^2 I_b} \gtrsim C \equiv \frac{h}{8\pi^2 I_c} \tag{2}$$

the energy eigenvalues are:

$$E = hBJ(J+1) + (A-B)hK^2. \tag{3}$$

In this model the quantum number K is a projection of rotational angular momentum on the body-fixed symmetry axis, and may take on the values:

$$K = \pm 1, \pm 2, \pm 3, \ldots, \pm J. \tag{4}$$

K loses the geometric meaning in the asymmetric top case, but retains the same allowed values. In the symmetric top

approximation there is an additional 2J+1 fold degeneracy associated with the third degree of rotational freedom. This, combined with that from the K quantum number, produces a 4J+2 fold degeneracy if K≠0 and 2J+1 if K=0. The rotational constants A,B, and C vary among vibrational modes[24].

The Schrödinger equation for the asymmetric top is not separable and must be solved by approximation methods[27]. Additional complications arise from coriolis coupling between rotational and vibrational modes[16,24,26,28]. Such a coupling, which perturbs the rotational levels of the ν_4 and ν_6 modes, was discovered in 1937 by Ebers and Nielsen[29] and was the first such resonance observed in any molecule. Further perturbations are caused by anharmonic (Fermi) interactions between vibrational modes[28]. These complications are important in high resolution work but will not be considered here.

5. The $\tilde{A}$ Excited State

The lowest-lying electronic excited state of formaldehyde is the $\tilde{a} - {}^3A_2$ level, but optical transitions between it and the ground state are weak due to the required spin flip[20]. There are, however, a series of strong transitions between the next higher excited electronic state, which for brevity will be called S_1, and the ground manifold of vibrational states.

For the present level of discussion, it will be assumed that in S_1 the molecule is planar, as it is in the ground state. The correct symmetry designation would then be $\tilde{A} - {}^1A_2$. The complications caused by the fact that the equilibrium configuration is bent are taken up in section II.A.7. The zero vibrational level of S_1 lies 28188 cm^{-1} above the ground level. The occupation of the vibrational modes in the excited state is again designated by a string of digits identifying the mode in question but for the excited state a superscript is appended to each mode designator to indicate the number of quanta in that mode. For example $4^2 6^1$ is an electronic excited state with two quanta of vibration in the fourth mode and one in the sixth mode; the S_1 electronic state is assumed. Figure (3) shows all the vibrational modes of the S_1 state with less than 1750 cm^{-1} of vibrational energy. The wave numbers of the figure come from the absorption measurements of Job, Sethuraman, and Innes[24]. The rotational structure of the excited state is similar to that of the ground state, except that the rotational constants differ.

FIGURE (3): Vibrational Levels in the $\tilde{A}$-$^1A_2$ Excited State of Formaldehyde. Levels are shown with their energy above the ground state in wave numbers. If they are seen in absorption from the ground state the wavelength of the absorption band center is indicated. The overall symmetry species of each state is listed, i.e., the product of the electronic A_2 and the vibrational symmetry.

a) These states exhibit dipole allowed absorption from the vibrationless ground state (cold bands).

b) These states are seen in absorption either as magnetic dipole transitions or as hot bands (starting from other than the zero vibrational level of the ground state).

c) These states have not been observed but are calculated to exist on the basis of known frequencies of overtones and combinations.

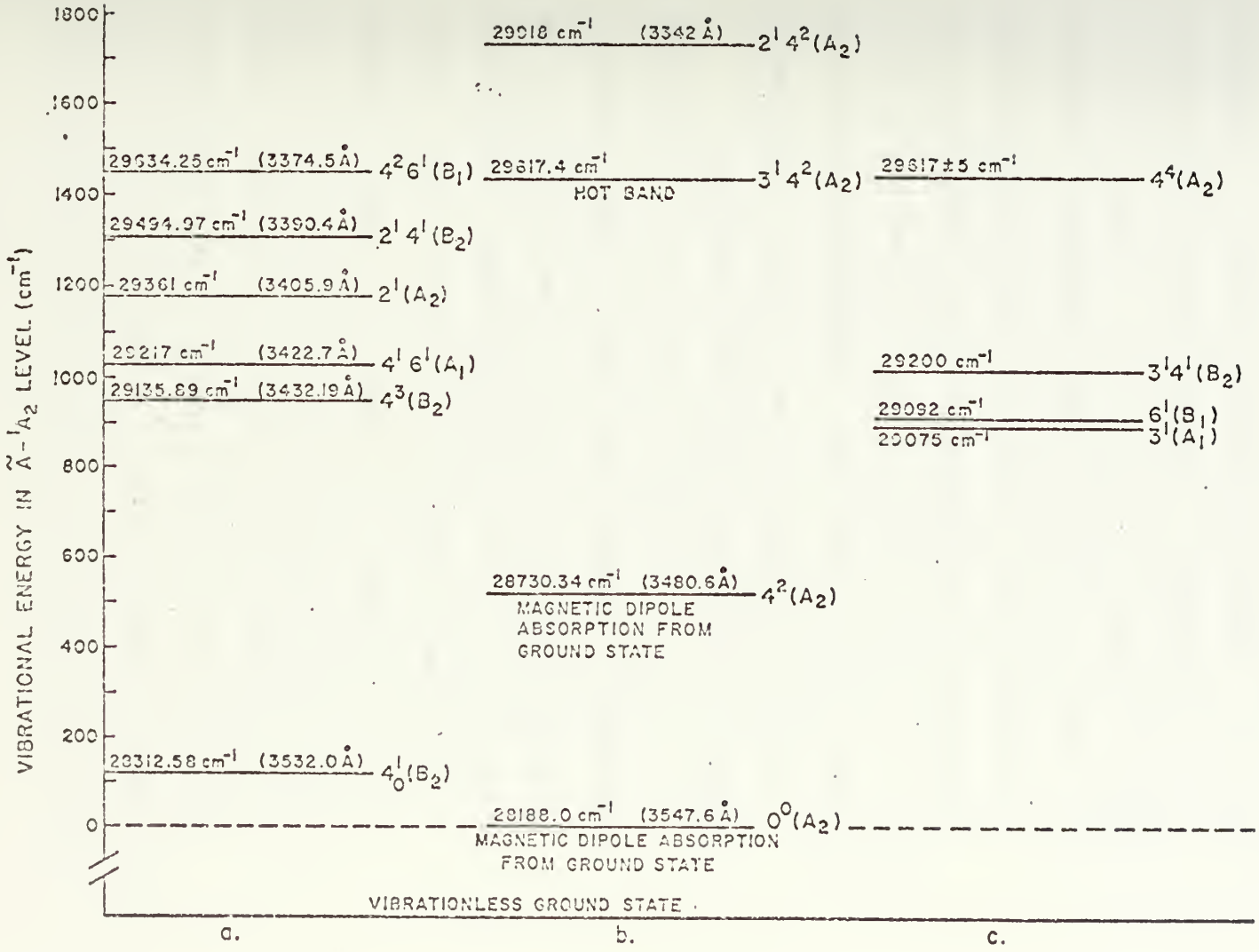
VIBRATIONAL ENERGY IN $\tilde{A}-{}^1A_2$ LEVEL (cm^{-1})
1800
1600
1400
1200
1000
800
600
400
200
0
29018 cm^{-1} (3342 Å) $2^1 4^2(A_2)$
29034.25 cm^{-1} (3374.5 Å) $4^2 6^1(B_1)$
29617.4 cm^{-1} $3^1 4^2(A_2)$
HOT BAND
29617±5 cm^{-1} $4^4(A_2)$
29494.97 cm^{-1} (3390.4 Å) $2^1 4^1(B_2)$
29361 cm^{-1} (3405.9 Å) $2^1(A_2)$
29217 cm^{-1} (3422.7 Å) $4^1 6^1(A_1)$
29135.89 cm^{-1} (3432.19 Å) $4^3(B_2)$
29200 cm^{-1} $3^1 4^1(B_2)$
29092 cm^{-1} $6^1(B_1)$
29075 cm^{-1} $3^1(A_1)$
28730.34 cm^{-1} (3480.6 Å) $4^2(A_2)$
MAGNETIC DIPOLE
ABSORPTION FROM
GROUND STATE
28312.58 cm^{-1} (3532.0 Å) $4_0^1(B_2)$
28188.0 cm^{-1} (3547.6 Å) $0^0(A_2)$
MAGNETIC DIPOLE ABSORPTION
FROM GROUND STATE
VIBRATIONLESS GROUND STATE
a.
b.
c.

6. Transitions and Selection Rules

The vibrational levels involved in a transition can be indicated by a compact notation due to Brand[30]. The state labeling system discussed above is a special case of this transition notation. As an example, the expression $2_1^0 4_3^2 6_1^1$ indicates a transition between the assumed S_1 excited state which is vibrating with two quanta in the fourth mode and one in the sixth, and the assumed ground (S_o) state which vibrates with one quantum in the second, three in the fourth, and one in the sixth modes. The direction of the transition (absorption or emission) must be separately indicated.

As mentioned earlier the dipole selection rules are calculated from the symmetry designations of the states involved. Figure (4) shows these rules and the direction of the transition moment relative to the body-fixed axes. In addition to identifying bands by the A, B, or C polarizations, they are frequently classified by whether the transition moment is perpendicular or parallel to the z axis, in which case they are called perpendicular or parallel bands. Notice that $A_1 \leftrightarrow A_2$ and $B_1 \leftrightarrow B_2$ transitions are not dipole allowed, thus considering only the electronic wave functions an $\tilde{A} - {}^1A_2$ to $\tilde{X} - {}^1A_1$ dipole transition cannot occur. In fact, the absorption from the vibrationless ground state to

	A_1	A_2	B_1	B_2
A_1	A	f	C	B
A_2		A	B	C
B_1			A	f
B_2				A

FIGURE (4): Dipole Selection Rules for a C_{2v}-C_{2v} Transition. (after Herzberg[23])

"f" indicates that the transition is forbidden. A,B, or C indicates the direction of the transition moment on the body-fixed coordinate system. For formaldehyde the a axis is along the C-O bond b axis is in the plane of the molecule perpendicular to the C-O bond, and the c axis is perpendicular to the molecular plane.

the vibrationless excited state - the 0-0 band - is seen only as a magnetic dipole transition[30].

When vibrational symmetry is considered a large number of bands become dipole allowed. In order to properly diagram the levels and the possible transitions one would require a seven dimensional plot, one dimension for each mode and one for the energy. To simplify matters, figure (5) considers only transitions between levels of the fourth mode. From the figure it can be seen that a transition from a particular ν_4 level of one electronic state is allowed only to alternate ν_4 levels of the other electronic state. Since, as will be explained later, the emission spectra originates from only a few of the lowest-lying vibrational states of S_1 while the absorption spectra originates almost entirely from the vibrationless ground state, the two spectra have very few bands in common.

The rotational selection rules depend upon the polarization of the band. In the symmetric top approximation:

$$\Delta J = 0, \pm 1; \quad \Delta K = 0$$
$$\Delta J = \pm 1 \text{ if } K = 0, \tag{5}$$

for a parallel band, and

$$\Delta J = 0, \pm 1; \quad \Delta K = \pm 1 \tag{6}$$

FIGURE (5): Some $\tilde{X}\text{-}^1A_1 \leftrightarrow \tilde{A}\text{-}^1A_2$ Transitions in Formaldehyde.

The figure illustrates several of the most intense transitions previously observed in fluorescence and emission. For simplicity only the out-of-plane bending (ν_4) mode is shown, although there are strong transitions involving the C-O stretching (ν_2) as well as combinations of the two. In emission these were the only modes observed to be active, although, as discussed later, ν_6 appears to be active in nitrogen laser excited fluorescence. Notice that only one of the absorption bands shown coincides with an allowed emission band. It is because of the $A_1 \not\leftrightarrow A_2$, $B_1 \not\leftrightarrow B_2$ selection rule that the absorption band system analyzed by Job, Sethuraman, and Innes,[24] Brand,[18] and Dieke and Kistiakowsky[26] bears almost no resemblance to that observed in emission by Brand[18] and Robinson[19]. The energy difference in the figure is not to scale; the electronic separation is about twenty-five times the vibrational separation.

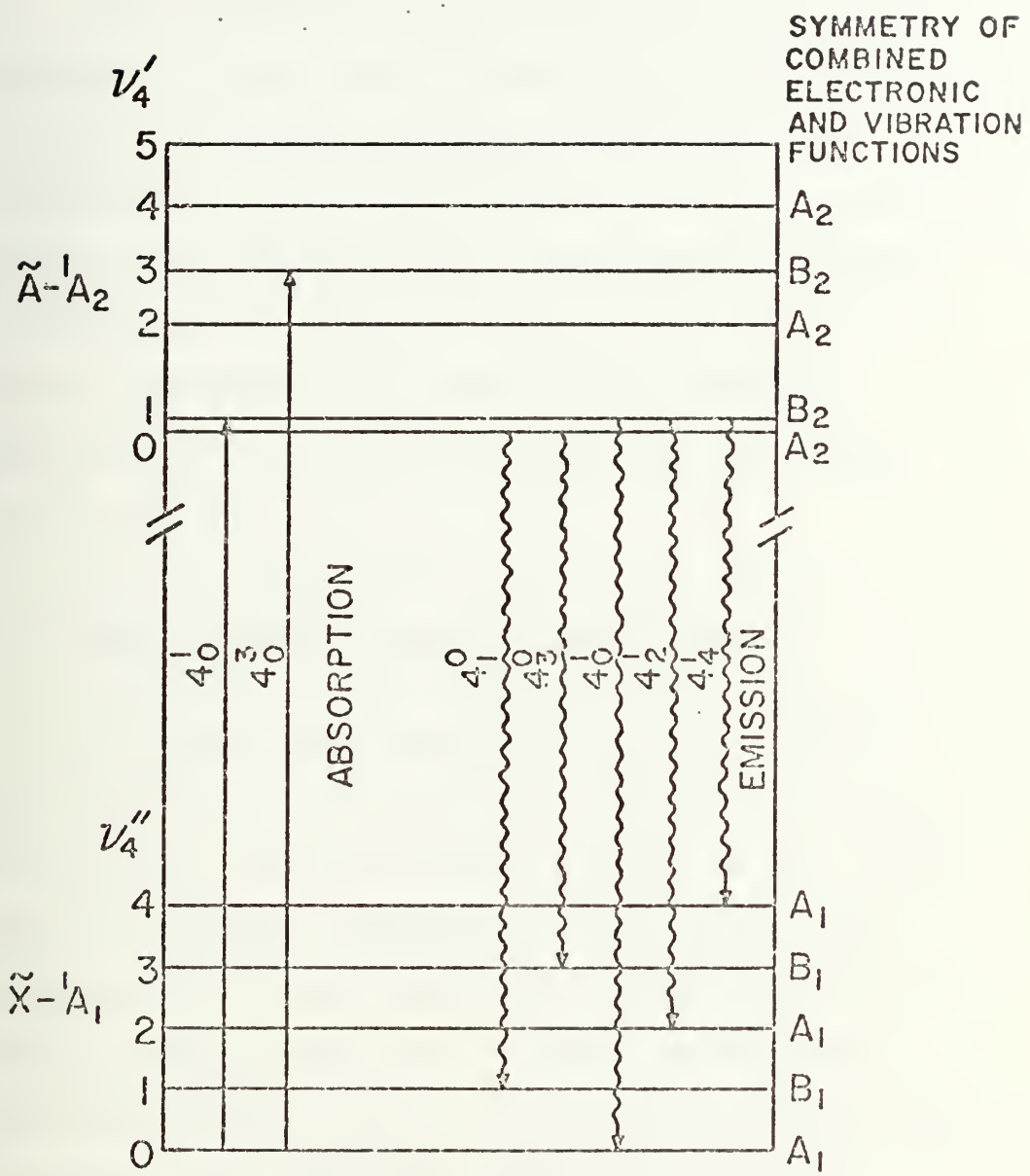
SYMMETRY OF COMBINED ELECTRONIC AND VIBRATION FUNCTIONS
ν_4'
5
4
3
2
1
0
$\tilde{A}\text{-}^1A_2$
A_2
B_2
A_2
B_2
A_2
4_0^1
4_0^3
ABSORPTION
4_1^0
4_3^0
4_0^1
4_2^1
4_4^1
EMISSION
ν_4''
4
3
2
1
0
$\tilde{X}\text{-}^1A_1$
A_1
B_1
A_1
B_1
A_1

for a perpendicular band.

The rotational transitions are classified by a scheme generalized from that used for diatomic molecules[26]. The change in J is labeled with an upper case P, Q, or R for J = -1, 0, +1 respectively. The change in K is labeled with a left superscript by the equivalent letters. Occasionally the value of K'' is appended as a right subscript, and the value of J'' is placed in parentheses. For example, ${}^{P}R_{1}(0)$ indicates a transition where $\Delta K = -1$, $\Delta J = +1$, and in the ground state $K = 1$ and $J = 0$.

7. The Non-Planar Nature of the Excited State

The early classification of the S_1 excited state as ${}^{1}A_{2}$ was based upon the assumption that the molecule was planar in that state. It has been shown that this is in fact not the case; the equilibrium configuration of the excited molecule is pyramidal[31,18,20] (see figure (6)). In this case there is only one symmetry element: the x-z plane. The appropriate point group for the S_1 state is thus C_s. A wave function that is symmetric under reflections through the x-z plane is designated A' and one which is anti-symmetric is A''. The proper designation of the electronic state S_1 is then $\tilde{A} - {}^{1}A''$.

The existence of two configurations with minimum potential energy, corresponding to bending angles of plus or

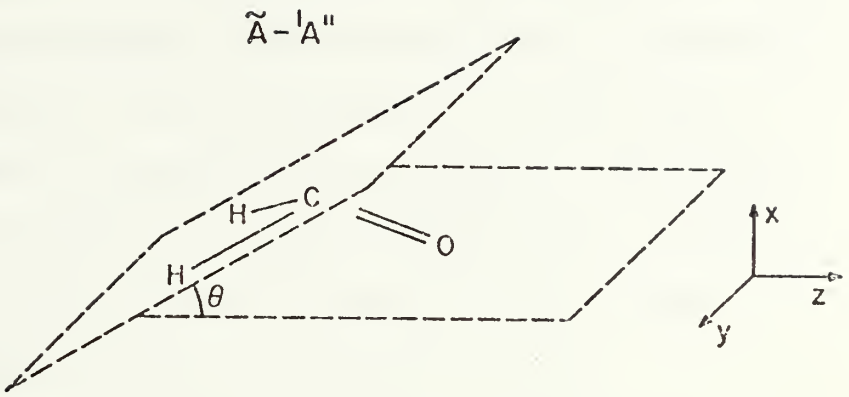

FIGURE (6): Pyramidal Shape of the $\tilde{A}$-$^1A''$ Excited State of Formaldehyde. This state is conventionally labeled with the planar symmetry designation $^1A_2$. The bending angle θ is defined as the angle formed between the plane containing the hydrogen and carbon atoms, and that containing the hydrogen and oxygen atoms. The equilibrium value of θ is 27°.

minus 27^{o}, produces a degeneracy which, through tunneling, causes inversion doubling. This doubling affects the character of the ν_4 vibration in the excited state. The actual eigenfunctions consist of symmetric and anti-symmetric combinations of states with positive and negative bending angles. This is the reason that the ν_4' levels of figure (5) are not evenly spaced in energy as would be expected for a harmonic oscillator. To help see how the doubling arises figure (7) shows a comparison among the levels and potential wells of: a, a pair of degenerate non-tunneling non-planar oscillators; b, the inversion doubled system; and c, a planar oscillator. It can be shown that the ν_4' levels of a $^1A_2$ state (ν_4' = 1, 2, 3, ...) and those of a $^1A''$ state (0^+, 0^-, 1^+, 1^-,...) have a one-to-one correspondence[20,24]. As ν_4' increases the energy levels of the two systems begin to coincide, since the shape of the non-rigid potential well is nearly the same as that of the rigid planar well at high energies. Because the symmetry labels a_1, a_2, b_1, b_2 can be used to designate the irreducible representations of the inversion doubled C_s point group, and the selection rules are not affected, it is the usual practice to refer to the S_1 electronic state as $^1A_2$.

It has been pointed out that a proper treatment of all vibrations in the excited state requires a G_4 point group[20]. Since this, again, is isomorphic with the C_{2v} point group the

FIGURE (7): Energy Levels of Non-Rigid Formaldehyde.

The figure indicates how the inversion doubling arises in the excited state, and why the rigid-planar (C_{2v}) notation is adequate to describe the v_4 vibrations.

a) Energy levels of two non-interacting oscillators: one vibrating about $\theta=27^{o}$ and the other about $\theta=-27^{o}$.

b) The inversion doubled system; tunneling connects the two oscillators and lifts the degeneracy.

c) Rigid-planar system; levels of an oscillator vibrating about a planar equilibrium position.

ENERGY LEVELS OF NON RIGID FORMALDEHYDE

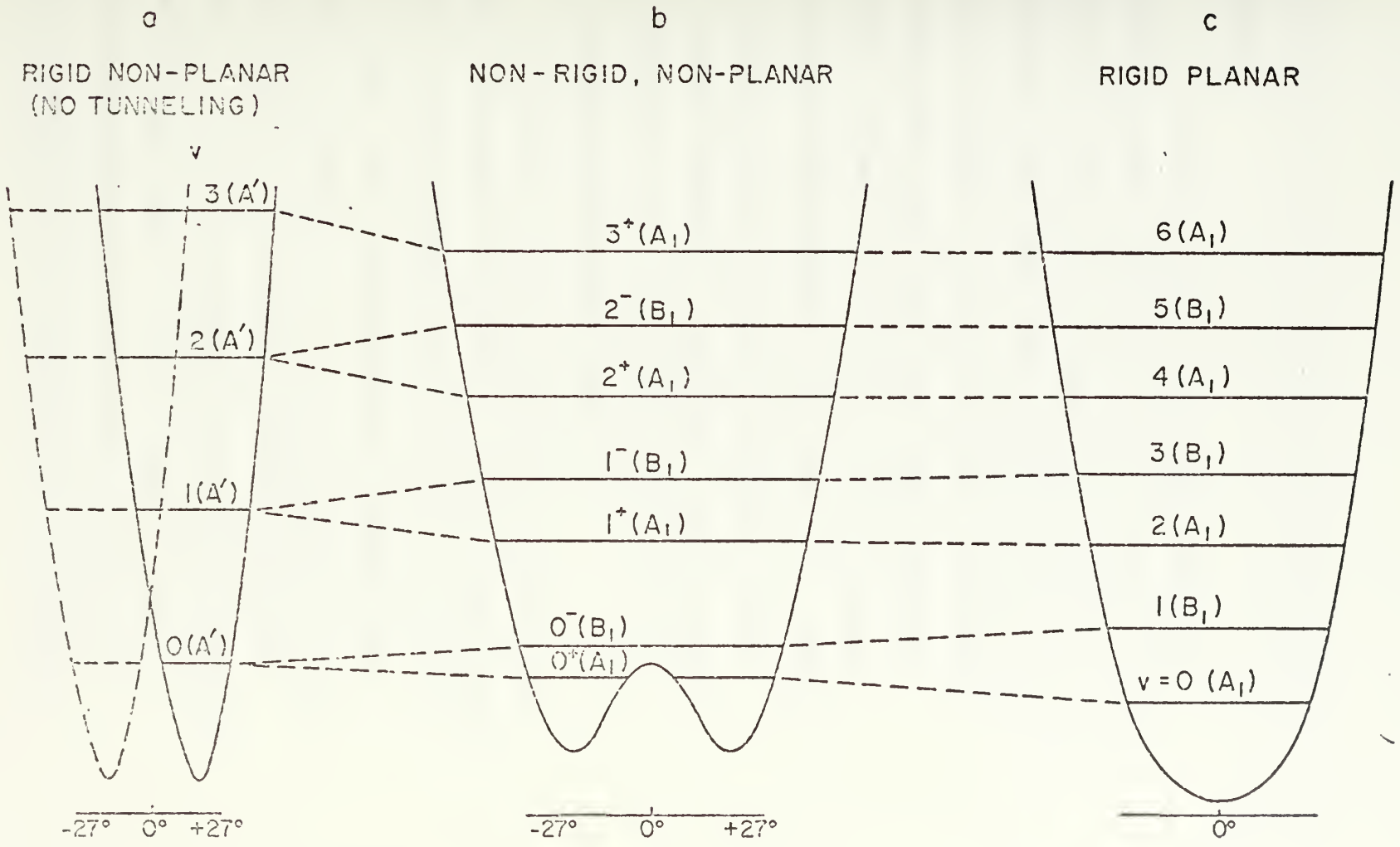

notation for the latter can fortunately still be used for practical purposes.

The pyramidal shape of the S_1 state affects the Frank-Condon factors. The most intense transitions will be between states which have wave functions that overlap significantly. In emission, since the excited state is not planar, the strongest transitions will be to those ground state vibrational levels which have a large probability amplitude to be bent out of the plane. These states are those with one or more quanta in the fourth mode. Downward transitions from any level of S_1 are therefore likely to end in states involving ν_4'' vibrations. From the lowest lying vibrational levels of S_1 the 4_3^0 and 4_4^1 transitions have the greatest Frank-Condon factors[18].

In absorption from the vibrationless ground state, however, the situation is different. Since the ground state is planar the wave function overlap with any of the excited states is poor. The Frank-Condon factors decrease monotonically as the number of excited bending quanta increases, thus the 4_0^1 band is the strongest absorption band which involves ν_4'. This is an additional reason why the absorption and emission band systems are almost completely different. The few common bands allowed by the selection rules have different branching ratios in absorption and in emission,

and a band that is comparatively strong in absorption is very likely to be quite weak in fluorescence.

8. The Observed Spectra

The structure and selection rules discussed above were deduced over the years from a large body of spectral data gathered in emission and absorption at both infrared and optical wavelengths. I have reversed the historical order by presenting the structure first. One starts by observing spectra however, and in the following section I will discuss some of the features of such spectra to be found in the literature, with the help of two figures taken from my own measurements. Both illustrations show many of the features of previously measured spectra.

The low resolution $\tilde{X} - {}^1A_1$ to $\tilde{A} - {}^1A_2$ band structure illustrated by figure (8) was first observed in an ether flame by Emiléus in 1926[32]. The same band system has since been produced by both optical and electric discharge excitation. The absorption spectra was first recorded by Henri and Shaou in 1929, and a complete rotational analysis of several absorption bands was made in 1934 by Dieke and Kistiakowsky[26]. This very readable paper is still the best introductory reference on the rotational structure of formaldehyde. Herzberg[21] calls it "a classic investigation which resulted

FIGURE (8): Emission Band Systems in Formaldehyde.

The figure shows a low resolution (12Å FWHM) photoelectric spectral scan of the high pressure fluorescence excited by the nitrogen laser. The strong bands between 3400Å and 5000Å are those which have been previously observed by Herzberg and Franz[34], Brand[18], Robinson[19], and others[32]. The transitions originate from the 4^0, 4^1, and $2^1 4^1$ states which are populated by collisions in the atmospheric-pressure vapor. The rise in the background is a combination of the low resolution and a series of comparatively weak transitions from the excited state directly populated by the laser. A higher resolution comparison of the two band systems as well as complete details of the experimental procedure can be found in a later chapter. The sharp spikes at 3371Å and 6742Å are caused by scattered light from the nitrogen laser, observed in first and second orders respectively. The apparent width of these lines indicates the resolution of the scan.

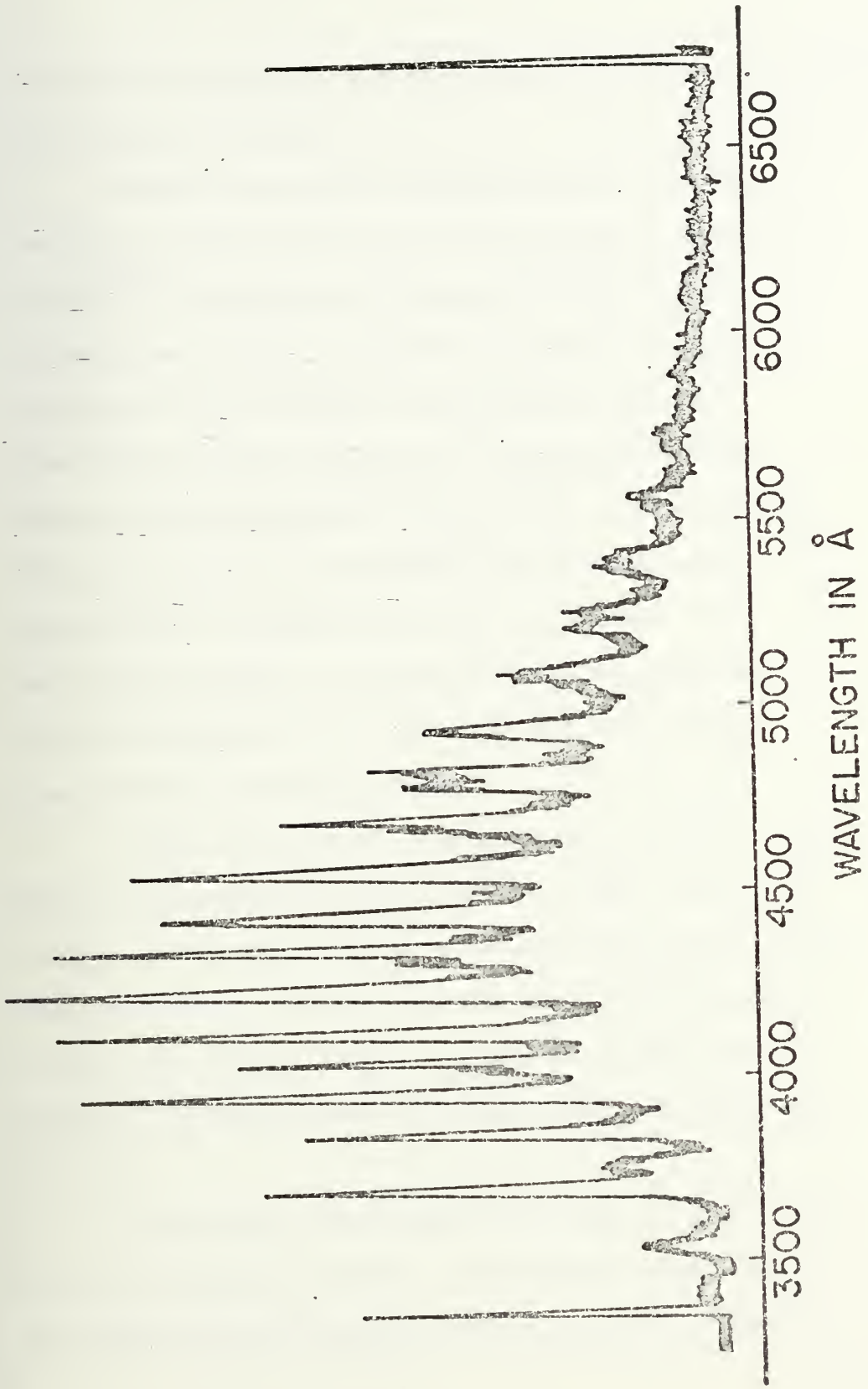
3500
4000
4500
5000
5500
6000
6500
WAVELENGTH IN Å

in the first unambiguous interpretation of an electronic spectrum of a polyatomic molecule."

Despite the success in identifying the rotational features of individual bands, it was not until a series of papers[16-18] by Brand written between 1950 and 1956 that a comprehensive vibrational analysis was made. The major obstacles to the vibrational identification were the dissimilarity between the emission and absorption band systems, and the anharmonic nature of the ν_4' vibration in the excited state. It was Walsh[35], in 1953, who first suggested that the excited state was not planar. His suggestion was based upon theoretical considerations but he cited the Frank-Condon factors deduced from Brand's measurements as additional support.

Brand's 1956 paper[18] unambiguously identified eighteen bands in fluorescence between 3400Å and 4900Å, and fourteen bands in absorption. Although much additional work has been done on the absorption spectrum, Brand's 1956 paper, supplemented by high resolution work on many of the same bands by Robinson[19] in 1956, remains the last word on the fluorescence spectrum.

Both Brand and Robinson used an electric discharge to excite the emission spectrum. Brand found that thirteen of the eighteen bands originated either from the 0^0 or the 4^1

levels, three from 2^1 and one each from $2^1 4^1$ and 2^2. Until the present work, spectrally resolved fluorescence had been observed only for transitions originating from these states. Using the same discharge excitation, Brand observed forty-six bands from D_2CO including a number of bands originating in the 4^2 and 4^3 states. He concluded that the failure to observe H_2CO bands originating from levels with significant excited state vibrational energy is due, not to failure to excite the states, but to predissociation which causes these states to decay by a non-radiative path[14]. Although this predissociation occurs with a quantum yield close to one it is not rapid enough to measurably broaden the absorption lines of formaldehyde until the vibrational energy is greater than 7000 cm^{-1},[9] and Job, Sethuraman, and Innes[24] have observed sharp absorption spectra for almost thirty bands extending from 3530Å to 2300Å.

The most striking feature of the structure of individual bands is a progression of very sharp sub-band heads. They exhibit alternating intensities and, in moderate resolution (0.5 cm^{-1}), appear as sharp spikes above the unresolved background. They are separated by about five angstroms, and decrease in intensity toward the violet end of the band (see figure (9)). These sub-bands occur in both perpendicular and parallel transitions and are characterized by the

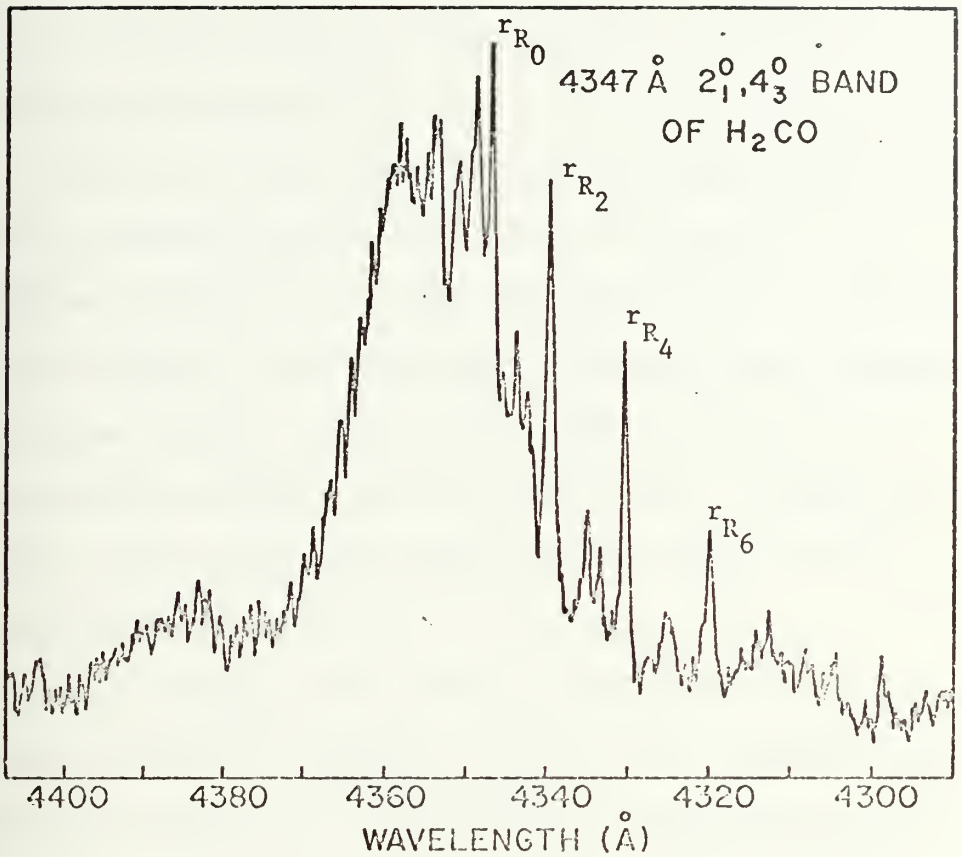

FIGURE (9): The 4347Å, 2_1^0 4_3^0, Emission Band of Formaldehyde. This figure shows a densitometer tracing of a portion of my plate VII. Experimental details of this 24 hour exposure may be found in a later chapter. The plate reproduces the general features and exact wavelengths of the spectra observed by Robinson.[33] The resolution is 0.1Å. The sharp spikes to the violet end of the band are r_R sub-band heads. The structure on the red side of the band is due to several branches that do not form heads. The 4347Å band originates from a vibrationally relaxed excited state, but the low humps at 4305Å and 4385Å are two of the new bands discovered here, which originate from levels populated directly by the nitrogen laser. They are not seen in spectra excited by other means, and are discussed in the experimental chapter.

rotational quantum number K. Parallel bands, however, do not form a sub-band head for $K''=0$.[26]

Equation (1) shows that the rotational energy in formaldehyde is linearly dependent upon $J(J+1)$ and upon K^2. The coefficient of the K^2 term is significantly greater than that for the J dependent term, because the low mass of the hydrogen atoms causes the moment of inertia about the C-O axis, I_a, to be much smaller than that about the other axes. A change in K, therefore, has a much larger effect upon the energy of the molecule than a change in J.

The prominent violet sub-band sequences are due to ^rR transitions and are adequately treated by the symmetric top approximation for $K''>3$.[26] For $K''\lesssim 3$ the perturbation to the symmetric top model, due to the non-zero differences between the large moments of inertia, lifts the degeneracy between the positive and negative values of K. This produces a splitting of the rotational lines and ^rR band heads, as well as a shift of the center of gravity of the split sub-band.

Although an absorption sub-band with $K''=0$ contains lines with all values of J, an $^rR_1$ sub-band will lack the $J=0$ lines, since $K\leq J$ from equation (4). For each increase in K there is a corresponding increase in the number of missing lines. When observed with medium resolution, where individual rotational lines are not resolved, the ^rR sub-band heads can be fixed with

an accuracy no better than about 1 cm^{-1} due to line center of gravity shift caused by the breakdown of the symmetric top approximation for low values of K and by the missing lines for higher values of K.[33]

The alternation of intensities of the K sub-bands is a nuclear spin effect. In the same way that such an alternation arises in the hydrogen molecule[26], states with even or odd quanta of angular momentum about the C-O axis possess either singlet or triplet nuclear spin functions. Since C-O rotation is characterized by K, alternate K sub-bands differ in intensity by a factor of three to one. The alternation is a function only of the nuclear degeneracy in the initial state of the transition. For emission, whether sub-bands with even or odd K' have the greater weight depends upon the rotational quantum number and the symmetry species of the excited state.

The nuclear function must be anti-symmetric with respect to the interchange of the hydrogen nuclei. This is equivalent to the C_2 symmetry operation; an A state is symmetric and a B state is anti-symmetric. In addition, rotational states with even K are symmetric with respect to the interchange and those with odd K are anti-symmetric. To provide the necessary overall anti-symmetry an A excited state with an even K' must be a nuclear singlet, and thus

will have a statistical weight of one. For a B species the lesser weight will be for odd K'. The usual designation of the transition, however, is by the value of K''. Therefore in emission, for ^{r}R transitions from A type excited states, the value of K'' will be even for the sub-bands with the statistical weight of three, and K'' will be odd for the intense sub-bands originating from a B level.

II. B. LIFETIMES AND COLLISIONS

When discussing molecular behavior it is necessary to make the distinction between the properties of the isolated molecule and those that are a function of the interaction between molecules. It is not always easy experimentally to distinguish between the two. The standard method for measurements in the vapor phase is to reduce the pressure of the gas until collisions are infrequent on the time scale of interest, or to make measurements at various pressures and extrapolate the results to obtain the zero pressure behavior. When I began making measurements in H_2CO it was my intention to follow this second technique.

The results repeatedly showed that collisions play an unexpectedly rich role in the physics of formaldehyde. For instance, when H_2CO at pressures above a few hundred torr is excited by a nitrogen laser, the resulting fluorescence originates almost entirely from the 4^0 and 4^1 states which lie more than 1400 cm^{-1} <u>below</u> the exciting energy. When the pressure was reduced below about 100 torr, I found that an entirely new band structure emerged in the spectrum. Even this structure cannot all be accounted for by fluorescence from the vibrational state excited directly by the nitrogen laser. Bands which must originate from states populated by collisions

persist in spectra taken at pressures as low as one torr where the mean lifetime of the unperturbed excited state is shorter than the hard-sphere collision time.

Collisions also appear to have an unusual influence upon formaldehyde lifetimes. The fluorescence decay curves I measured cannot be described by a single rate; the emission intensity from most bands decreases rapidly in time for almost a decade with one characteristic rate, and then more slowly with a second rate. The two rates do not have a similar pressure dependence. In addition the faster decay becomes independent of the collision rate at pressures above about 60 torr. Even this behavior varies quantitatively among bands and with the introduction of buffer gasses. The traditional methods for extrapolating molecular lifetimes to zero pressure do not predict this physically interesting phenomenon.

In searching for an explanation for these unexpected results, I found a branch of the literature on molecular collisions which has been developed by a few authors over the last ten years or so[36-41]. Their theories deal with quantum mechanical effects and with systems that exhibit non-radiative transitions similar to the predissociation present in formaldehyde. They are capable of reproducing to varying degrees some of the anomalous behavior I have observed.

There appear to be only scattered and fragmenting experimental tests of these theories in the literature, partly because they are hard to apply unambiguously to real systems, due to the complexity of molecular structure.

In order to assist the reader to understand the data which will be presented in the experimental chapter I shall discuss, in the following sections, background that is ultimately pertinent to the molecular collision theories. A description of the nature of the nitrogen laser excitation is followed by a review of the present knowledge of the predissociation mechanism. The classical theory for the pressure dependence of molecular lifetimes is discussed, followed by a short introduction to the recent theories. The details of those theories will be presented as required, in the experimental chapter when discussing the data.

1. Nitrogen Laser Excitation

The fact that the spectral output of the nitrogen laser spans a little over half an Angstrom (4.4 cm^{-1}) has led several authors to incorrect ideas about the manner in which it excites formaldehyde. For example, Houston and Moore[2] state "...since [the nitrogen laser] is spectrally broad compared to the formaldehyde linewidth, absorption should not depend strongly on the linewidth." The nitrogen laser output

is in fact composed of almost thirty extremely narrow lines. The width of each, according to a high resolution study by Parks, Rao, and Javan[42], is about one third the doppler width. For 300°K nitrogen, I find this yields a line width of about .001Å (.01 cm^{-1}). Since the doppler width (full width at half maximum) of the formaldehyde absorption at the 400°K of my experiments is about .005Å (.04 cm^{-1}), and since the average separation of lines in the $4_0^2\ 6_0^1$ band is fewer than 10 per Angstrom (less than 1 per cm^{-1}),[28] only a few nitrogen laser lines are likely to interact with formaldehyde. Because the probability of an exact overlap is small any broadening of the H_2CO lines will be extremely important.

Sakurai et al.[11] have suggested that as many as 18 overlaps might exist, but a comparison of the nitrogen laser lines given by Parks, Rao, and Javan and the absorption lines given by Sethuraman, Job and Innes yields only four good candidates for such an overlap. These four, and a few other lines that may overlap due to broadening mechanisms or possible small errors in the measurements, are listed in Table I; they all belong to the $4^2\ 6^1$ vibrational state. There is no evidence for the assertion by Yeung and Moore[1] or Houston and Moore[2] that the nitrogen laser may overlap some high-lying rotational lines of the $2_0^1\ 4_0^1$ band of H_2CO, although it does excite that state in D_2CO. The important things to note in

TABLE I: POSSIBLE NITROGEN LASER - H_2CO $S_1 \leftarrow S_0$ OVERLAPS

H_2CO Line[a]	σ (cm^{-1})	N_2 Laser Line[b]	σ (cm^{-1})	Difference (cm^{-1})
$4_0^2\ 6_0^1\ {}^rQ_2(9)$	29658.80	$\pi_o - \pi_o$ P(8)*	29658.796	.004
$4_0^2\ 6_0^1\ {}^rR_1(1)$	29661.27	$\pi_1 - \pi_1$ P(15)	29661.270	.000
$4_0^2\ 6_0^1\ {}^rQ_1(12)$	29652.82	$\pi_2 - \pi_2$ P(7)	29652.821	.001
$4_0^2\ 6_0^1\ {}^rQ_1(7)$	29653.04	$\pi_2 - \pi_2$ P(10)	29653.051	.011
$4_0^2\ 6_0^1\ {}^rR_1(9)$	29662.51	$\pi_o - \pi_o$ P(5)	29662.478	.032
$4_0^2\ 6_0^1\ {}^rQ_1(4)$	29655.30	$\pi_1 - \pi_1$ P(8)	29665.266	.034
$4_0^2\ 6_0^1\ {}^rQ_3(13)$	29658.49	$\pi_1 - \pi_1$ P(5) $\pi_o - \pi_o$ P(12)	29658.440	.050
$4_0^2\ 6_0^1\ {}^rQ_2(9)$	29658.10	$\pi_o - \pi_o$ P(9)*	29658.045	.055
$4_0^2\ 6_0^1\ {}^rQ_1(3)$	29655.21	$\pi_1 - \pi_1$ P(8)	29655.266	.056

All wavenumbers are vacuum wavenumbers.

a) From Sethuraman, Job, and Innes (Reference 28).

b) From Park, Rao, and Javan (Reference 42).

* Line listed as one of "most intense single transitions" by Park et al.

Table I are that all the lines have K' less than or equal to three, and the J values, while varied, are relatively low.

The fact that several formaldehyde levels are probably excited by the nitrogen laser and that several of these may be excited only in the wings of the absorption profile will complicate any theoretical explanation of the lifetime behavior of the subsequent fluorescence. Excitation using a choice of single nitrogen laser lines, possibly using a Fabry-Perot cavity for spectral filtering, could simplify the problem.

2. Predissociative and Radiative Lifetimes

The primary decay mode for the S_1 state in H_2CO is predissociation to either H_2+CO or H+HCO.[2] For the $4^2 6^1$ vibrational state excited by the nitrogen laser the quantum yield for the H_2+CO branch is about 79%.[43] That for the radical product is close to 21% and very little decays by fluorescence. In spite of this, since the photon emission rate is proportional to the population of the S_1 level, monitoring the fluorescence intensity as a function of time gives a measure of that population. It does not, however, provide a measure of the oscillator strength of the transition since the radiation decay rate is much slower than that for predissociation.

Lifetimes measured in nanoseconds approach the limit of electronic detection methods. The problem is compounded by the very small quantum yield for fluorescence, due to predissociation from the S_1 state. If it were necessary to work at the millitorr pressures required by molecules with more normal decay rates, lifetime measurements in H_2CO would be extremely difficult to make. Fortunately, in order to get the same ratio of decay rate to collision rate in H_2CO as in D_2CO, for example, the H_2CO pressure may be fifty times greater. Using a geometric cross section and the 400°K temperature of my experiments, the formaldehyde collision time at one torr is greater than 150 nanoseconds; thus measurements of the short H_2CO decay times are almost collision-free at pressures less than a few torr.

The processes involved in S_1 predissociation of formaldehyde are not well understood. Houston and Moore[2] have shown that the decay does not proceed directly from H_2CO to the decay products H_2 + CO. By monitoring the production rate of the CO product after laser excitation they have shown that the rate of appearance of CO is fifty times slower than the decay of excited H_2CO. In the time between the disappearance of S_1 formaldehyde and the production of CO there must be some intermediate state which, with Houston and Moore, I will

call (I).

Two candidates for the state (I) are the $T_1(\tilde{a}\text{-}^3A_2)$ state and the high vibrational levels of the $S_o(\tilde{X}\text{-}^1A_1)$ ground state. There are objections to both possibilities. The coupling of the S_1 to T_1 manifold by collisions can explain certain effects upon the predissociation rate of formaldehyde vapor caused by the quenching action of triplet-state benzene molecules,[2] but there is no mechanism that can satisfactorily couple the states at zero pressure. In addition, the T_1 state does not correlate directly to the molecular decay product. The S_0 state, on the other hand, correlates directly to both molecular and radical products. Yeung and Moore[15] have also theoretically reproduced the observed variation of lifetimes with vibrational energy in the S_1 state by considering the $S_1 \rightarrow S_0$ non-radiative coupling. Their work, however, did not reproduce the order of magnitude of the measured lifetimes, and is not compatable with the long intermediate state lifetime later shown to exist. Houston and Moore explain the situation in the zero pressure limit:

> For a long lived S_0 to form a dissipative manifold for S_1 its level density must be greater than $2\pi c\tau$, where τ is the shorter of S_1 and S_0 lifetimes. For measured values of $\tau(S_1)$, this required density is much greater than that calculated for H_2CO (S_0), about $10/cm^{-1}$ at the S_1 origin. While there is no evidence for much higher level densities, the possibility cannot be ruled out. Perhaps a geometry such as HCOH plays a role.[2]

I will show later that the anomalous pressure dependence of formaldehyde lifetimes can shed some light on the nature of the intermediate state.

3. Collision Theories

The normal linear, or Stern-Volmer, behavior of decay rate as a function of pressure is a classical phenomenon. It is named for the researchers who first discussed it in 1919 as a relationship between the quantum yield and pressure in continuous excitation experiments.[44] The derivation for decay rate as a function of pressure is quite simple: If a system has a series of decay modes i, each possessing an individual decay rate k_i, the population N will vary according to the following equation,

$$N(t) \alpha e^{-\Sigma k_i t} . \qquad (7)$$

If collisions induce a decay, the rate k_c for such a decay should be proportional to the collision rate times a cross section. Since the collision rate is proportional to pressure,

$$k_c = \alpha \sigma P \qquad (8)$$

where σ is a quenching cross section and α is dependent upon the temperature T and molecular weight M of the gas in question.

Its value can be derived from statistical mechanics:

$$\alpha = 8(\pi\ kTM)^{-1/2} . \qquad (9)$$

For 400°K formaldehyde the value of α is $3.61\times10^{21}\ s^{-1}cm^{-2}torr^{-1}$.

If all the other rates are summed to yield a zero pressure rate k_o, the measured rate of decay will have the form,

$$k_{measured} = k_o + \alpha\sigma\ P . \qquad (10)$$

Therefore, a plot of measured rate against pressure should yield, in this classical model, a straight line; the zero intercept is the zero pressure rate and the slope yields a collision quenching cross section. Since the rate is the inverse of the lifetime, it is usual to plot $1/\tau$ against pressure. Such a plot is called a Stern-Volmer plot, and equation (10) is a form of the Stern-Volmer equation. It is often written:

$$k_{measured} = k_o + k_q\ P. \qquad (11)$$

$k_q \equiv \alpha\sigma$ is called the quenching rate and is dependent upon temperature, whereas σ, the cross section, is not.

The published literature on formaldehyde lifetimes, and the observation that the average distance between molecules is much greater than the molecular diameter even for a gas at atmospheric pressure, had led me to believe that the

Stern-Volmer equation (10) would be quite adequate to describe the behavior of the molecule. It soon became clear that it was not, but there are two classes of modern molecular collision theories which may explain the double decays and pressure-independent lifetimes. The first[36] requires that the fluorescence which is observed should originate from several different ro-vibronic states. (This is somewhat restricted by the $10\mathring{A}$ bandwidth of my measurements.) The model requires that the various observed levels possess different quenching rates and different zero pressure lifetimes. The values of these parameters are adjusted to reproduce the two decay rates and non-Stern-Volmer behavior. The several states could be populated directly by the laser or by collisions subsequent to the initial excitation.

The second class of theory involves certain quantum mechanical effects.[38-41] Quantum beats between the $4^2 6^1$ excited state levels and levels of the predissociation intermediate state (I) or possibly other close-lying vibrational levels of S_1 might explain the non-exponential decay curves. The appearance of pressure-independent lifetimes for sufficiently high pressures can be caused by a broadening of the (I) levels by collisions.[37] If these interactions become sufficiently frequent to broaden the levels of (I)

into a continuum, an increase in the collision rate cannot make the (I) levels any more continuous. Since the true eigenstates of the collision-perturbed molecule will be a superposition of S_0 and (I) states, when the (I) state becomes continuous the effective Hamiltonian for the molecule will no longer change with pressure, and pressure-independent lifetimes result.

Specifics of these theories are model dependent. They will be discussed after the data from these experiments have been presented.

II.C. REVIEW OF H_2CO LIFETIME MEASUREMENTS

Before explaining my experiments, it is valuable to review the previous measurements of H_2CO lifetimes, if only to help the reader distinguish between those and mine. The literature on the spectra of the molecule has already been discussed. This presentation is essentially in historical order, and the work done on D_2CO, triplet H_2CO, and HDCO will be mentioned only when it sheds light on H_2CO studies.

In 1955, before there was a general understanding of the structure of the S_1 state of formaldehyde, Cohen and Reid[45] undertook to measure the integrated absorption coefficient of what is now known as the 4_0^1 band. They wished to determine if the upper level were a triplet state as had been suggested by Walsh.[31] They were able to calculate from their absorption measurements a radiative lifetime of 5×10^{-5} seconds for the 4_0^1 transition. There are, in fact, many transitions possible from 4^1; some of them are more probable than 4_0^1. The radiative lifetime of this state, therefore, is not governed just by the Frank-Condon factor for 4_0^1 but the sum of Frank-Condon factors for all possible 4_n^1 transitions. Thus the lifetime of the 4^1 state should be shorter than that calculated from the Einstein A coefficient of the 4_0^1 absorption. From their measurement I estimate a radiative

lifetime for the 4^1 state of 1×10^{-5} seconds.

In 1957 and 1958, Pople and Sidman[46,47] calculated, on theoretical grounds, an oscillator strength of 3×10^{-4} for the 4_0^1 absorption. This is an excellent agreement with the 1957 value of 2.4×10^{-4} measured by House.[48] Estimating the Frank-Condon factor from Brand's measurements, Jeunehomme and Duncan[10] have converted this oscillator strength to a radiative lifetime of 1.45×10^{-5} seconds.

A direct experimental lifetime measurement was also made by Jeunehomme and Duncan[10] in 1964. A fast electric discharge excited the S_1 state and the time-resolved fluorescence was observed. Working at pressures of 5 to 300 millitorr, they measured a lifetime of $(2.3\pm.3)\times10^{-7}$ seconds for the 0^o band. In addition, fluorescence at 3690Å was seen to show a lifetime of $(1.7\pm.3)\times10^{-7}$ seconds. They could not distinguish between fluorescence of the $2_0^1\ 4_2^0$ and $2_0^0\ 4_1^0$ bands near this wavelength, but the measurement hinted that the lifetimes shorten with increased vibrational energy in the excited state; the $2^1\ 4^0$ and the $2^0\ 4^0$ levels are separated by 1173 cm^{-1}. They noted the discrepancy between their measurements and the lifetimes implied by the integrated absorption measurements but did not suggest that predissociation was the cause.

The lifetime of nitrogen laser excited formaldehyde was first reported by Sakurai, Capelle, and Broida[11] in 1971.

The fluorescence output was detected through an interference filter which transmitted light between 4200Å and 5000Å and then displayed on a sampling oscilloscope. They measured a lifetime of 27±2 nanoseconds which did not vary over a range of 0.3 to 3.8 torr. Higher pressures were not used because of polymerization at the 300°K temperature of their apparatus.

The experiment was repeated by Aoki, Morikawa, and Sakurai[12] in 1972. The fluorescence signal was viewed through an ultraviolet cutoff filter which had a half-attenuation point at about 4000Å and complete cutoff below 3600Å. Their measurement yielded a lifetime of 18±1 nanoseconds which did not vary between one and ten torr. A measurement was also made of the lifetime using a mixture of air at atmospheric pressure and an unspecified pressure of formaldehyde. Assuming Stern-Volmer behavior, this and their unbuffered measurements yielded a quenching cross section of $3.1^{\pm}.5$ 10^{-18} cm^2. They do not appear to have observed the lifetime behavior at any intermediate buffer gas pressure.

Aoki et al.[12] also show a spectrum of fluorescence from 20 torr H_2CO excited by a nitrogen laser. Their resolution was 200Å. This spectrum shows a broad peak of intensity between 4000 and 5000Å, and a second, lower intensity peak centered around 6400Å. Their paper makes no comment

about the second peak. It was in an attempt to investigate this feature that I first began to record nitrogen laser excited fluorescence spectra, although I have since shown it to be spurious.

In 1973 Yeung and Moore[1] reporeted a comprehensive study of the lifetimes of many vibrational states of D_2CO and HDCO using a tunable ultraviolet laser as an excitation source. In addition they were able to determine lifetimes and self-quenching rates, k_c, of three vibrational levels in H_2CO; 4^1, $2^1 4^3$, and $2^2 4^1$. These observations, as did those on the other isotopic species, showed that lifetimes decreased rapidly with increasing vibrational energy. ($\tau_o(4^1) = 282ns$, $\tau_o(2^1 4^3) = 29ns$, $\tau_o(2^2 4^1) = 20ns$.) The exciting laser had a spectral width of about one Angstrom, and the fluorescence was observed through a 200Å bandwidth interference filter centered on either 4200Å or 4400Å.

In their D_2CO data, when using this broad observing bandwidth, Yeung and Moore saw double exponential decays, but when the strong D_2CO fluorescence excited by a doubled ruby laser was observed through a 22Å bandwidth monochrometer, only single exponential decays were seen. Since 22Å width is sufficient to resolve between bands of fluorescence but 200Å is not, they attributed the slow decay to emission from

vibrational levels populated by collisions. It is not clear whether they saw the double decays in any of the three H_2CO bands or not.

In a subsequent theoretical paper Yeung and Moore[15] assumed that predissociation takes place via radiationless transfer from the S_1 state to the high-lying vibrations of S_0 which then dissociates. They showed, given this assumption, that the lifetimes should decrease rapidly as the energy of the excited state vibration increased. They noted that although they had adequate data on D_2CO lifetimes, more information on the H_2CO lifetimes in various vibrational states was needed.

Well after I started the research reported in this dissertation, two recent studies came to light. In 1976 Andreyev, Antonov, Knyazev, and Letokhov[13] reported two-step photoionization of H_2CO by excitation using nitrogen and hydrogen lasers. The nitrogen pulse excited the S_1 $4^2 6^1$ level and the hydrogen laser pulse ionized the excited molecules. Although their primary goal was to show the feasibility of the ionization process, they also were able to take lifetime data on the $4^2 6^1$ state by varying the time between the N_2 and H_2 laser pulses and monitoring the ionization current. Their decay curve for 0.9 torr H_2CO shows distinct non-exponential behavior. For this reason, they quote no

measured lifetime in their paper; however their results correspond to two lifetimes of about 14 and 20 nanoseconds, measured at one torr. Because they observed photoelectrons, spectral filtering is not applicable to their experiment.

Another series of formaldehyde lifetime measurements made by C. B. Moore's group is reported in A. P. Baronavski's 1976 Ph.D. dissertation.[8] Baronavski measured, among other things: spectrally resolved lifetimes of nitrogen laser excited D_2CO, as well as the low resolution fluorescence spectrum; the broadband emission lifetime of N_2 laser excited H_2CO; and some preliminary results of broadband fluorescence resulting from single line excitation of several individual rotational levels of the 4^1 state in H_2CO ($\tau \gtrsim 100$ns). For this last experiment, he used a tunable dye laser and Tektronix model R7912 Transient Digitizer system.

This equipment was not available when he studied N_2 laser excitation of H_2CO and he could not electronically resolve the fast 20 nanosecond lifetimes of the $4^2 6^1$ state. Instead he photographed the weak fluorescence curve from several laser pulses on the face of an oscilloscope, and faired a curve through the resulting noisy signal. Such a technique is valid if enough photons arrive at one time so that the vertical input to the oscilloscope is proportional to the probability of arrival of a photon. If however the signal

is so weak that photon pulses arrive separately at the oscilloscope, then the trace height photographed from the scope face will equal to that of a single photon pulse height, independent of arrival time. For these measurements Baronavski's data appears to fall between the two cases and the extent to which his photographs yield the true lifetime is not clear. He quotes a value for the lifetime of nitrogen laser excited fluorescence viewed through a 200Å band width interference fileter, centered at 4400Å, of 46 nanoseconds ± 10%.

The spectrally resolved D_2CO fluorescence in Baronavski's work exhibited both double exponential decays and non-Stern-Volmer pressure dependence. The double exponentials persisted even at low pressures and when viewed with as small a bandwidth as six Angstroms. Little theoretical justification for this behavior was given. Although no pressure studies were made for the single line excitation of the slowly decaying 4^1 level, most of the fluorescence curves showed double exponential behavior also. The lifetimes varied randomly with the rotational quantum number J within about a factor of two.

It is interesting to note that the only trait Baronavski found which distinguished those rotational levels which fluoresce with double decays from those which do not is the value of K. Out of the 20 lines individually excited, 15

with $K \leq 3$ possessed double decays (one did not) and 4 with $K \geq 4$ showed only single decay rates. Although the cause of this apparent trend is not clear, I find it hard to avoid speculating that it may be somehow related to the breakdown of the symmetric top approximation for $K \leq 3$.

Although it is not certain that the $4^2 6^1$ band should act like the 4^1 band in respect to the double decay of singly excited lines, it should be noted that all the candidates for the nitrogen laser-formaldehyde absorption line overlaps in Table I have $K \leq 3$.

In summary, until the work reported here, the nitrogen laser excited fluorescence lifetime of H_2CO formaldehyde has been observed with, at best, 200Å resolution around a single wavelength. That wavelength differs for each reported experiment. There is little agreement among the various measurements made. There is a definite double decay in the measurement made by Andreyev et al. and hints of it in the figure of the decay curve shown by Aoki et al. There is no information in the literature concerning the effect of pressure on H_2CO above ten torr where the collision time begins to exceed the zero pressure lifetime, except for one measurement of an unspecified partial pressure of formaldehyde in the presence of air at atmospheric pressure. Some of the experiments described in the following chapter should help resolve the conflicts and

fill in the gaps, but as usual the results raise new questions which will require further experimental work to answer.

CHAPTER III

EXPERIMENTAL APPARATUS

III. EXPERIMENTAL APPARATUS

This chapter describes the experimental equipment used. It is organized around the block diagram of figure (10). A brief overview of the apparatus is first given and then each block is explained in more detail.

Starting from the top of figure (10): the nitrogen laser pulse was focused and directed through a heated cell filled with formaldehyde vapor. The resulting fluorescence was focused onto the slit of a spectrometer and dispersed light was detected either by a photographic plate or a photomultiplier tube. Photographic plates were scanned by a microdensitometer the output of which was graphed by a chart recorder. This tracing was then analyzed to produce wavelength data. The wavelengths were calibrated with an iron hollow cathode lamp comparison spectrum and Crosswhite's tables[49].

When the photomultipler was used, the electrical output was amplified and processed by a boxcar integrator. The analog output of the boxcar was recorded directly to produce spectra when the spectrometer grating was scanned. If the spectrometer was fixed at one wavelength, the boxcar integrator could itself be scanned in time and its output would be proportional to the fluorescence decay curve at the fixed wavelength. To simplify the measurement of lifetimes

the decay signal from the boxcar was further processed by a home-built logarithmic amplifier. Both the decay curve and its logarithm were recorded on a dual trace chart recorder. The lifetime could be easily calculated from the logarithmic plot. Photoelectric spectra were calibrated with a thorium hollow cathode lamp and Chaffee's thorium atlas[50].

1. Nitrogen Laser

Details of the construction of the home-built nitrogen laser used in these experiments are given in the appendix. Of importance here is the nature of its output. The pulse width (fwhm) was 8 nanoseconds, and the peak power used for all experiments was about 100 kilowatts. The pulse rate was 15 per second. The beam had a rectangular cross section 25mm by 4mm and had a divergence angle of about 8 milliradians. The spectral content of this laser is shown in figure (11). Radio-frequency shielding for the laser was achieved by enclosing all of the laser parts including the power supply and connecting cables in a single metallic enclosure, and filtering the AC power line to the system. Further mention of the laser's radio-frequency emission is made in the sections on photodetection, and on the boxcar integrator.

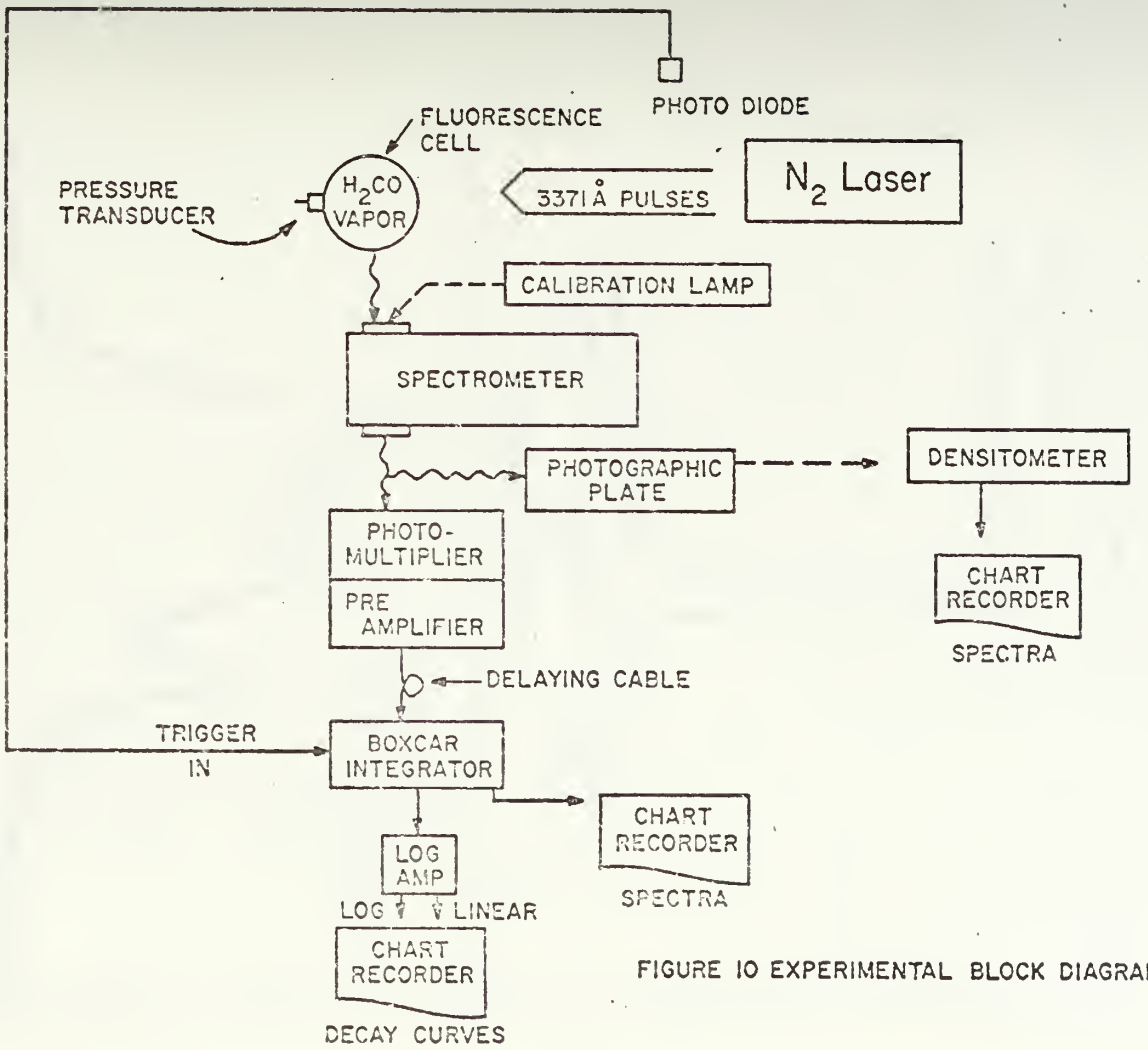

FIGURE 10 EXPERIMENTAL BLOCK DIAGRAM

Fig. 11

Nitrogen Laser Spectrum

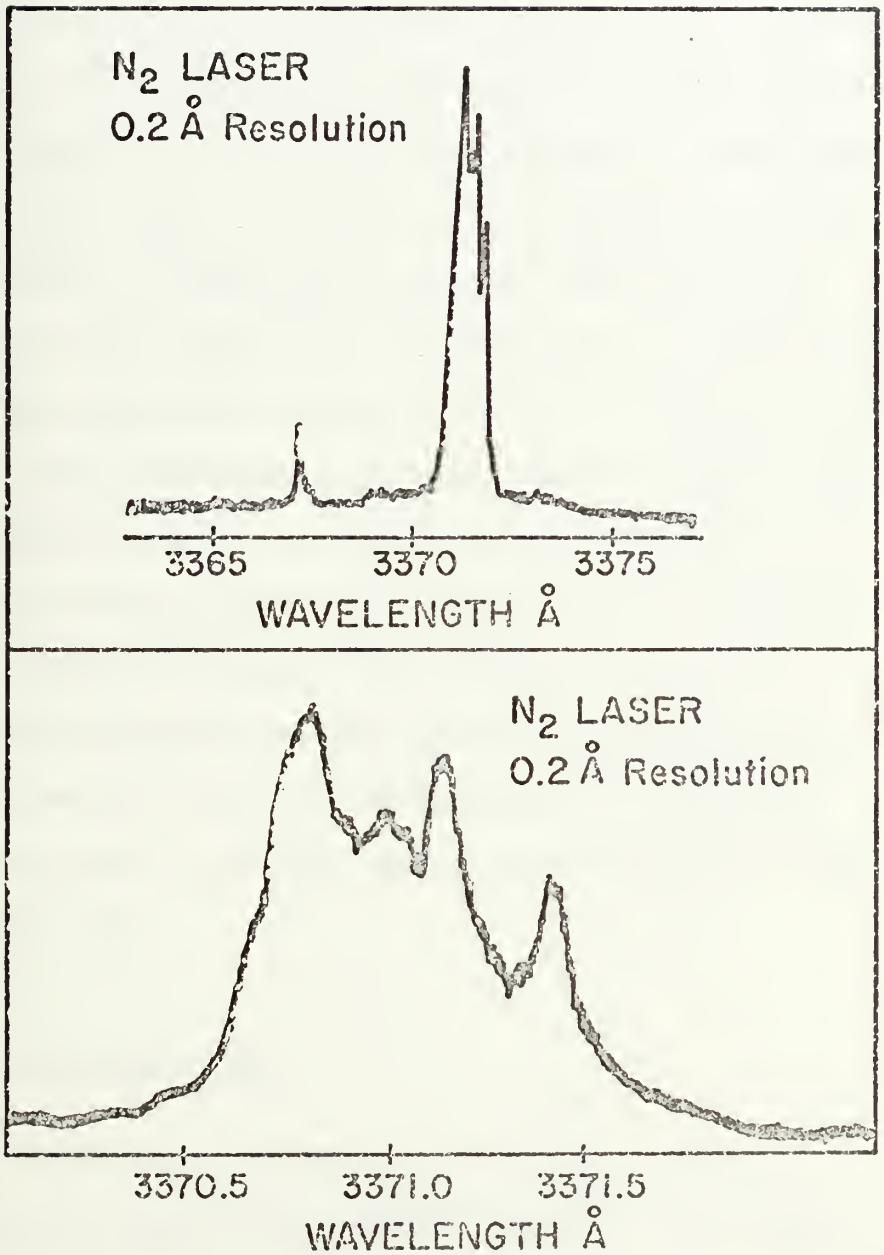

2. Experimental Geometry

Figure (12) shows the geometry of the experiments. The nitrogen laser beam is directed vertically by a mirror and focused with a long focal length quartz lens. The beam passing into the cell is therefore an extremely narrow pencil of light. The diverging laser beam exitting the fluorescence cell is redirected and refocused back through it. Fluorescence from the focal region is viewed facing the edge of the beam. The thin line of fluorescence, which is visible in 20 torr H_2CO with a dark adapted eye, is focused onto the spectrometer slit by an aspheric glass lens. The distances between the lens cell and spectrometer were empirically chosen to produce the most intense output from the spectrometer. The result was a compromise between matching the f-number of the spectrometer with the convergence angle of the light focused from the lens, and producing the smallest possible image on the entrance slit so that that portion of the light which is within the acceptance angle of the spectrometer grating will get through the narrow slit.

3. Fluorescence Cell

Figure (13) illustrates the cell used. It was constructed of brass silver-soldered together. The windows

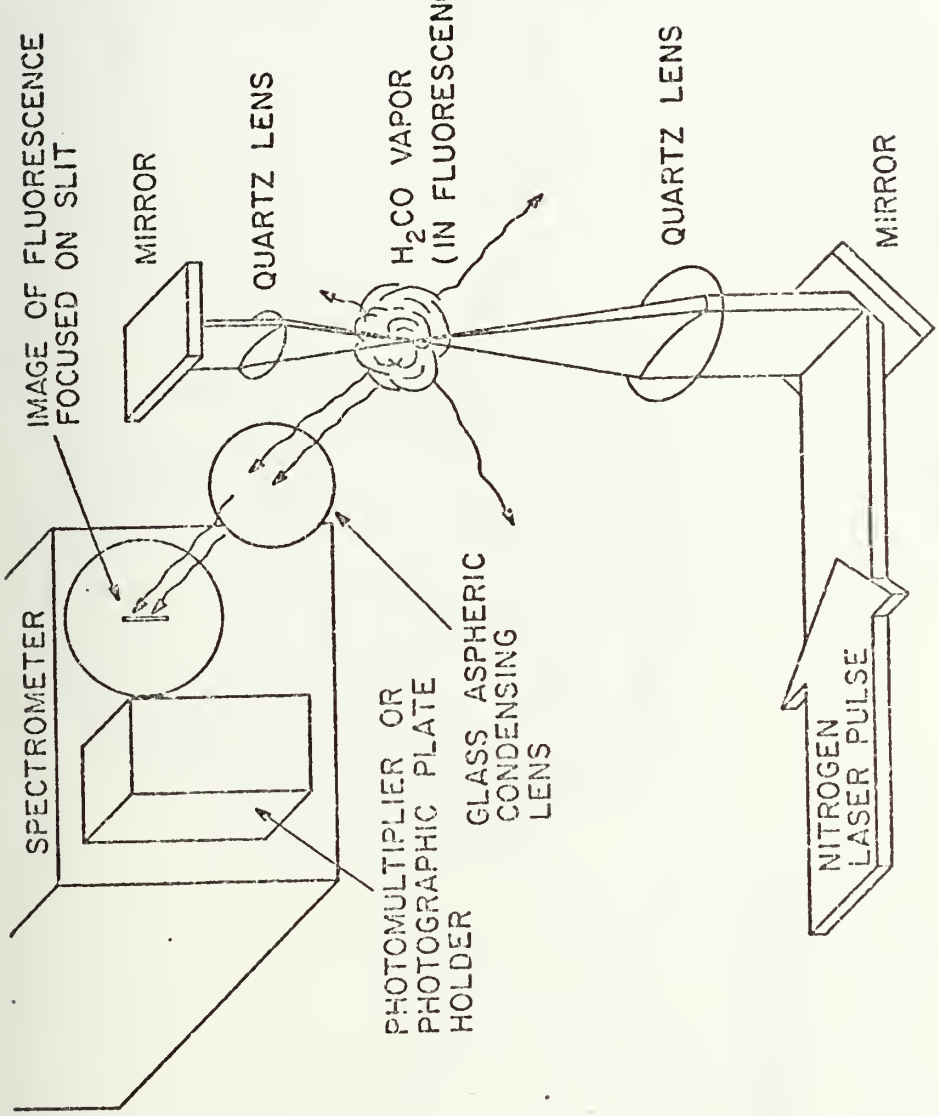

FIGURE 12 EXPERIMENTAL GEOMETRY

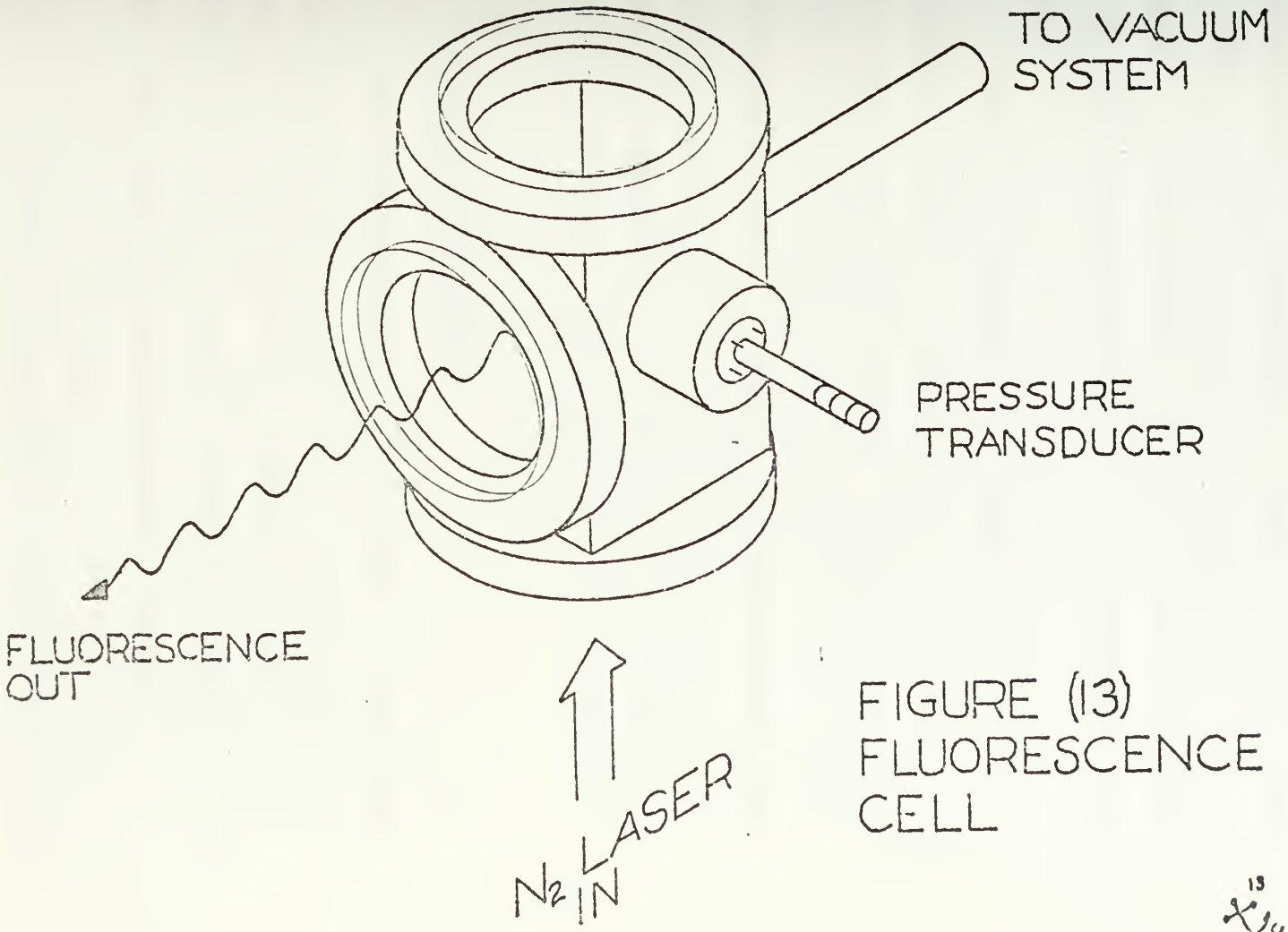

FIGURE (13)
FLUORESCENCE CELL

were quartz and sealed to the cell by O-rings. The window through which the fluorescence was viewed was 4.5 cm in diameter. An additional small window was placed in the side so that the intensity of the broad-band fluorescence could be monitored at the same time that spectrally filtered emission was being measured.

The cell was heated by electrical heat tape. This was necessary to prevent the formaldehyde from polymerizing. Heat tape, being opaque, was not suitable to prevent condensation of the polymer on the windows. For this purpose three old hair dryers were modified to produce a slow high-temperature flow of air over the surface of all windows. The temperature of the cell was monitored by a chromel-alumel thermocouple and was maintained within ± five degrees of 130°C at all times.

4. Pressure Monitoring

Pressure measurement in the presence of formaldehyde vapor presents special problems. If a pressure gauge is not thoroughly heated, polymer will condense in it and will plug any narrow passages. Accurate manometer and mechanical gauges have piping sensitive to such condensation and are difficult to heat. Most electrical gauges lose their calibration when heated. A device which substantially overcomes these problems

is a strain gauge pressure transducer. The CEC 4-313 transducer used in these experiments measured the pressure difference between that at a reference port and that on the face of 1.25 cm diameter diaphram. It was mounted so that the diaphram was flush with the inner fluorescence-cell wall, and was held in a thick brass housing so that a uniform temperature would be maintained over the entire transducer. It was sealed to the cell with a silicone rubber O-ring. The sensor output ranged from + to -13 millivolts proportional to the differential pressure over the range of ±520 torr.

The transducer, as purchased, was temperature compensated so that its output would be independent of temperature over a wide range including the 130°C temperature used. The gauge was calibrated against a precision Wallace and Tiernan mechanical gauge which was also used to monitor the pressure at the reference port. Small zero drifts in the electrical output corresponding to a pressure measurement of about ±1 torr were found to occur over a period of 24 hours, but the proportionally constant between the electrical output and the differential pressure remaind constant. For that reason the calibration was checked at operating temperature both before and after every series of measurements. This amounted to a calibration check about every two hours. With this additional calibration the

system could measure pressure with an accuracy of ±0.5 torr.

5. Gas Handling System

Because of the low fluorescence yield, emission could not be spectrally resolved at pressures below one torr. For this reason only a mechanical vacuum pump was required. The cell is, however, suitable for high vacuum work and showed no leaks on a helium leak detector. The vacuum pump was connected to the cell (with copper tubing) through a series of valves. The valve manifold allows for the system to be pumped to a pressure of less than 10 millitorr, and for the controlled inlet of buffer gasses, or H_2CO vapor.

Formaldehyde vapor was produced by the pyrolysis of the polymer, paraformaldehyde (Fisher Scientific). The powder was maintained in a separate bulb and heated as necessary to produce the required monomer pressure in the fluorescence cell. The cell would then be sealed off with a valve. It was found that the pressure in such a sealed cell would remain constant over a period of at least several hours if the formaldehyde partial pressure was less than about 150 torr. At higher partial pressures there was a slow decrease in pressure caused by polymerization at some isolated cool place in the copper tubing. If condensation had taken place it was necessary to

pump the cell out overnight while it was still heated to remove the polymer; otherwise there would be a rise in pressure if the cell were sealed with a partial pressure of formaldehyde less than 20 torr. The formaldehyde used in these experiments was not recovered, but pumped from the cell by the mechanical pump which was vented to the laboratory's toxic gas ventilation system. The elaborate distillation procedures of Spence and Wild[51] were not used for these experiments since only the monomer can exist at the 130°C temperature maintained in the cell.

An annoying experimental problem was caused by the formation of photochemical sludge on the window surface where the nitrogen laser beam entered and exitted. The beam was focused to provide a thin line of fluorescence to image on the spectrometer slit and had a cross section of about 0.5 mm by 2.5 mm when it passed through the windows. The brown deposit that formed absorbed a large portion of the laser light and drastically reduce the fluorescence signal. When spectra were being taken of atmospheric pressure formaldehyde, the cell had to be moved slightly relative to the fixed position of the laser beam every fifteen minutes or so, so that the exciting light could pass through a clear portion of the windows. This became tedious during twenty-four hour photographic exposures.

At H_2CO pressures around 40 torr it took several hours for the sludge to build up sufficiently to decrease the fluorescence signal by half. The sludge can be removed by scraping followed by the use of an ultrasonic sink and a commercial glass cleaning solution.

At the end of a twenty-four hour photographic exposure where the H_2CO pressure had been about 760 torr, most of the inside of the cell was found to be coated with a similar brown sticky sludge. It was not so thoroughly bonded to the cell as that which formed on the windows where the laser beam had passed.

6. Spectrometers

Two spectrometers were used. For the photographic spectra the laser and gas handling equipment were moved to the university's Molecular Astrophysics Laboratory in order to use the SPEX Model 1704 one meter f-9 Czerney-Turner spectrometer located there. The spectra were photographed in first order of a 600 groove per millimeter 3000Å blazed grating without a grating mask. A 20 micron wide entrance slit was used, and this, combined with the reciprocal dispersion of 16Å/mm at the focal plane yielded an expected bandwidth of 0.3Å.

All the useful photographic data came from twenty-four hour exposures on type II a-0 Kodak Spectroscopic plates which

had been baked at 60°C in flowing dry nitrogen for four hours prior to exposure. No image could be obtained of wavelengths longer than 4800Å either on II a-0 or II a-F plates. Very faint images of bands out to 5200Å were obtained on a Kodak 127-04 plate sensitized in the same way as were the II a-0 plates. The photographic spectrometer was available for only a short period of time and therefore only seven plates were exposed, only four of which were usable.

An iron calibration spectrum of a Westinghouse iron hollow cathode lamp was exposed on the plates next to the formaldehyde spectrum. The plates were traced with a Grant series 800 Comparator and recorded on chart paper. A quadratic least squares fit to the iron line wavelengths was made. The mean square deviation of the iron lines from the least squares fit was, for all plates, less than 0.06Å.

Photoelectric spectra and lifetime measurements were made using a McPherson Model 218 one-third meter f-5.3 scanning monochrometer. A 1200 groove per millimeter grating blazed at 5000Å was used. Using a series of thorium lines to calibrate the monochrometer, its wavelength counter was found to be accurate within ±0.3Å over the range of 3300 to 6000Å. The counter values for different scans were found to be repeatable to within ±0.2Å. The bandwidth of this instrument was experimentally determined to be 2.5Å per 100 microns slit width.

When observing the high pressure, vibrationally relaxed spectrum with the 2.5Å bandwidth, the following additional calibration procedure was used for each band investigated. The spectrometer scan was started at a wavelength well below that of the band to be studied. Several thorium lines were recorded, and then, while the spectrometer continued to scan and the chart recorder continued to advance, the thorium lamp would be removed and the nitrogen laser excited fluorescence would be directed into the spectrometer. When the band of interest had been recorded, the output of the thorium lamp was again focused on the entrance slit, and a second set of calibration wavelengths was recorded.

7. Photodetection

Light emerging from the exit slit of the McPherson 218 monochrometer was detected by an uncooled RCA 31025Q photomultiplier tube (quartz envelope) in a Pacific Photometric model 3150 radio-frequency shilded housing. The tube supply voltage was 1500 volts. Photoelectron pulses were amplified by an Ortec model 9301 fast preamplifier, which provided a gain of ten. It was connected directly to the output of the tube housing. The amplified pulses were delayed by 100 feet of RG 58/U coaxial cable before presentation to the boxcar

integrator, since the integrator requires a minimum of 100 ns delay after it is triggered before it can process a sample. This unavoidably introduced some dispersion to the fluorescence decay curves necessitating corrections which will be discussed later.

Care in shielding the cable, use of the shielded photomultiplier housing, and direct shielding for the nitrogen laser reduced the electrical laser noise arriving at the boxcar integrator input to less than one millivolt amplitude. This was less than the noise level of the preamplifier, and more than ten times less than the pulse height generated by a single photon.

8. Boxcar Integrator

A Princeton Applied Research Corporation (PAR) model 162 boxcar integrator provided both signal averaging and amplification of the fluorescence pulses. It was triggered by a photodiode which responded to light scattered from the front window of the nitrogen laser. After a delay set on the instrument's mainframe, the boxcar would sample the input signal and add it to the samples taken of previous pulses. To record spectra, the delay was set to produce maximum response, the spectrometer wavelength was scanned and the samples of the amplified and delayed photomultiplier output were exponentially

averaged by the boxcar*. If the scan rate was slow enough this would produce a continuous output equal to the instantaneous average input pulse height times the gain of the boxcar's amplifiers. For lifetime measurements the spectrometer wavelength was fixed and the delay time was scanned at a rate of 30 nsec per minute. The laser pulse rate was 15 per second. Thus each pulse was sampled with a slightly different delay. Again, exponential averaging was used, and with the slow scan rate, properly reproduced the shape of the input signal. It is worth noting that this instrument can correctly integrate low light signals for lifetime work, since it adds the irregular photoelectron pulses for each laser pulse to those of successive laser pulses, unlike the photographic method which superimposes them. It can, of course, properly sum smooth signals as well.

Two gating plug-ins were used. For the high pressure spectrum measurements a PAR 164 integrator set for a

---

*Exponential averaging causes the output voltage to asymptotically approach the boxcar gain times the true average of the sampled input signal level. It is a form of weighted averaging where the most recent repetition has more influence on the output level than the one preceding it which, in turn, has more influence than the sample preceding it. Early repetitions have a negligible influence. "Early" in this context means that sufficient time has elapsed since the pulse in question so that the aperture has been open to sample signals for longer than five instrument time constants. When the input signal is scanned, the scan rate must be slow relative to this time constant in order that the output will accurately follow the changing input.

25 nanosecond gate width was used. This gate width was unsuitable for the rapidly decaying low pressure bands and so for both lifetime and low pressure spectra measurements a PAR model 163 sampled integrator with a Tektronix S-1 sampling head was used. This produced a 350 picosecond aperture. Since this latter plug-in could only provide exponential averaging, and could not algebraically sum successive pulses, single point analysis of very low intensity signals was not possible.

The necessity to average exponentially placed a limit of about 10 millivolts on the minimum signal that could be measured, since the averaged input level must be large enough that the output voltage will be well above the noise level introduced by the boxcar circuits, and be within the linear region of the processor's amplifiers.

An additional limit to the minimum level of signals that could be averaged was given by the weak rf noise generated by laser firing, which took the form of a damped ringing. Since this was really a signal that repeats from pulse to pulse, it was also integrated by the boxcar, and produced an output on the most sensitive boxcar scale of about 10 millivolts. For comparison, a representative decay curve would yield a boxcar output varying from one volt at maximum down to several millivolts at the point where measurements were

stopped (about 250 nsec after pulse initiation). When taking spectra the laser's RF emission was unimportant since the same portion of the electrical "noise" waveform was sampled on each pulse, and it merely contributed an addition to the baseline. When measuring lifetimes, however, the electrical laser emission yielded a series of small oscillations with a period of about 5 nanoseconds which would be superimposed on the fluorescence curve.

9. Logarithmic Amplifier

When investigating spectra the (analog) output of the boxcar integrator was recorded directly by a chart recorder, but when measuring the fluorescence decay curves the boxcar output was further processed by a logarithmic amplifier which I built for the purpose. Figure (14) shows the circuit diagram of this amplifier. Since the log amp chip would be damaged by inputs greater than about four volts, the supply voltage to the operational amplifiers which drive the chip inputs were limited to ± four volts[52]. A monitor of the input to the log amp chip was provided to show when the input signal was so large that it saturated the input amplifiers. Both the monitor and its logarithm were recorded by a chart recorder.

FIGURE(14) LOGARITHMIC AMPLIFIER

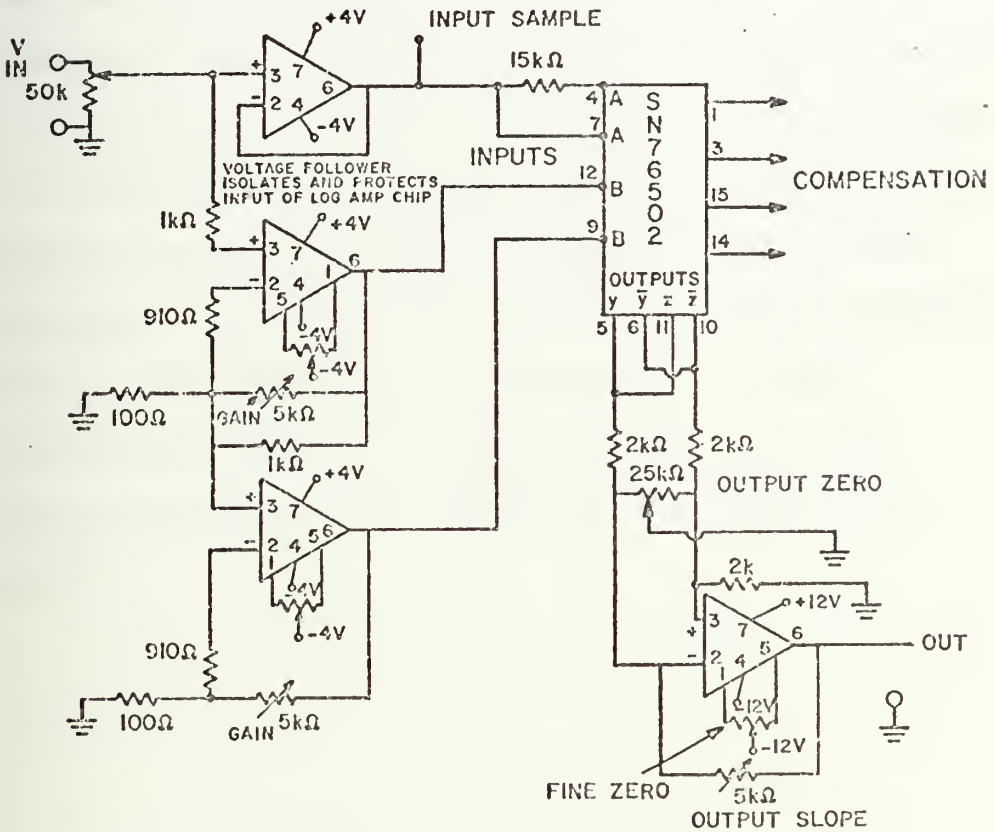

ALL OP-AMPS ARE 741

The output of this amplifier was proportional to the logarithm of its input between 3 volts and 3×10^{-4} volts. The maximum difference between the calculated log of the input and the amplifiers logarithmic output was 2%, in the range used for these experiments (3 volts to 1 millivolt input). If the fluorescence decay curve were exponential, its logarithm would be a straight line. The slope of this line could be converted to a lifetime, knowing the proportionality constant between the amplifier's output and the natural logarithm. This constant was measured to an accuracy of ± 0.3% using a Leeds and Northrup Millivolt Potentiometer as a voltage source. The chart recorder which measured the output from the log amplifier during the experiments was calibrated by the same voltage source.

CHAPTER IV

RESULTS AND DISCUSSION

IV. RESULTS AND DISCUSSION

In this chapter the data will be presented in three sections. Spectra taken at high pressure where the vibrational relaxation time is much shorter than the lifetime of the excited molecules will be discussed first. Next the spectra taken at pressures where the collision time is less than or the order of the mean molecular lifetime (for brevity, low pressure spectra) will be presented. These show an entirely new band structure. The variation of the spectra with pressure is also considered here. In the third section the lifetime data are presented and the application of collision theories to these data are discussed.

Each of the three sections is organized in the same way. The data are initially summarized and discussed, so that the important points of the analysis are presented first. This is followed by a sub-section on the experimental details, which will contain a more complete description of the data, details of its processing, and miscellaneous points of interest. Included here will be a number of figures which show representative samples of the raw data. They have been copied directly from the original charts by a reducing Xerox machine. It was necessary to darken the lines on a few of them, where the originals had been made in red ink, in order that a usable

copy could be made, but in those cases I have used a fine drawing pen and attempted to trace curves as accurately as possible. Additional scales have been drawn on these figures to aid in interpretation.

IV. A. VIBRATIONALLY RELAXED SPECTRA

1. Data Summary

Table II lists the fluorescence bands observed in atmospheric pressure formaldehyde vapor which had been excited by a pulsed nitrogen laser. With the exception of a few bands with wavelengths shorter than 4000Å, which originated from the 2^1 state, all the bands detected at this pressure originate from the 4^1 or 4^0 excited states. Little trace of the fluorescence from the state originally excited by the laser can be found in these spectra.

The spectra measurements are of three different types. The first type is composed of photographic plates for wavelengths between 3370 and 4800Å, having a resolution of about 0.1Å. Photoelectric spectra with a resolution of 2.5Å were taken for a number of bands between 4500 and 5600Å. Some of these overlap the photographic coverage so that the precision of the two methods can be compared. Photoelectric spectra with a 5Å bandwidth were taken for all bands out to 6400Å. There were weaker bands beyond this wavelength, but these could not be investigated with the available equipment.

To help visualize the data presented in Table II, figures (15), (16), and (17) illustrate the entire high pressure spectrum observed. Figure (15) is a direct (reduced)

TABLE II: BANDS EXCITED BY THE NITROGEN LASER IN ATMOSPHERIC PRESSURE FORMALDEHYDE VAPOR.

Photoelectric Intensity	Designation	λ (Å) (band center)	σ (cm^{-1}) (Photographic)	σ (cm^{-1}) Photoelectric	Previous Measurements[a] or Predictions[b]
0.8	$2_0^1\ 4_1^0$	3544	(†)		28207 (28210)
5.5	4_1^0	3697.7	27036		27036 (27036)
1.8	$2_1^0\ 4_0^1$	3762	(†)		26569*
	$2_1^1\ 4_1^0$	3776	(†)		26470 (26471)
4.0	4_2^1	3846.5	25990		25991
5.1	$2_0^1\ 4_3^0$	3860	25896		25895
7.3	$2_1^0\ 4_1^0$	3951.8	25298		25297 (25297)
5.6	4_3^0	4044.1	24720		24721 (24722)
7.2	$2_1^0\ 4_2^1$	4120.7	24261		24259 (24260)
6.2	4_4^1	4220.0	23690		23687
6.6	$2_2^0\ 4_1^0$	4239.6	23581		23579 (23580)
6.0	$2_1^0\ 4_3^0$	4347.5	22996		22997 (22999)
5.0	$2_2^0\ 4_2^1$	4434.0	22547		22547
4.0	4_5^0	(4457.8)	(22426)		[22424]

TABLE II: continued

Photoelectric Intensity	Designation	λ (Å) (band center)	σ (cm^{-1}) (Photographic)	σ (cm^{-1}) Photoelectric	Previous Measurements[a] or Predictions[b]
4.9	$2_1^0\ 4_4^1$	4550.6	21969	21969	21971
	$2_3^0\ 4_1^0$	4569.6	21877	21876	21880
2.6	$2_2^0\ 4_3^0$	4696.2	21289	21290	21294
2.1	$2_3^0\ 4_2^1$	4794.6	20851	20849	[20859]
2.1	$2_1^0\ 4_5^0$	4825.9	20715	20709	20712
2.0	$2_2^0\ 4_4^1$	4931		20274	20271
	$2_4^0\ 4_1^0$	4949.0		20200	[20203]
	4_7^0	4962		20148	[20147]
1.3	$2_1^0\ 4_6^1$	5075		19699	[19697]
1.6	$2_3^0\ 4_3^0$	5099.5		19605	19613 [19604]
0.9	$2_4^0\ 4_2^1$	5209		19192	[19192]
0.8	$2_2^0\ 4_5^0$	5255		19024	[19020]
0.5	$2_3^0\ 4_4^1$	5378		18589	[18594]

TABLE II: continued

Photoelectric Intensity	Designation	λ (Å) (band center)	σ (cm^{-1}) (Photographic)	σ (cm^{-1}) Photoelectric	Previous Measurements[a] or Predictions[b]
0.5	$2_5^0\ 4_1^0$	5390		18548	[18547]
0.5	$2_1^0\ 4_7^0$	5421		18441	[18448]
0.3	$2_2^0\ 4_6^1$	5554		18000	[18012]
0.3	$2_4^0\ 4_3^0$	5571		17947	[17942]
0.1	4_9^0	5590		17884	[17889]
0.2	$(2_5^0\ 4_2^1)$	5708±8		17515±20	[17540]
0.2	$(2_1^0\ 4_8^1)$	5737±8		17425±20	[17442]
0.2	$(2_3^0\ 4_5^0)$	5758±8		17360±20	[17349]
0.2	$(2_4^0\ 4_4^1)$	5897±8		16955±20	[16937]
0.1	(4_{10}^1)	5985±8		16704±20	[16886]
0.1	$(2_3^0\ 4_6^1)$	6105±8		16375±20	[16347]

TABLE II: continued

* Misprint in Brand; his table reads 27569.

† Too weak for accurate measurement.

[a] Values from Brand[17,18]; those in parentheses () from high resolution work of Robinson[19].

[b] Wave numbers in brackets [] are calculated from Brand's[18] anharmonic constants. They have not been measured elsewhere.

copy of densitometer tracings of two plates and shows the range of photographic coverage (3371 to 4800Å). Figure (16) is a 10Å bandwidth photoelectric scan of the spectrum of 560 torr formaldehyde vapor, and covers the range of 3371 to 6000Å. Notice that while the K sub-bands are not evident in figure (16) it is usually possible even with this resolution to tell which bands are overlapped by others. Figure (17) illustrates the high pressure photoelectrically detected spectrum (5Å bandwidth) between 5000 and 6400Å.

All bands below 4700Å have been studied previously by Brand[18] or Robinson[33], but with two exceptions, those with wavelengths longer than that have not been identified before. Brand[18] mentioned the existence of bands beyond 5000Å but he could not unambiguously identify them due to the weakness of the images on his plates and the fact that each band was overlapped by one or two others.

The observations Brand made on the bands out to a wavelength of 4700Å enabled him to calculate the anharmonic constants ω_{22}, ω_{44}, and ω_{24}. Using these, it is possible to calculate a predicted wave number for any transition involving ground state harmonics of ν_2'' or ν_4''. These predictions were invaluable in the process of identifying the bands beyond 4800Å. They yielded the measured wavelengths to within the

FIGURE (15): Photographic Spectrum of High Pressure Formaldehyde 3370Å to 4750Å. This is a direct copy, produced by a reducing xerox machine, of the densitometer tracing.

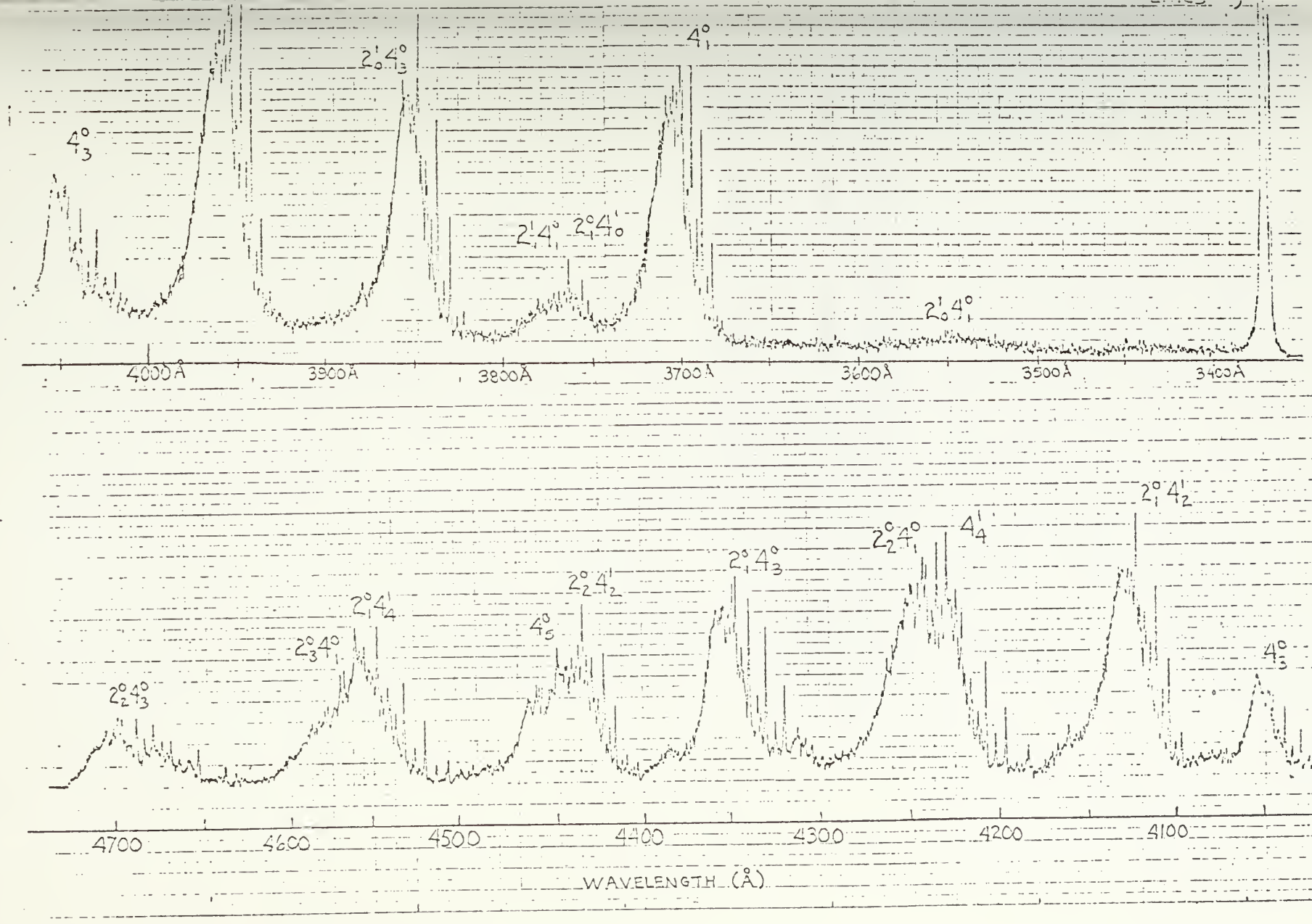
4^0_3
$2^1_0 4^0_3$
4^0
$2^1 4^0$ $2^0 4^1_0$
$2^1_0 4^0_1$
4000Å
3900Å
3800Å
3700Å
3600Å
3500Å
3400Å
$2^0_2 4^0_3$
$2^0_3 4^0_1$
$2^0 4^1_4$
4^0_5
$2^0_2 4^1_2$
$2^0_1 4^0_3$
$2^0_2 4^0_1$
4^1_4
$2^0_1 4^1_2$
4^0_3
4700
4600
4500
4400
4300
4200
4100
WAVELENGTH (Å)

FIGURE (16): 10Å Bandwidth Photoelectric Spectrum of High Pressure Formaldehyde 3371Å to 6000Å. This is a copy of the original scan, (curve darkened by hand). The formaldehyde pressure was 558 torr.

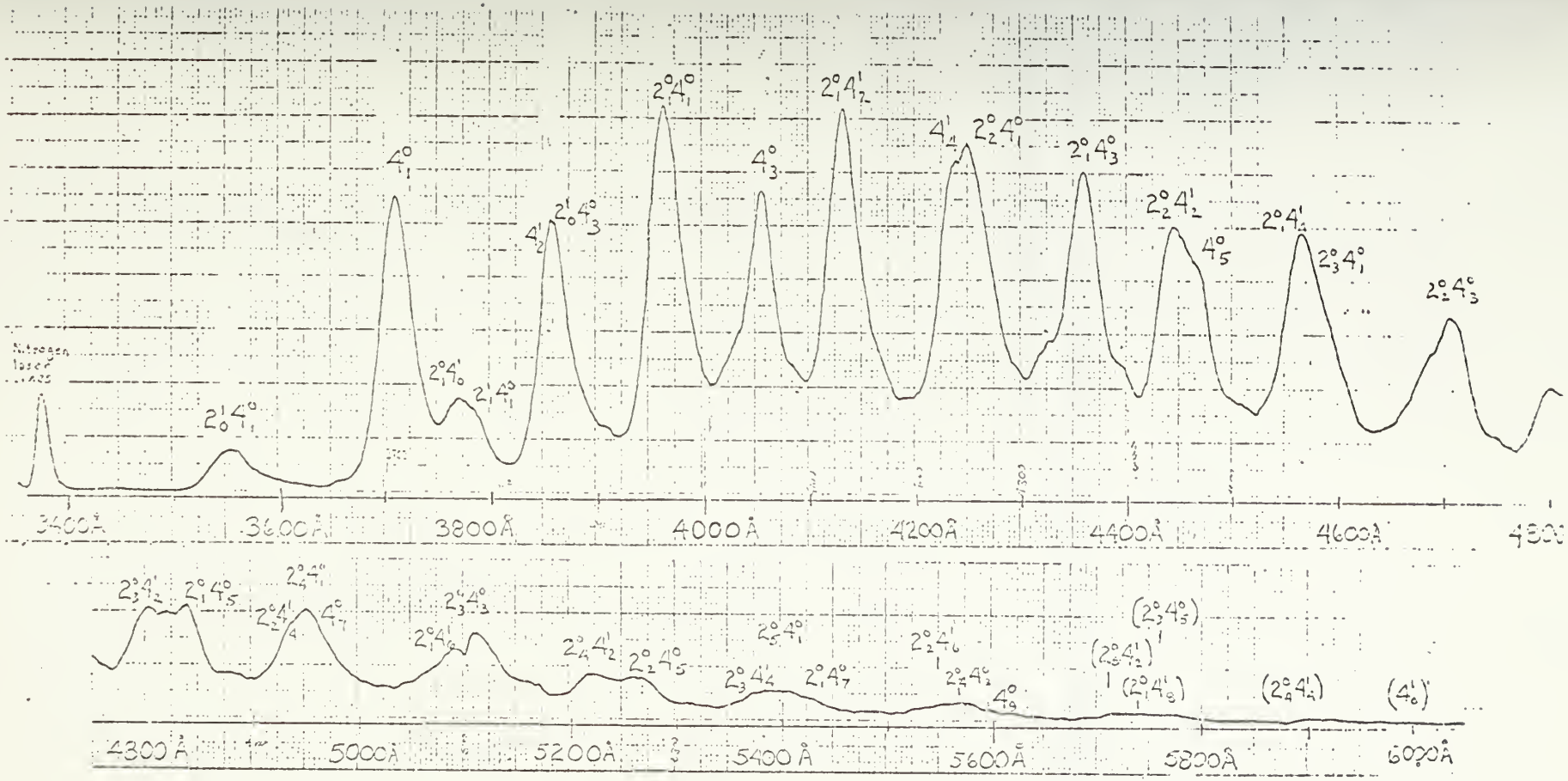
Nitrogen
3400Å
3600Å
3800Å
4000Å
4200Å
4400Å
4600Å
4300Å
5000Å
5200Å
5400Å
5600Å
5800Å
6000Å

FIGURE (17): 2.5Å Bandwidth Spectrum of High Pressure Formaldehyde; 5000Å to 6400Å.

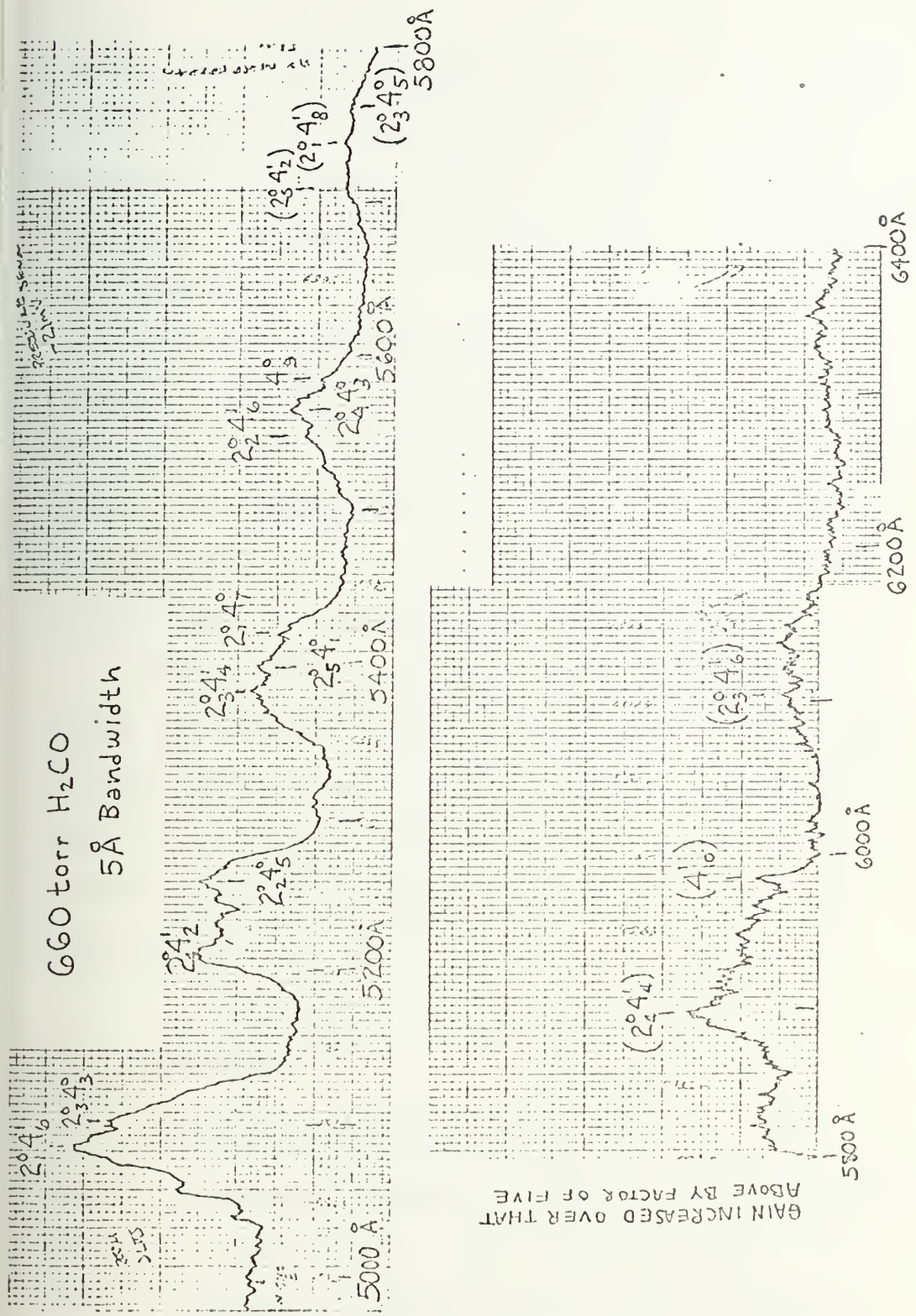
660 torr H_2CO
5Å Bandwidth
5000 Å
5200Å
5400Å
5600 Å
5800Å
$2^0 4_6$
$2^0 3_3$
$2^0 4_3$
$2^0 4_2$
$2^0 2_2$
$2^0 4_5$
$2^0 3_4$
$2^0 4^1$
$2^0 2_1 6$
$2^0 5^4$
$2^0 4_3$
$(2^0 4_2)$
$(2^0 4_1)$
$(2^0 4_5)$
GAIN INCREASED OVER THAT ABOVE BY FACTOR OF FIVE
5500 Å
6000Å
6200Å
6400Å
$(2^0 4_4)$
(4^1_0)
$(2^0 4_6)$

±0.5Å accuracy of the photoelectric measurements for all bands out to 5600Å. Beyond that wavelength, my band centers are estimates with an accuracy no better than ±8Å. The predictions using Brand's anharmonic constants are also compatable with those measurements.

The wave numbers listed in Table II are quoted only to the nearest cm^{-1}, even though in the case of the photographic measurements they have a greater precision, because K sub-band heads cannot be defined to better accuracy. As was mentioned in the background chapter, this is due to the missing rotational lines and the breakdown of the symmetric top model.

Figures (15) and (16) show hints of other bands in between the strong, previously identified ones. The suggestion of other bands is clearest at 4310 and 4390Å. (See also figure (9).) In the section on low pressure spectra these are shown to be bands originating from the $4^2 6^1$ and the $4^1 6^1$ excited states.

2. Discussion

The paucity of evidence for bands originating from the state excited by the laser to be found in the high pressure spectrum is not unreasonable. The collision time at atmospheric pressure is about 0.2 nanoseconds, one hundred

times shorter than the unperturbed lifetime of the $4^2 6^1$ state and thus vibrational equilibrium is achieved before most of the molecules radiate or dissociate. The equilibrium Boltzman ratio between the population of the $4^2 6^1$ and the 4^0 or 4^1 states should be about one to three hundred. In addition, since the unperturbed predissociation lifetime for the lower-lying excited states is an order of magnitude longer than that of the laser-excited states, more of the lower states will radiate instead of dissociating.

The agreement between my measurements and the predictions made with the anharmonic constants of Brand shows that the ground state molecular potential function for ν_2'' and ν_4'' can be adequately represented up to 10,000 cm^{-1} of vibrational energy by an harmonic well using only quadratic correction to level spacings. The shape of the potential is important for determining the nature of the predissociation mechanism. It is certainly possible to extend the measurements reported here to longer wavelengths; the band structure clearly extends to at least 6700Å and photon counting techniques could be used to investigate it.

In the case of the vibrationally relaxed emission, since it is the use of photoelectric detection, not the use of a different excitation mechanism, that is the major difference between my long wavelength measurements and Brand's shorter

wavelength observations, it may be possible that a continuous electric-discharge excitation might be used for such experiments instead of the pulsed laser excitation. Use of the laser does have the advantage that the 3371Å light is not energetic enough to produce the dissociation product CO in an excited electronic state and therefore the spectrum observed from the laser-excited formaldehyde does not have masking CO bands. Continuous excitation, however, would probably produce more time-averaged fluorescence.

3. Miscellaneous

It is worth noting the reason why photoelectric measurements are capable of extending the band structure further to the red than photographic methods. In the first place, modern photo-cathodes are more sensitive detectors of light than photographic emulsions. Furthermore, there is a minimum intensity of light below which a plate will not respond to light no matter how long an exposure is made. This is called reciprocity failure. An additional non-linearity in the photographic process is intermittency. When the same amount of energy is incident on similar photographic plates the image density is less when the energy comes as pulses than if it is continuous. The extremely short fluorescence pulses aggravate this effect. Finally, the sensitivity of photographic

plates falls off rapidly above about 4800Å.

Photoelectric detection has another advantage over photographic methods when attempting to detect low light levels. For a given instrumental dispersion, the density of an emission image on a photographic plate is independent of the entrance slit width; the wider the slit the wider the image, but the image density remains constant. The resolution is therefore independent of the light intensity if any light can be detected at all. With photoelectric detection, on the other hand, one can trade off resolution for signal strength. The photocathode responds to all light falling upon it, and the wider the slit, the more light is detected. Since it is the progression of the K sub-bands that confirms the band center predictions, a spectrometer bandwidth only sufficient to resolve this structure may be used for band identification.

The major analysis problem was the overlapping of bands. Figure (18) and (19) show examples of photographic and photoelectric spectra of two overlapping bands. The overlaps are caused by the fact that $3\nu_4''$ equals $2\nu_2''$ within five cm^{-1}. It would not be possible to separate the overlapping bands at all if it were not for the selection rules which require, for transitions involving only ν_4'' and ν_2'', that $4^1 \not\vdash 4_{odd}$ and $4^0 \not\vdash 4_{even}$ (selection rules place no restriction

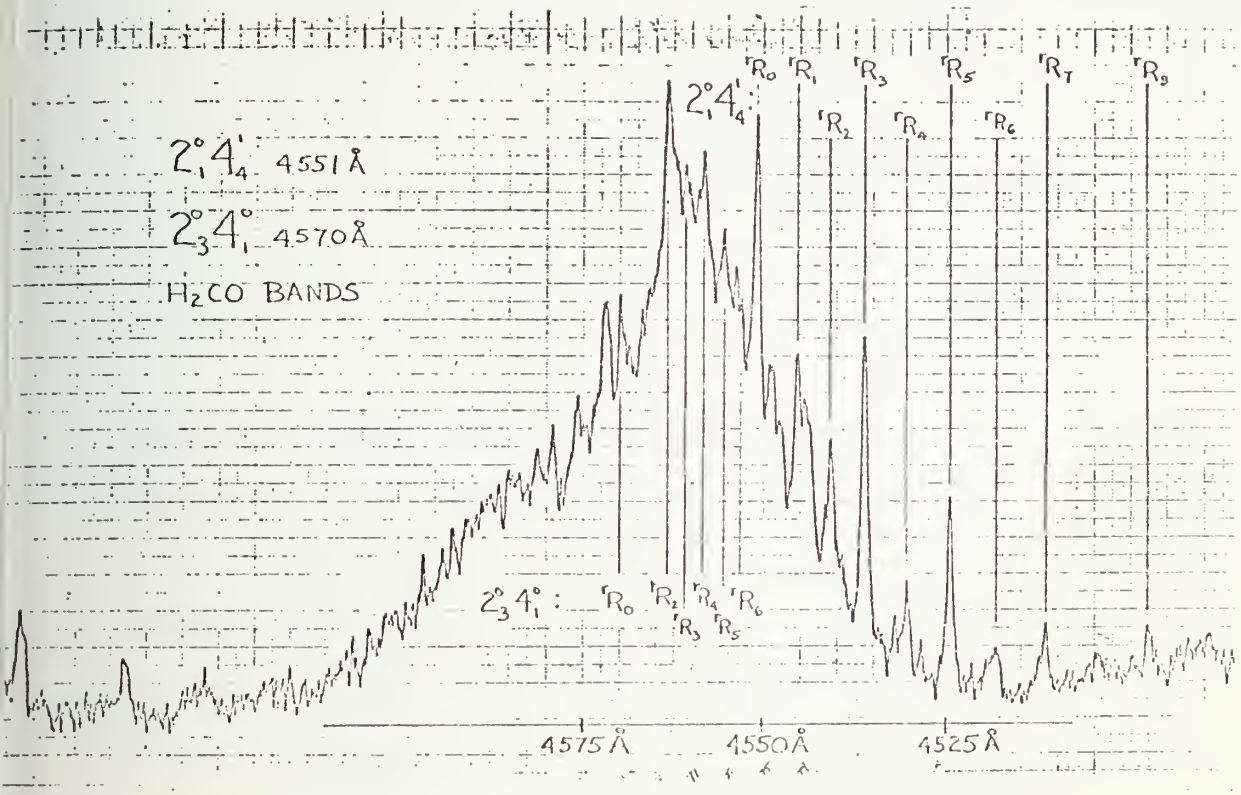

FIGURE (18): Photographic Spectrum of 4551 and 4570Å Bands.

FIGURE (19): Photoelectric Spectrum of 4551Å and 4570Å Bands. The smooth structure to the far left is part of the thorium ramp calibration spectrum. It shows the approximate bandwidth of the measurements. Note that the sense of wavelength increase is reversed from that of Figure (18).

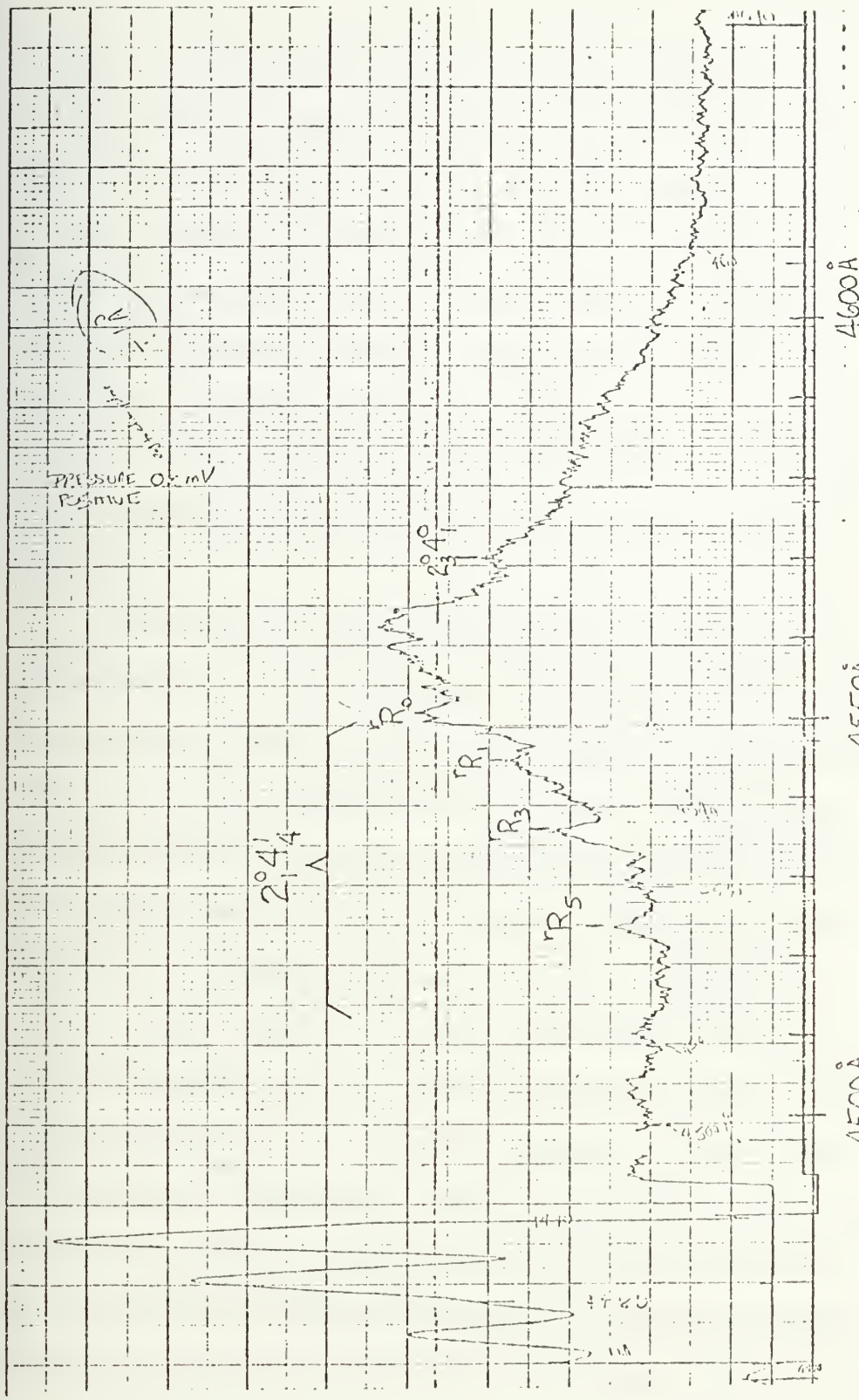
PRESSURE 0.1 mV
REMOVE
2°44'
R0
R1
R3
R5
23°4'
4600Å
4550Å
4500Å

on v_2''). For example, a $2_2^0 4_4^1$ transition is allowed, but a $2_4^0 4_1^1$ transition (which, neglecting anharmonic terms, would have the same wavelength) is not. The $2_4^0 4_1^0$ transition is allowed, however, and since there is only a difference of 124 cm^{-1} between the 4^1 and 4^0 excited states, the $2_2^0 4_4^1$ and the $2_4^0 4_1^0$ transitions overlap. These bands are overlapped by the 4_7^0 band as well, the three band centers all lying within 126 cm^{-1} of each other. The $2_4^0 4_1^0$ and 4_7^0 bands are separated by more than 10 cm^{-1} due to the anharmonic nature of the potential.

There are two types of evidence which make it possible to identify the overlapping bands. The first is the predictions of the anharmonic model. The constants Brand quotes are labeled with the old mode designations and they yield the transition wavelengths when the excited state wave numbers which he quotes in his 1956 paper[18] are used. The presently accepted values are slightly different from those. It is not worthwhile to recalculate ω_{22}, ω_{44}, and ω_{24} since these factors are used in an empirical formula designed only to fit the observed transition wavelengths and which does not make a direct statement about the potential-well parameters. Recalculation would merely show that another quadratic model can be constructed reproducing the transition wave numbers with slightly different empirical parameters. It would provide no new information. The

important point is that a quadratic model is sufficient to predict transition wavelengths accurately out to at least the 4^1_{10} band.

The other evidence which was used to identify overlapping bands was the regular progression of K sub-bands. The spacing and intensity alternation were both useful in the identification process. Recall from the background chapter that sub-bands with K'' even are strong for 4^0_n bands and weak for 4^1_n bands. If some K structure could not be observed, the band centers listed in Table II have been placed in parentheses to indicate that they are supported only by the predicted wavelengths.

A listing of the sub-band spacing that supports the identifications made in Table II is given in Table III. The listed K spacing should be viewed as accurate for the photographic spectra, but only as a support for the band assignment in the case of the photoelectric spectra. For bands whose K structure had been previously measured, I have included those measurements in Table III for reference. Brand[16] indicated that he had measured the K structure of bands other than those which he published, although it appears that they were ultraviolet bands. My measurements of K structure for bands with wavelengths longer than 4650Å are, to my knowledge, the first to have been made.

Copies of several representative spectra are shown in figures (20) through (22). All wave numbers are vacuum wave numbers converted from the measured wavelengths using Edlén's formula[53].

Photographic spectra of the bands out to about 5200Å might be obtained if a solution to the window sludge problem could be found. A baked 127-04 plate showed faint band images at these wavelengths after a twenty-four hour exposure, and there is little doubt that a usable plate could be obtained if the initial fluorescence strength could be maintained over a 24 hour period. In addition, more powerful nitrogen lasers exist, and if the window problem could be solved, they could provide more intense fluorescence. (My photoelectric measurements indicate that the fluorescence strength is still proportional to the laser power up to 150 KW, the maximum laser output used.)

FIGURE (20): Photographic Spectra: 4434Å, 4458Å and 4696Å Bands.

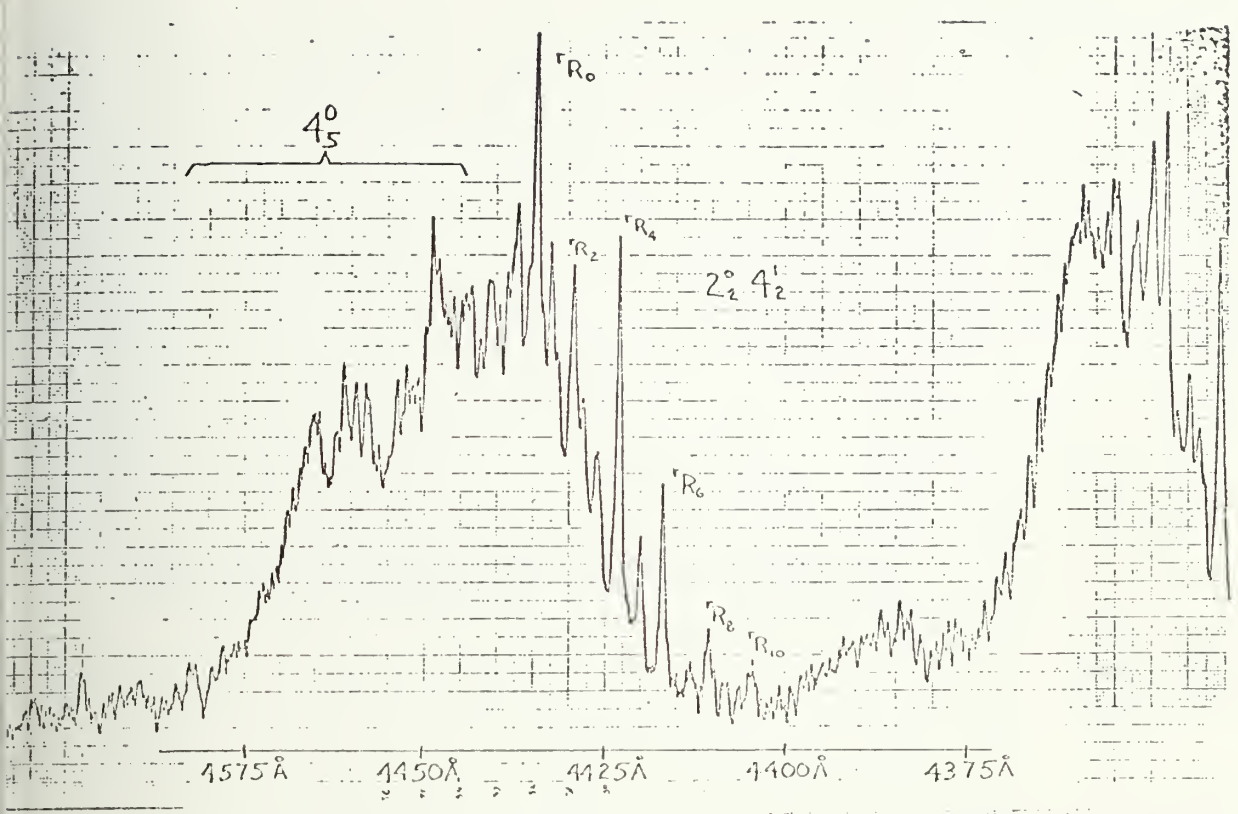
4_5^0
$^rR_0$
$^rR_2$
$^rR_4$
$2_2^0 4_2^1$
$^rR_6$
$^rR_8$
$^rR_{10}$
4575 Å
4450 Å
4425 Å
4400 Å
4375 Å

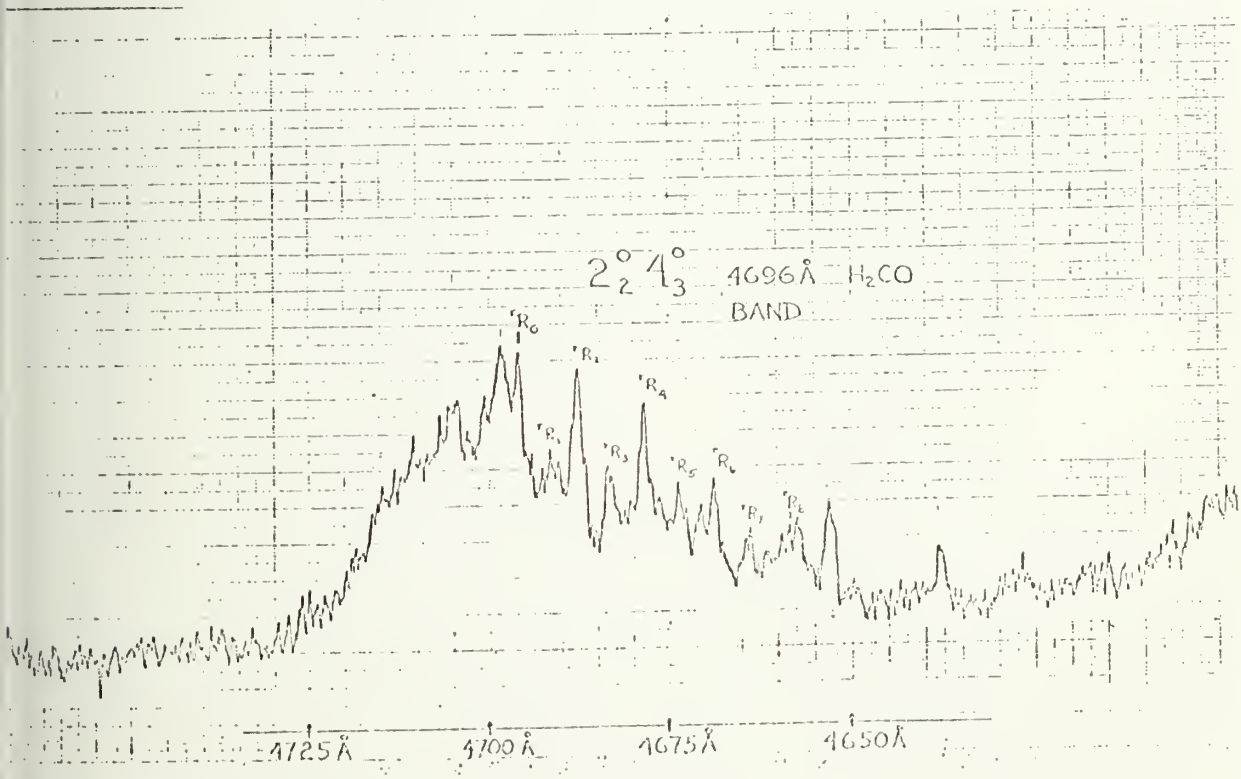
$2_2^0 4_3^0$ 4696 Å H_2CO
BAND
$^rR_0$
$^rR_1$
$^rR_2$
$^rR_3$
$^rR_4$
$^rR_5$
$^rR_6$
$^rR_7$
$^rR_8$
4725 Å
4700 Å
4675 Å
4650 Å

FIGURE (21): Photoelectric Spectrum: 4696Å Band.

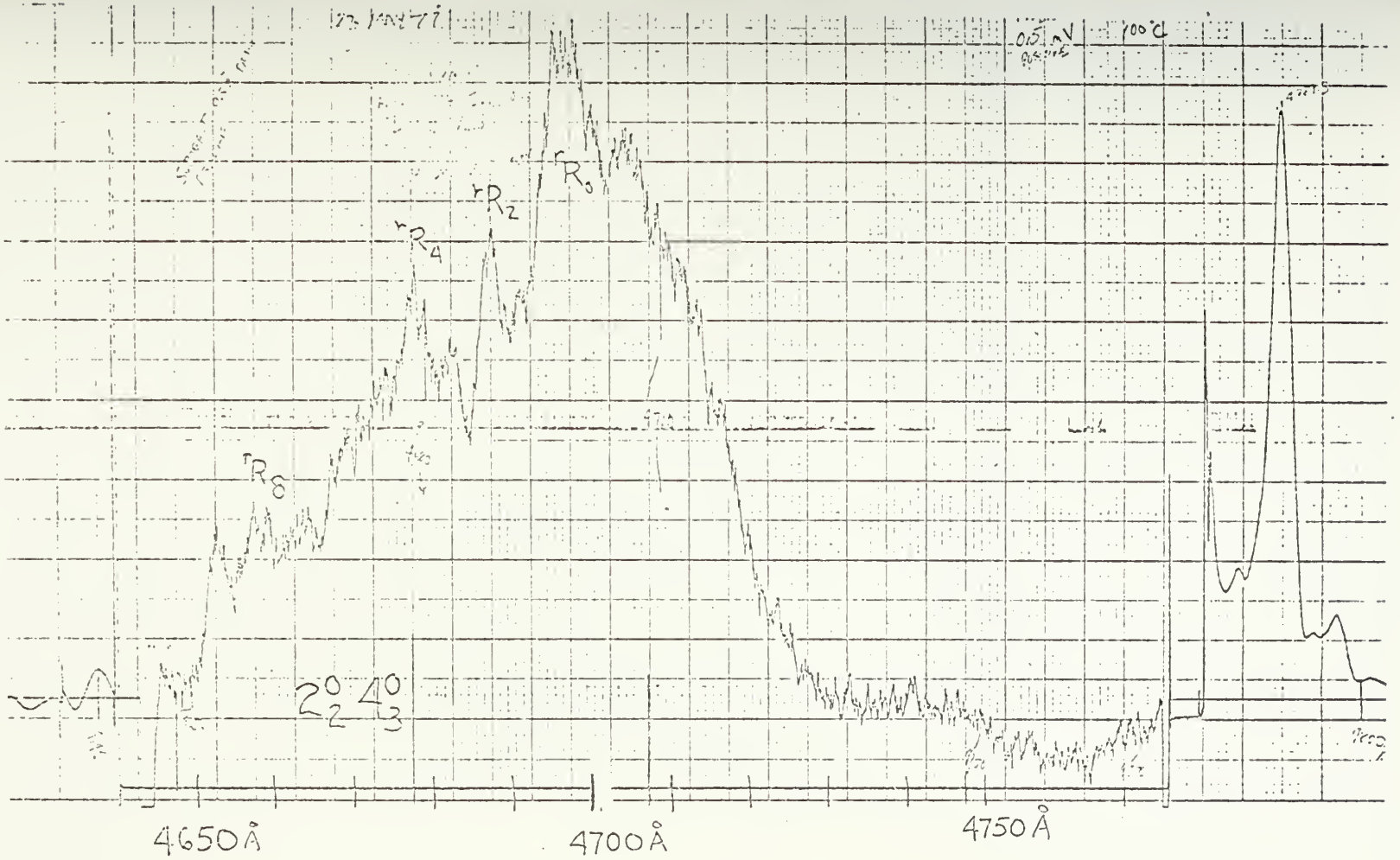
$^rR_6$
$^rR_4$
$^rR_2$
$^rR_0$
$2_2^0 4_3^0$
4650Å
4700Å
4750Å

FIGURE (22): Photoelectric Spectrum: 5500Å to 5600Å.

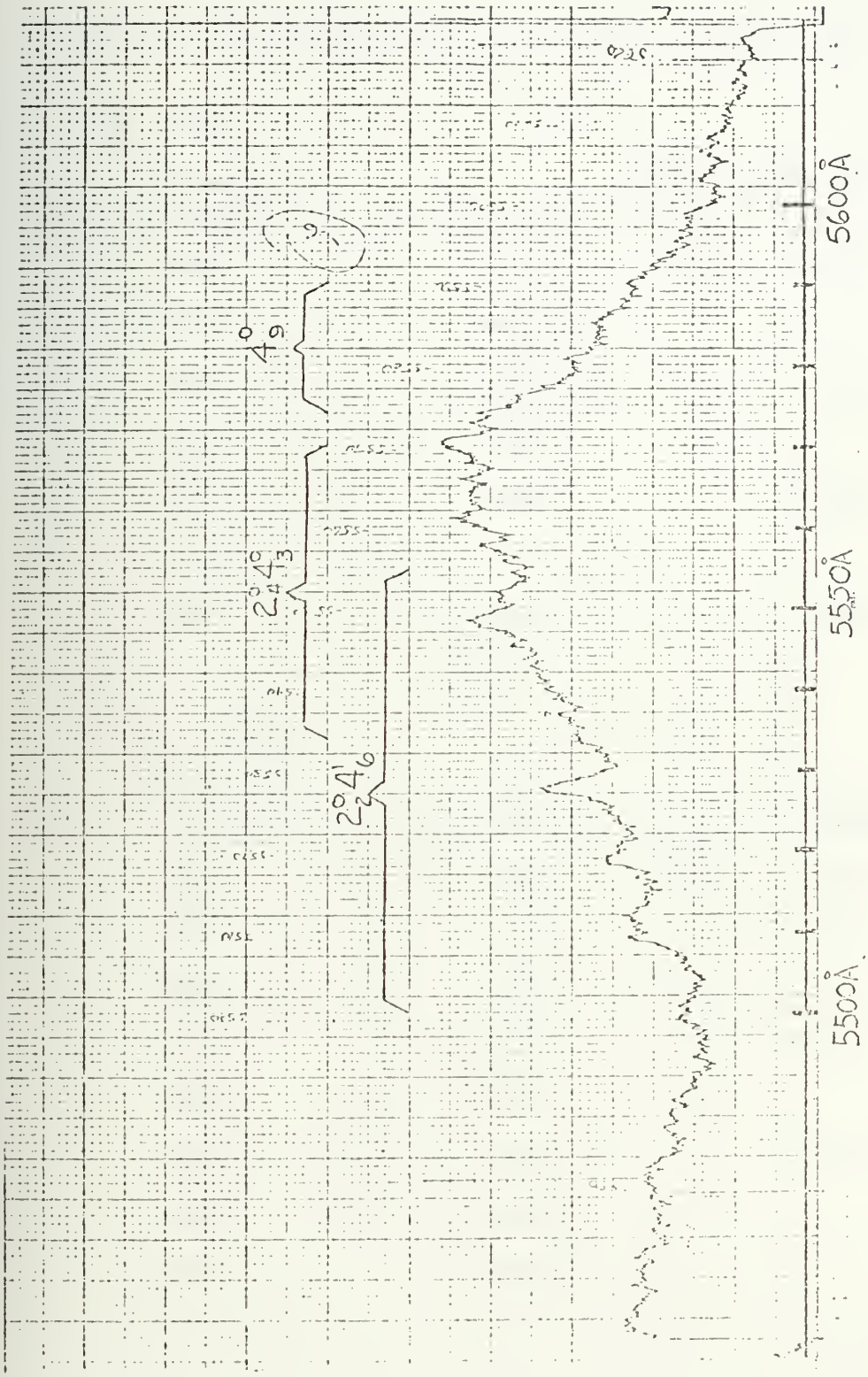
5600Å
5550Å
5500Å
2°49'
2°48'
2°46'

TABLE III: K STRUCTURE OF VIBRATIONALLY RELAXED BANDS

4_3^0 4044Å

K''	Photographic σ (cm^{-1})	Δ	λ (Air)Å	Previous Measurements: Brand	Robinson
0	24720	20	4044.1	24721	24722
1	24740	22	4040.9		
2	24762	26	4037.3		24764
3	24788	29	4033.1		
4	24817		4028.4		24818
---	---	67	---		
6	24884		4017.5		24883

$2_1^0 4_2^1$ 4121Å

K''	Photographic σ (cm^{-1})	Δ	λ (Air)Å	Brand	Robinson
0	24261	26	4120.7	24259	24260
1	24287	20	4116.2		24284
2	24307	19	4112.9		
3	24326	19	4109.8		24325
4	24345	22	4106.5		
5	24367	19	4102.7		24366
6	24386	21	4099.0		
7	24407		4096.0		

TABLE III: continued

4_4^1 4220Å

K''	Photographic σ (cm^{-1})	Δ	λ (Air)Å	Previous Measurements Brand
0	23690	26	4220.1	23687
1	23716	49	4215.4	
3	23765	28	4206.6	
4	23793	35	4201.7	
5	23828	73	4195.5	
7	23901		4182.7	

$2_2^0\,4_1^0$ 4240Å

K''	Photographic σ (cm^{-1})	Δ	λ (Air)Å	Brand	Robinson
0	23581	34	4239.6	23579	23580
2	23615	29	4233.3	23612	23613
4	23644	29	4228.2	23642	23643
6	23673		4223.1	23670	23671

TABLE III: continued

$2_1^0\ 4_3^0$ 4347Å

K''	Photographic σ (cm^{-1})	Δ	λ (Air)Å	Previous Measurements Brand	Robinson
0	23000	16	4346.6	22997	22999
1	23016	22	4343.6		
2	23038	24	4339.3		23038
3	23062	25	4335.0		
4	23087	27	4330.2		23087
5	23114	29	4325.1		
6	23143		4319.8		23142

$2_2^0\ 4_2^1$ 4434Å

K''	Photographic σ (cm^{-1})	Δ	λ (Air)Å	Brand
0	22547	25	4434.0	22547
2	22572	33	4429.0	
4	22605	31	4422.6	
6	22636	32	4416.6	
8	22668	32	4010.2	
10	22700		4404.0	

TABLE III: continued

$2_1^0 4_4^1$ 4551Å

K''	Photographic σ (cm^{-1})	Δ	λ (Air)Å	Photoelectric σ	Previous Measurements Brand
0	21969	27	4550.6	21969	20271
1	21996	21	4545.0	21997	
2	22017	23	4540.7		
3	22040	28	4535.9	22041	
4	22068	29	4530.2	22070	
5	22097	30	4524.3	22099	
6	22127	33	4518.1		
7	22160	35	4511.3		
8	22195	34	4504.2		
9	22229		4497.4		

$2_3^0 4_1^0$ 4570Å

K''	Photographic σ (cm^{-1})	Δ	λ (Air)Å	Photoelectric	Brand
0	21877	32	4569.6	21876	21881
2	21909	12	4563.1		21912
3	21921	12	4560.5		21923
4	21933	14	4558.0		21934
5	21947	12	4555.23		--
6	21959		4552.7		21959

TABLE III: continued

$2_2^0 4_3^0$ 4696Å

K''	Photographic σ (cm^{-1})	Δ	λ (Air)Å	Photoelectric	Brand
0	21289	21	4696.2	21290	21294
1	21310	17	4691.4		
2	21327	19	4687.6		
3	21346	24	4683.5		
4	21370	21	4678.2		
5	21391	23	4673.5	21394	
6	21414	23	4686.6	21413	
7	21437	25	4663.5		
8	21462		4658.2	21464	

$2_2^0 4_4^1$ 4931.5Å

K''	Photoelectric σ (cm^{-1})	Δ	λ (Air)Å	Brand
0	20274	23	4931	20271
1	20297	16	4926	
2	20313	21	4922	
3	20334	22	4916	
4	20356	26	4911	
5	20382		4905	

TABLE III: continued

$2_1^0 4_6^1$ 5075Å

K''	Photoelectric σ (cm^{-1})	Δ	λ (Air)Å	
0	19699		5075	
1		54		Note: This band is strongly mixed with lines of the $2_3^0 4_3^0$ 5099Å band. More resolution is needed to unambiguously separate them.
2	(19753)	25	5061	
3	19778	30	5055	
4	19808	40	5047	
5	19848		5037	

$2_3^0 4_3^0$ 5100Å

K''	Photoelectric σ (cm^{-1})	Δ	λ (Air)Å	Brand†
0	19604	39	5099	19613
2	19643	42	5089	
4	19685	47	5079	
6	19732		5066	

†Value quoted in Brand's 1951 paper[17] but not mentioned in his summary of all bands in his 1956 paper[18]. Using the values of the anharmonic constants given in the latter article the predicted band center is calculated to be at 19605 cm^{-1}.

TABLE III: continued

$2_4^0\ 4_2^1$ 5209 Å

K''	Photoelectric σ (cm^{-1})	Δ	λ(Air) Å
0	19192	24	5209
2	19216	13	5203
3	19229	26	5199
5	19255	24	5192
7	19279	25	5186
9	19304	25	5179
11	19329	34	5172
(13)	(19363)		5163

$2_2^0\ 4_5^0$ 5255 Å

K''	Photoelectric σ (cm^{-1})	Δ	λ(Air) Å
0	19024	17	5255
1	19041	21	5250
2	19062	18	5245
3	19080	19	5240
4	19098	19	5235
5	19117		5229

TABLE III: continued

$2_3^0 4_4^1$ 5378Å

K''	Photoelectric σ (cm^{-1})	Δ	λ (Air)Å
0	18587		5378
		17	
1	18604		5374
		39	
3	18643		5362
		40	
5	18683		5351

$2_2^0 4_6^1$ 5552Å

K''	Photoelectric σ (cm^{-1})	Δ	λ (Air)Å
0	18000		5554
		57	
1	--		
		30	
2	18057		5536
		29	
3	18087		5527
		30	
4	18116		5518
		32	
5	18146		5509
6	18178		5500

TABLE III: continued

$2_4^0\ 4_3^0$ 5571Å

K''	Photoelectric σ (cm^{-1})	Δ	λ (Air)Å
0	17947	31	5570
1	17978	30	5561
2	18008	57	
4	18065		5434

4_9^0 5590

K''	Photoelectric σ (cm^{-1})	Δ	λ (Air)Å
0	17884	16	5590
1	17900	15	5585
2	17915	19	5580
(3)	17934		5574

IV. B. LOW PRESSURE SPECTRUM

1. Data Summary

In the course of making preliminary lifetime measurements at a formaldehyde pressure of 40 torr, it was found that relatively strong fluorescence with a lifetime less than 20ns appeared at wavelengths where no known bands existed. In order to investigate this fluorescence a series of spectral scans were made at low H_2CO pressure. A completely new band structure appeared in these scans. Figure (23) illustrates the difference between the high and low pressure spectra. None of the low pressure bands have previously been seen.

Because of the obvious importance of collisional energy transfer in producing these spectra, the effects on the H_2CO fluorescence caused by variable partial pressures of nitrogen buffer gas were also measured. All measurements presented in this section were made using the PAR model 163 sampled integrator plug-in with the PAR 162 boxcar. The observation was made for each pulse about 10 nanoseconds after the peak of the nitrogen laser pulse.

Table IV lists the low pressure band wavelengths and their designations. The bands were identified by the coincidence of the measured wavelengths with calculated transition wavelengths. Consideration was given, when making these identifications, to all the excited state vibrational levels shown

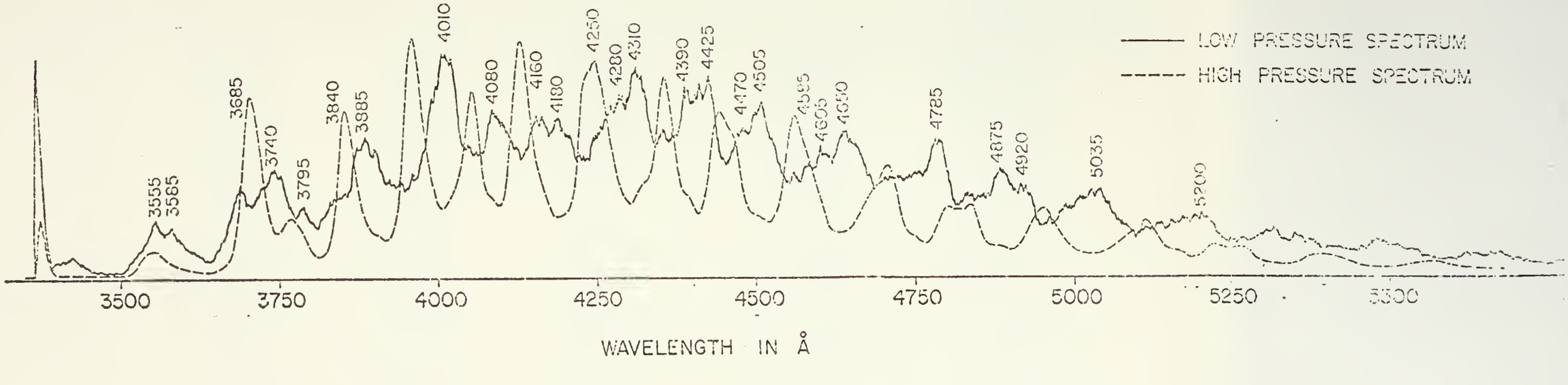

FIGURE (23): High and Low Pressure Spectra

TABLE IV: LOW PRESSURE BANDS

Nitrogen Laser Excited Fluorescence Seen at Pressures Below 40 torr

λ (Air) ± 3Å	Relative Intensity at 40 torr	Identification	Assumed Transition type; polarization[b]	σ [a] calculated (cm^{-1} vacuum)	σ measured (cm^{-1} vacuum)	Pressure Dependence of Band: Change of $(\frac{I_{band}}{I_{4010Å}})$ with increasing pressure
3555	2.0	$3_1^0\ 4_0^2\ 6_0^1$	$A_1 \leftarrow B_1$; C	28133	28120±25	no change
3583	2.0	$2_1^0\ 4_0^2\ 6_0^1$	$A_1 \leftarrow B_1$; C	27888	27900±24	no change
3685	3.0	$(4_0^2\ 6_2^1)$	$(A_1 \leftarrow B_1$; C)	(27132)	27130±22	increase
3740	3.5	$4_0^1\ 6_2^1$	$A_1 \leftarrow A_1$; A	26715	26730±21	increase
3795	2.0	$2_1^0\ 4_1^1\ 6_0^1$	$B_1 \leftarrow A_1$; C	26325	26345±21	increase
3840	2.0	$3_0^1\ 4_2^2\ 6_1^0$	$B_2 \leftarrow A_2$; C	26044	26034±21	increase
3885	4.5	$4_3^1\ 6_0^1$	$B_1 \leftarrow A_1$; C	25750	25733±20	increase
4010	7.0	$4_3^2\ 6_1^1$	$A_2 \leftarrow B_1$; B	24916	24930±20	reference band
4080	5.0	$2_2^0\ 4_0^1\ 6_1^1$	$B_2 \leftarrow A_1$; C	24494	24505±18	increase
4160	5.0	$(2_1^0\ 4_3^1\ 6_0^1)$	$(B_1 \leftarrow A_1$; C)	24028	24030±18	no change
4180	5.0	$2_1^0\ 4_2^1\ 6_1^1$	$B_2 \leftarrow A_1$; B	23911	23920±17	increase

continued

4250	3.0	$2_2^0\ 3_1^0\ 4_1^2\ 6_0^1$	$B_1 \leftarrow B_1$; A	23524	23525±17	no change
4280	5.5	$4_4^1\ 6_1^1$	$B_2 \leftarrow A_1$; B	23340	23360±17	increase
4310	6.5	$2_1^0\ 4_3^2\ 6_1^1$	$A_2 \leftarrow B_1$; B	23194	23195±17	no change
4390	5.0	$2_3^0\ 4_0^1\ 6_1^1$	$B_2 \leftarrow A_1$; B	22789	22775±16	increase
4425	6.0	$4_5^2\ 6_1^1$	$A_2 \leftarrow B_1$; B	22611	22590±16	no change
4470	4.5	$2_2^0\ 3_1^0\ 4_2^2\ 6_0^1$	$A_1 \leftarrow B_1$; C	22367	22365±16	no change
4505	5.5	$2_2^0\ 4_2^1\ 6_1^1$	$B_2 \leftarrow A_1$; B	22200	22190±15	increase
4585	3.5	$2_1^0\ 3_1^0\ 4_4^2\ 6_0^1$	$A_1 \leftarrow B_1$; C	21791	21805±15	no change
4605	4.0	$2_1^0\ 3_1^0\ 4_3^2\ 6_1^1$	$A_2 \leftarrow B_1$; B	21693	21710±14	no change
4650	4.5	$2_2^0\ 4_3^2\ 6_1^1$	$A_2 \leftarrow B_1$; B	21489	21500±14	no change
4785	4.0	$2_1^0\ 4_5^2\ 6_1^1$	$A_2 \leftarrow B_1$; B	20899	20900±13	no change
4875	3.5	$(2_3^0\ 4_2^1\ 6_1^1)$	$(B_2 \leftarrow A_1$; B)	(20510)	20510±13	no change
4920	3.0	$4_7^2\ 6_1^1$	$A_2 \leftarrow B_1$; B	20334	20320±12	no change
5035±10Å	2.5	$(2_2^0\ 3_1^0\ 4_2^2\ 6_2^1)$	$(A_1 \leftarrow B_1)$; C	(19865)	19860±40	no change

continued

5200±10Å	2.0	$(2_2^0\ 4_5^2\ 6_1^1)$	$(A_2 \leftarrow B_1;\ B)$	(19207)	19230±40	no change

Entrys in parentheses do not agree with the qualitative pressure dependence data, except for the last two where the difficulty in assigning a band center, due to the low fluorescence intensity, makes any vibrational assignment somewhat speculative.

a) Values calculated from Brand's[18] measurements of the ν_2'' and ν_4'' progressions, extensions to higher overtones using his anharmonic parameters, and the values of ν_3'' and ν_6'' from Moule and Walsh[20]. Anharmonicity of the third and sixth modes is ignored since the parameters are not known. This generates only small errors with this resolution since few overtones of ν_3'' and ν_6'' are required to fit the observations.

b) Transition type based upon the band identification.

in figure (3) (those below the exciting laser energy), all ground state modes, and the applicable selection rules. The choice of 7.5Å resolution resulted from the best compromise between signal strength and slit width.

The low pressure spectrum shows progressions in ν_4'' with either 0, 1, or 2 quanta in mode six. The fluorescence could be identified as arising only from the $4^2 6^1$ or $4^1 6^1$ levels. Occasionally one quantum of ν_3'' was required to match the observed wavelengths.

Figure (24) illustrates the change in a representative section of the low pressure spectrum when the H_2CO pressure (without buffer gas) was varied from one to twenty torr. Notice that the 4080 and 4505Å bands change more rapidly with pressure than, for example, the 4010 or 4310Å bands. This type of qualitative pressure dependence is listed for each band in Table IV. On the assumption (justified later) that the $4^2 6^1$ state is the one excited by the nitrogen laser, and that the $4^1 6^1$ state is subsequently populated by collisions, the 4010Å ($4_3^2 6_1^1$) band is used as a standard to which the other band strengths are compared. The ratio of each band intensity to that of the 4010Å band was calculated for each pressure in figure (24). The resulting ratios either increased with increasing pressure or stayed the same. No band had a decreasing ratio.

FIGURE (24): Nitrogen Laser Excited H_2CO Spectrum as a Function of Formaldehyde Pressure, One to Twenty Torr.

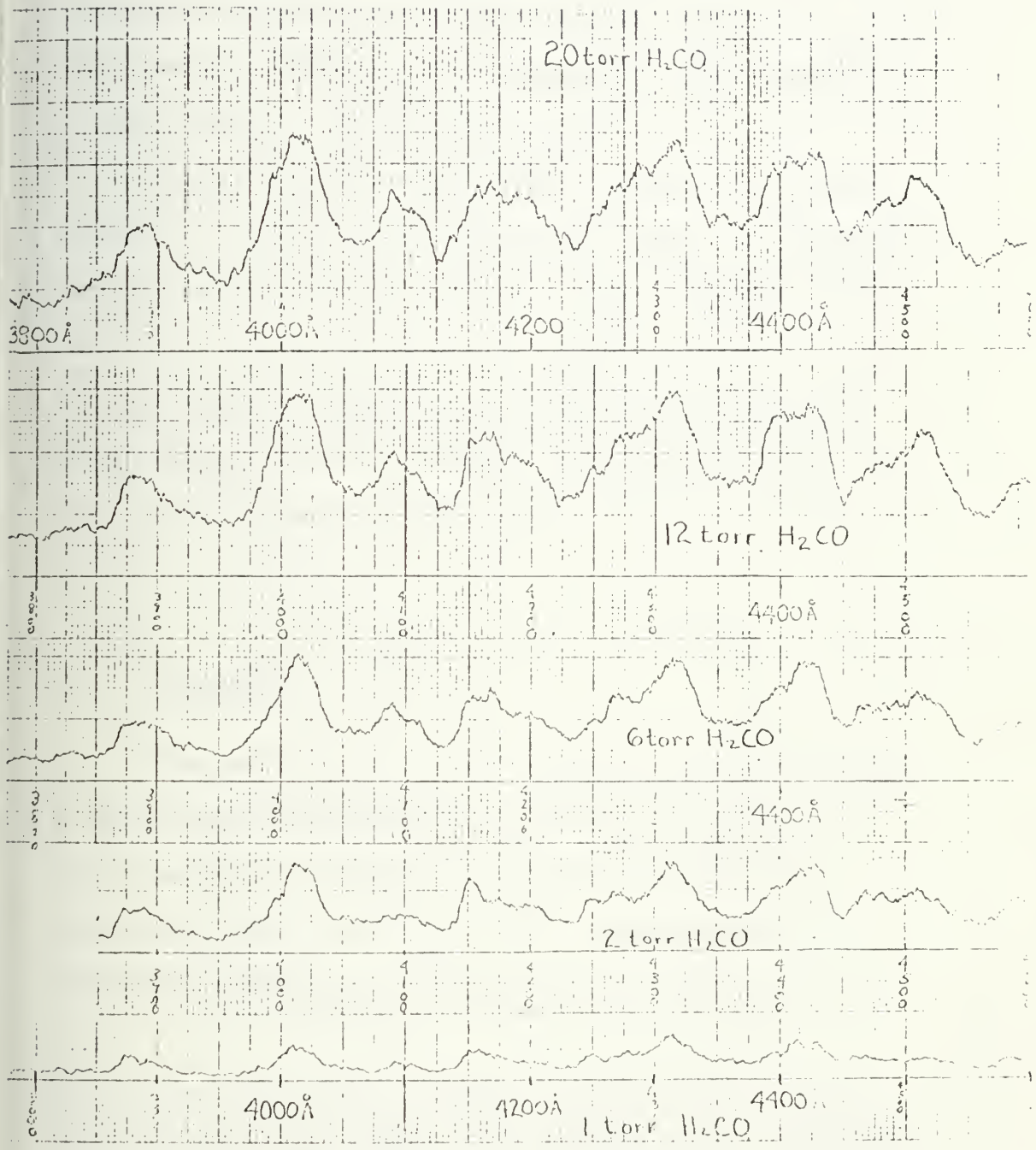
20torr H₂CO
3800Å
4000Å
4200
4400Å
12 torr H₂CO
4400Å
6torr H₂CO
4400Å
2 torr H₂CO
4000Å
4200Å
4400
1 torr H₂CO

Figure (25) shows the behavior of the spectrum as the formaldehyde pressure is increased from ten to 360 torr. The high pressure, vibrationally relaxed bands emerge distinctly at about 120 torr and dominate at 360 torr.

Figure (26) shows the effect of changing the partial pressure of a nitrogen buffer gas while holding the formaldehyde partial pressure constant at 30 torr.* The same qualitative behavior as shown in figure (25) is evident. Notice that the nitrogen does not relax the excited molecule as efficiently as formaldehyde itself. The shape of the spectrum of 240 torr H_2CO closely approximates that of 30 torr H_2CO in the presence of 734 torr of nitrogen.

2. Discussion

The emission spectrum of N_2 laser excited formaldehyde is clearly being influenced by collisions at pressures as low as one torr. Although the identification of the two fluorescing states as $4^2 6^1$ and $4^1 6^1$ is based primarily on wavelength considerations, the presence of two different

---

*It is worth noting that although a nitrogen laser is used for excitation, the nitrogen buffer gas used in the experiments illustrated by figure (26) is not affected by the laser light. The laser transitions are between two excited electronic states in N_2 and are not connected to the nitrogen ground state.

FIGURE (25): H_2CO Spectrum as a Function of Pressure, 10 to 360 Torr.

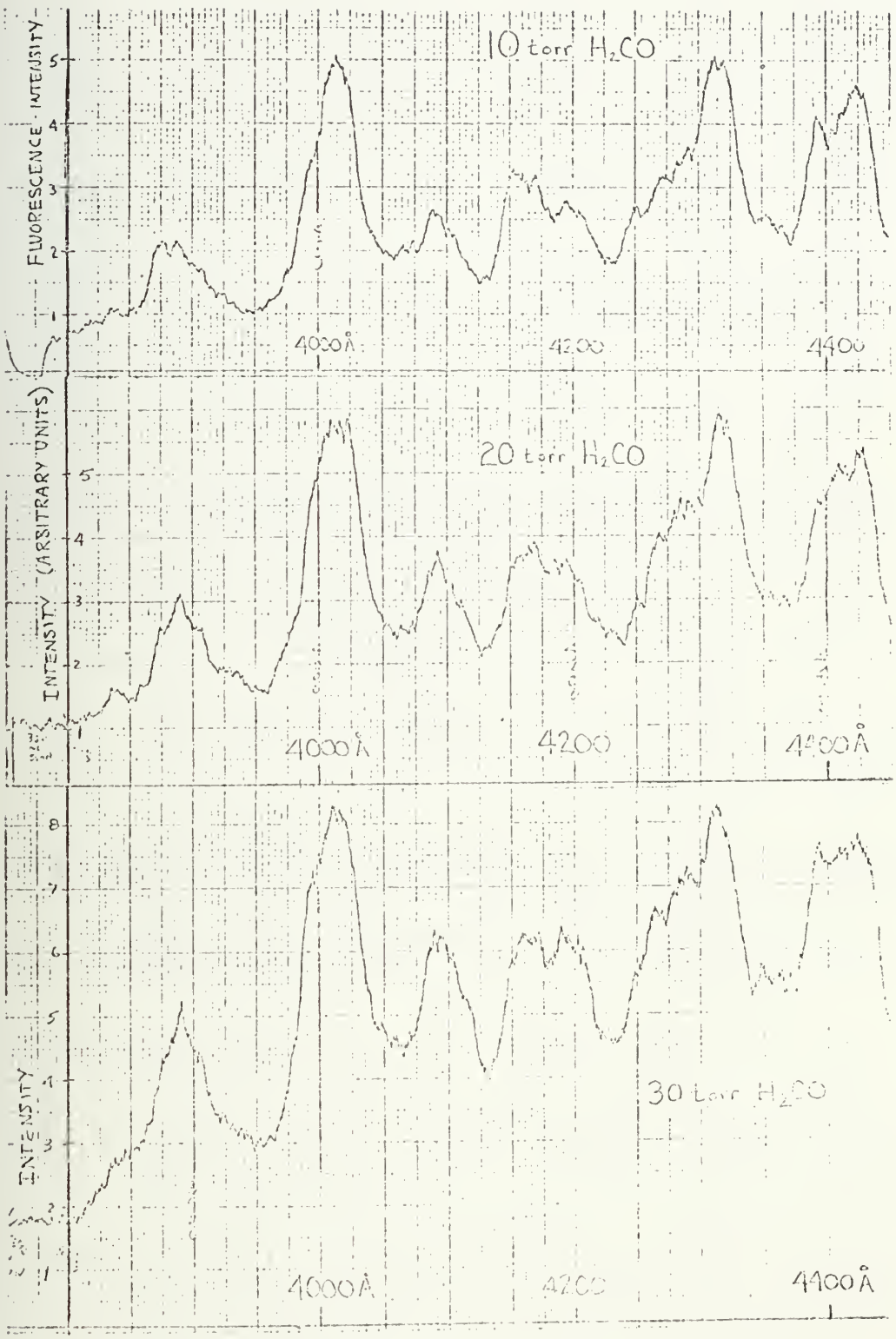
FLUORESCENCE INTENSITY
10 torr H_2CO
4000Å
4200
4400
INTENSITY (ARBITRARY UNITS)
20 torr H_2CO
4000Å
4200
4400Å
INTENSITY
30 torr H_2CO
4000Å
4200
4400Å

Figure (25)

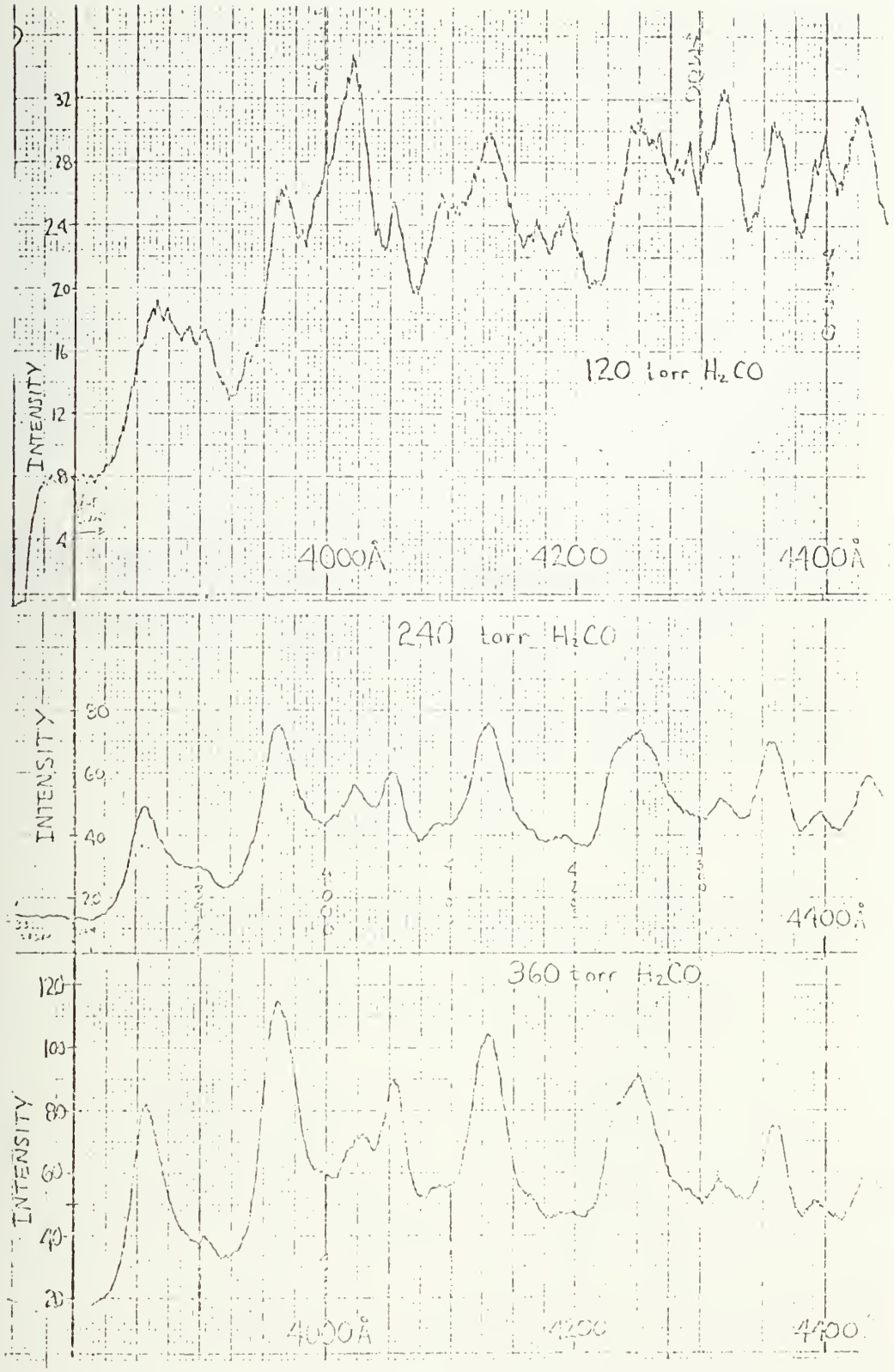

Figure (25): continued

FIGURE (26): H_2CO Spectrum as a Function of N_2 Buffer Gas Pressure.

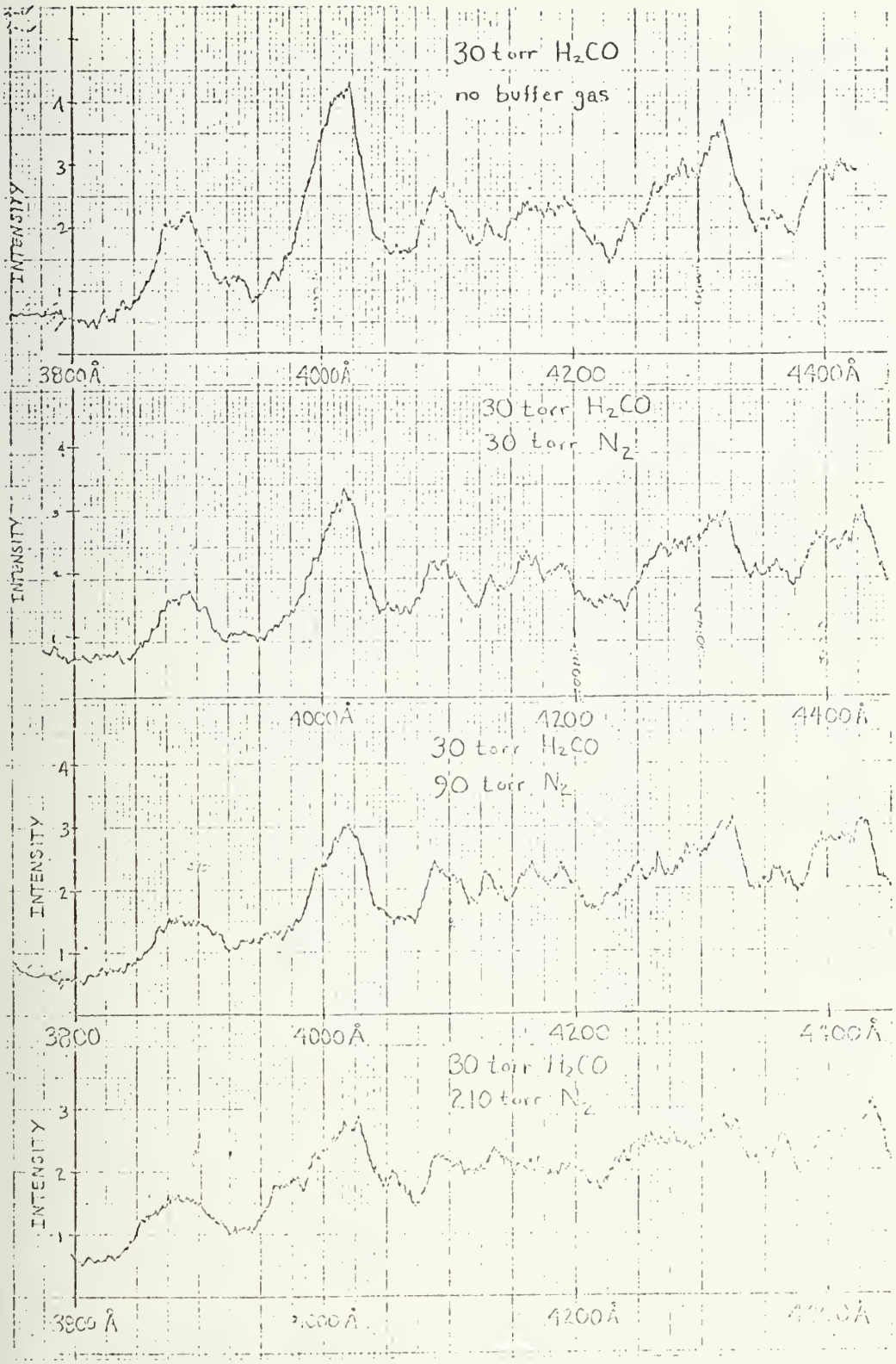
30 torr H_2CO
no buffer gas
INTENSITY
3800Å
4000Å
4200
4400Å
30 torr H_2CO
30 torr N_2
INTENSITY
4000Å
4200
4400Å
30 torr H_2CO
90 torr N_2
INTENSITY
3800
4000Å
4200
4400Å
30 torr H_2CO
210 torr N_2
INTENSITY
3800 Å
4000Å
4200Å

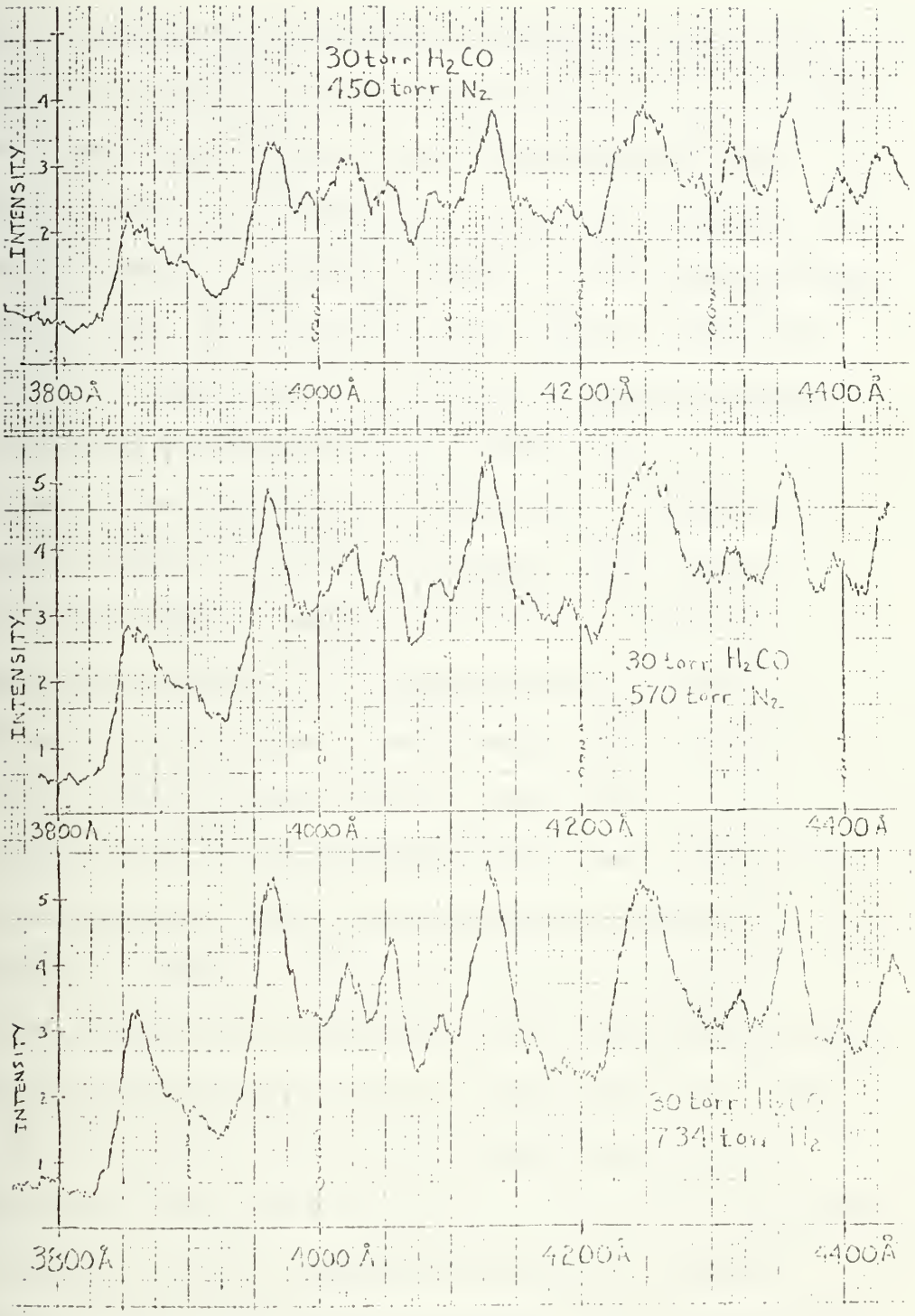

Figure (26): continued

excited state vibrational levels at pressures as low as one torr is strongly supported by the spectral pressure dependence and lifetime measurements. It is rather surprising that the $4^1 6^1$ bands should have almost one half the intensity of the $4^2 6^1$ bands at the lowest pressure for which a measurement could be made. If a collision cross section is calculated for a hard sphere with the radius of 1.2Å (the equilibrium ground state C-O distance) the collision time at one torr would be about 150ns. Since the fluorescence for each pulse is sampled through a 350 picosecond window, opened eighteen nanoseconds after the beginning of the laser pulse, this would imply only about one in ten molecules has suffered a collision when the lowest pressure measurements were made. The actual excited-state collision cross section is almost certainly larger than that determined by ground-state internuclear spacings. If the cross section were twice that calculated by using a 1.2Å radius, more than half of the molecules would have suffered collisions before the measurement. Furthermore the pressure measured is only good to ±0.5 torr. In any case a very strong coupling exists between the two vibrational states seen fluorescing in low pressure formaldehyde. If the $4^1 6^1$ and $4^2 6^1$ designations are correct then the coupling exists in the inversion doubled, out-of-plane-bending vibrational mode.

An independent support for the band identification comes from the changes in the spectrum with pressure. When the qualitative pressure dependence was compared to the band designations that had been made using only the wavelength data, the agreement was quite good. As would be expected, the fluorescence intensity for the $4^1 6^1$ state, which must be populated by collisions subsequent to the laser excitation, increased more rapidly with pressure than that from the $4^2 6^1$ bands. The three bands for which this dependence did not agree with the designations made by wavelength considerations are listed in parentheses in Table IV. The lifetime information presented in section IV.C also supports the contention that there are two different states fluorescing in low-pressure nitrogen laser-excited formaldehyde.

To confirm the band identification more resolution would be needed. Resolution sufficient to detect K structure may not be enough for positive identification at very low pressures since only a few low K values may be excited by the laser (possibly only one). The distinctive progression of sub-bands may not appear in a low pressure spectrum. If the pressure is raised so that a rotational equilibrium can be achieved, thus producing many K sub-bands, the spectrum will be complicated by vibrational energy transfer as well. In any event a usable signal could not be obtained with the

present apparatus at a resolution much less than 7.5Å. The band identifications presented in Table IV are consistent with the data taken at this resolution. I have been unable to discover another identification scheme that is consistent, but it is quite possible that the measured centers of a few bands are in error to the extent that their designations given here are not correct.

3. Miscellaneous

The calculated wavelengths for each band identification found in Table IV were obtained using the measured values of the ν_2'' and ν_4'' harmonics. Since only the fundamentals of ν_3'' and ν_6'' have been previously observed (only in IR absorption) the anharmonic constants for these latter vibrations are not known. If they are similar to those for the second and the fourth modes, an error of perhaps 10 cm^{-1} is made by ignoring them for low occupation numbers in these modes. Since the measurements are accurate to no better than ± 20 cm^{-1}, neglecting the ν_3'' and ν_6'' anharmonic corrections when calculating the predicted transition wave numbers does not produce a major error.

A possible objection to the band identifications given here is raised by the fact that the $4^2 6^1$ and the $3^1 4^2$ bands are separated by only 17 cm^{-1} (see figure (3)). If the

selection rules allow a $4^2_n 6^1_1$ band they also allow a $3^1_0 4^2_n 6^0_1$ band (n must be odd). The energy for a transition involving the third mode would be only 17 cm^{-1} less than that for the corresponding transition involving only the fourth and sixth modes. I have chosen the $4^2 6^1$ identification in all cases for several reasons: In most cases the substitution of the 3^1 for the 6^1 vibration in the identification takes the calculated wave number further from the measured value. It also changes the band polarization from perpendicular to the weaker parallel (type A) polarization. In addition, because the $3^1 4^2$ state cannot be excited by the laser due to selection rules, it must be populated by collisions. The pressure dependence of the bands in question does not, therefore, support a $3^1_0 4^2_n 6^0_1$ designation. The possibility cannot, however, be ruled completely out. Everything said above about the $3^1 4^2$ state applies as well to the 4^4 state, except that this state has never been observed. The actual 4^4 energy may be even closer to the $4^2 6^1$ energy than the $3^1 4^2$ state's energy[28]. The presence of $4^4_n 6^0_1$ (n odd) can thus also not be ruled out.

The quantitative intensity values shown in Figures (25) and (26) as a function of pressure should not be heavily relied on. Window sludge formation and slowly decreasing laser power with continued operation may have combined to

decrease the excitation energy from one spectrum to the next. The broad-band fluorescence monitored through the side window decreased by several percent over each spectrum taken, a period of about 20 minutes apiece. The spectra were taken in order of increasing pressure. Additionally, the intensity scales are not the same for Figures (24), (25), or (26). The band shape and relative intensities within a single spectrum, however, if not the absolute intensities, should be accurate to a few percent.

The cell windows were less susceptible to the formation of sludge at the low pressures used in the experiments illustrated by Figure (24). These sections of low pressure spectra were measured in order of decreasing pressure. If the exciting light intensity had been decreasing in time, therefore, it might be expected that the observations would show the observed band strengths were not proportional to pressure; that they would decrease faster than the pressure. The opposite, however, is true. The integrated fluorescence intensity, as well as the individual band strength, increases more rapidly between 0 and 10 torr than between 10 and 20 torr. Apparently collisions are not only transferring energy but quenching fluorescence as well, for other experiments have shown that the laser is not saturating the transition. Figure (27) illustrates the quantitative

change in band strength for a few bands measured by the experiments shown in Figure (24). Notice that the scatter of the intensity ratios ($I_{4010\text{Å}}/I_{band}$) does not support more than a qualitative statement that the ratios change with pressure or that they do not.

The spectra of the dissociation products of H_2CO were not observed in either the low or high pressure laser-excited spectra. The lowest electronic excited state of HCO [54-56] and CO [57] require much more energy than the laser photons can deliver. Since the ground state energy of HCO + H or CO + H_2 is greater than or equal to the formaldehyde ground state energy, the N_2 laser cannot produce CO or HCO electronic fluorescence. Although CH is not known to be a dissociation product of H_2CO, the strong 4315Å band of CH [58] has the approximate shape and placement of the 4310Å band observed in the low pressure spectrum. The same shape is also, however, possessed by many of the bands originating from the $4^2 6^1$ state of formaldehyde (4010, 4424, 4785, 4920Å) but these bands do not correspond to any CH bands. The measured lifetime of the 4310Å band fluorescence also does not support its designation as a CH band.

FIGURE (27): Pressure Dependence of 4010, 4310, 4080, 4505Å.

Band intensities between one and 20 torr. Data comes from the spectra shown in figure (24).

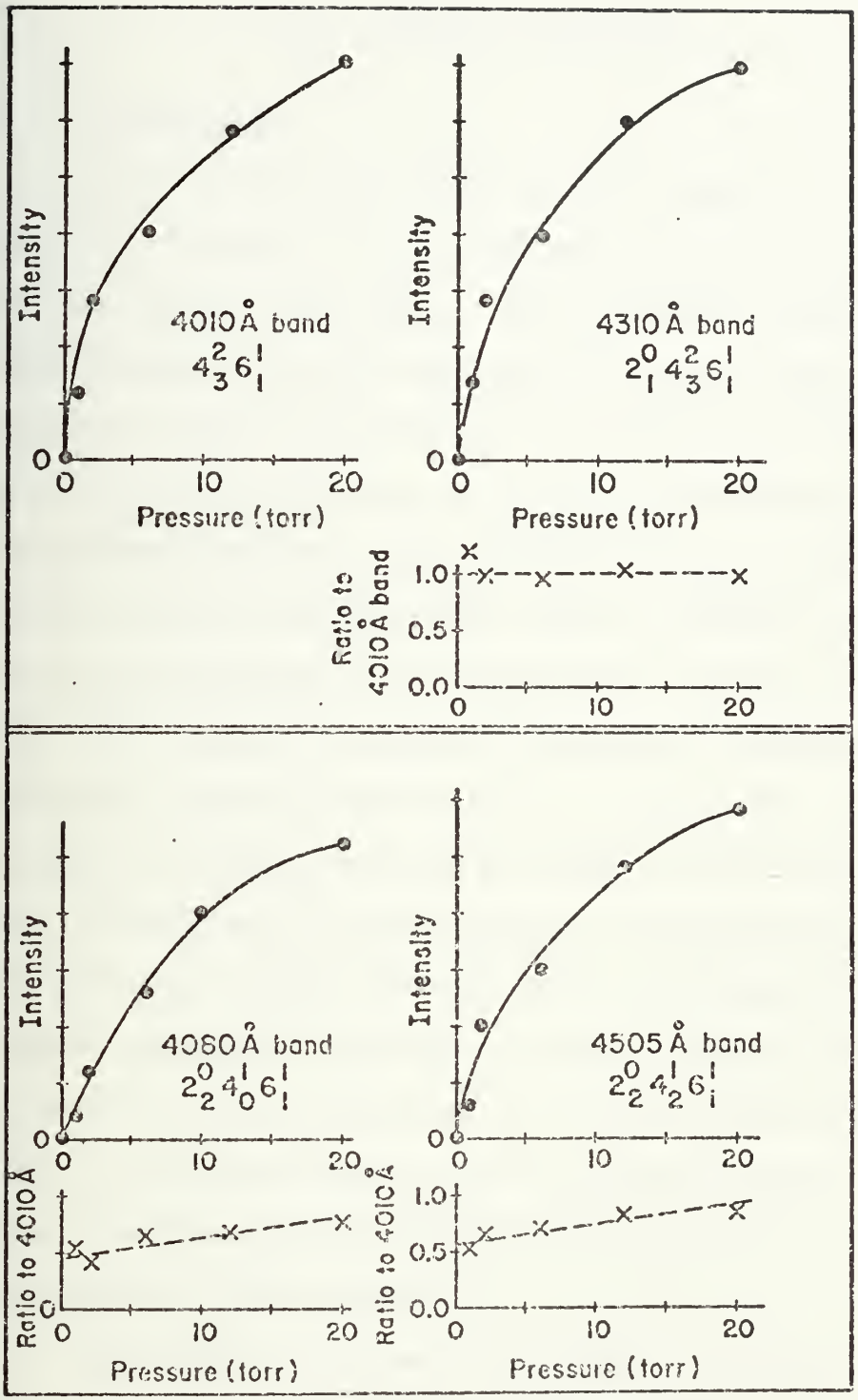
Intensity
4010 Å band
$4_3^2 6_1^1$
Pressure (torr)
Intensity
4310 Å band
$2_1^0 4_3^2 6_1^1$
Pressure (torr)
Ratio to 4010 Å band
Intensity
4080 Å band
$2_2^0 4_0^1 6_1^1$
Ratio to 4010 Å
Pressure (torr)
Intensity
4505 Å band
$2_2^0 4_2^1 6_1^1$
Ratio to 4010 Å
Pressure (torr)

IV.C. LIFETIME MEASUREMENTS

1. Data Summary

The experiments reported here were originally undertaken to investigate the lack of agreement among the previously published lifetime measurements. After making the spectral studies reported in the last sections, it was clear that meaningful lifetime measurements in formaldehyde had to be made by observing the fluorescence with a limited bandwidth. The 10Å (FWHM) bandwidth chosen for the experiments reported here is a factor of twenty smaller than the narrowest bandwidth used for any previously reported formaldehyde lifetime measurements. This inevitably reduced the intensity of the detected fluorescence signal by the same factor. Consequently, I have been unable to measure lifetimes at pressures less than one torr. As was shown in the last section, there still appear to be significant collisional effects on the fluorescence at that pressure. Although it may not be possible to make a linear extrapolation of the Stern-Volmer plots shown in this section to give a zero pressure lifetime, work described here has revealed interesting new collisional effects occurring in formaldehyde at higher pressures.

This section describes measurements of the H_2CO collisional self-quenching effect on the S_1 lifetime for pressures between one and 300 torr. Measurements have been

made on six different bands. Four of them are low pressure bands identified in IV.B. as $4_3^2\ 6_1^1$, $2_1^0\ 4_3^2\ 6_1^1$, $2_3^0\ 4_0^1\ 6_1^1$ and $2_2^0\ 4_2^1\ 6_1^1$. The other two bands for which self-quenching studies were made were $2_0^1\ 4_3^0$ and $2_1^0\ 4_1^0$. The fluorescence from these two previously known bands was much weaker than that from the low pressure bands. Additional experiments were made to study the effect of an argon buffer gas on the fluorescence lifetimes for three low pressure bands.

This section will begin with examples of the lifetime data and illustrate the behavior of both the individual decay curves and their changes with pressure. Having thus explained the notation and introduced the new phenomena, the data for all bands will be summarized. The discussion section will compare these results among themselves and with previous measurements and will present possible explanations for the shape of the decay curves and the non-linear Stern-Volmer plots. Subsection three will discuss the processing of the raw data and corrections for instrumental effects.

Figure (28) illustrates several unprocessed decay curves for the 4505Å ($2_2^0\ 4_2^1\ 6_1^1$) band. Small corrections to the raw lifetime data, of which this is an example, had to be made due to the dispersion introduced by the measuring apparatus. These corrections will be considered in Section 3. The important

points to notice about figure (28) are the existence of two rates in the logarithmic plot and how these rates change with pressure. This behavior is characteristic of all the low pressure bands studied. About 15 nanoseconds after the excitation (well after the nitrogen laser has ceased to emit) the fluorescence decreases with a rapid rate corresponding to a short lifetime, τ_S. After a time, which varies with the pressure, the decay slows and the fluorescence decreases with a rate characterized by a longer lifetime, τ_L. From figure (28) it can be seen that the short lifetime, τ_S, changes with pressure, but the gradual change with pressure of τ_L is not obvious.

It was also found that the magnitude of the short lifetime varied significantly between bands, but that of the long lifetime did not. This behavior is illustrated for a small segment of the spectrum by figure (29).

The existence of two lifetimes in the decay curves is probably <u>not</u> an effect of the initial excitation of two different states with two different lifetimes. On the contrary, it is most likely due to collisional effects which build up population in states responsible for the long lifetime after the laser excitation, so that the long lifetime is not a characteristic of the originally excited ro-vibronic state or states. This will be discussed in much more detail in sections b and c.

FIGURE (28): Decay Curves for 4505Å Band. The figure illustrates the fluorescence intensity as a function of time at three different pressures. These plots are direct copies of the chart recorder output. For each pressure two curves are shown. The lower, narrow peak is the actual fluorescence decay curve, the upper one is its logarithm. The time scales of the linear and log plots are displaced relative to each other by six nanoseconds (two small divisions) due to the separation between the pens on the chart recorder. The best estimate of the slope of the logarithmic plot was drawn on the chart paper. Lines of maximum and minimum possible slope were also drawn, in order to estimate the probable error, but they have not reproduced well. All decay curves are shown to the same time scale, but not the same vertical scale. The attenuation of the signal was changed for each measurement to provide the optimum input to the logarithmic amplifier. Therefore, the relative intensity between different decay curves cannot be compared.

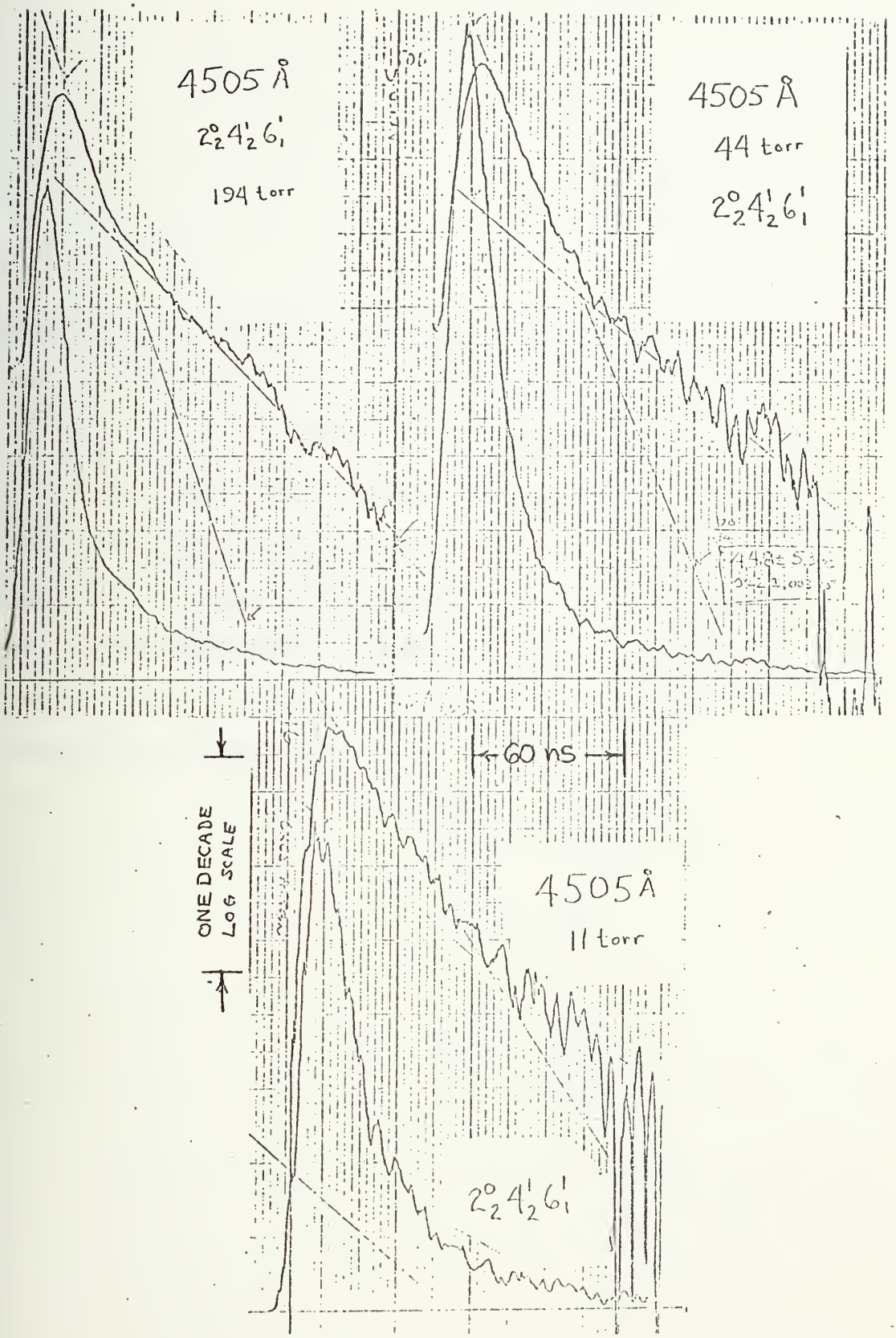
4505 Å
$2_2^0 4_2^1 6_1^1$
194 torr
4505 Å
44 torr
$2_2^0 4_2^1 6_1^1$
60 ns
ONE DECADE
LOG SCALE
4505 Å
11 torr
$2_2^0 4_2^1 6_1^1$

FIGURE (28)

FIGURE (29): Lifetime vs. Wavelength 4380Å to 4425Å.

The measurements illustrated span the range between the $2_3^0\ 4_0^1\ 6_1^1$ and the $4_5^2\ 6_1^1$ bands. The wavelength error shown is the full width at half maximum resolution of the spectrometer and the vertical error bars come from estimates of the maximum and minimum possible slope of the logarithmic decay plot. Notice that there is no systematic variation of the long lifetime with wavelength although there is such a variation of the short lifetime.

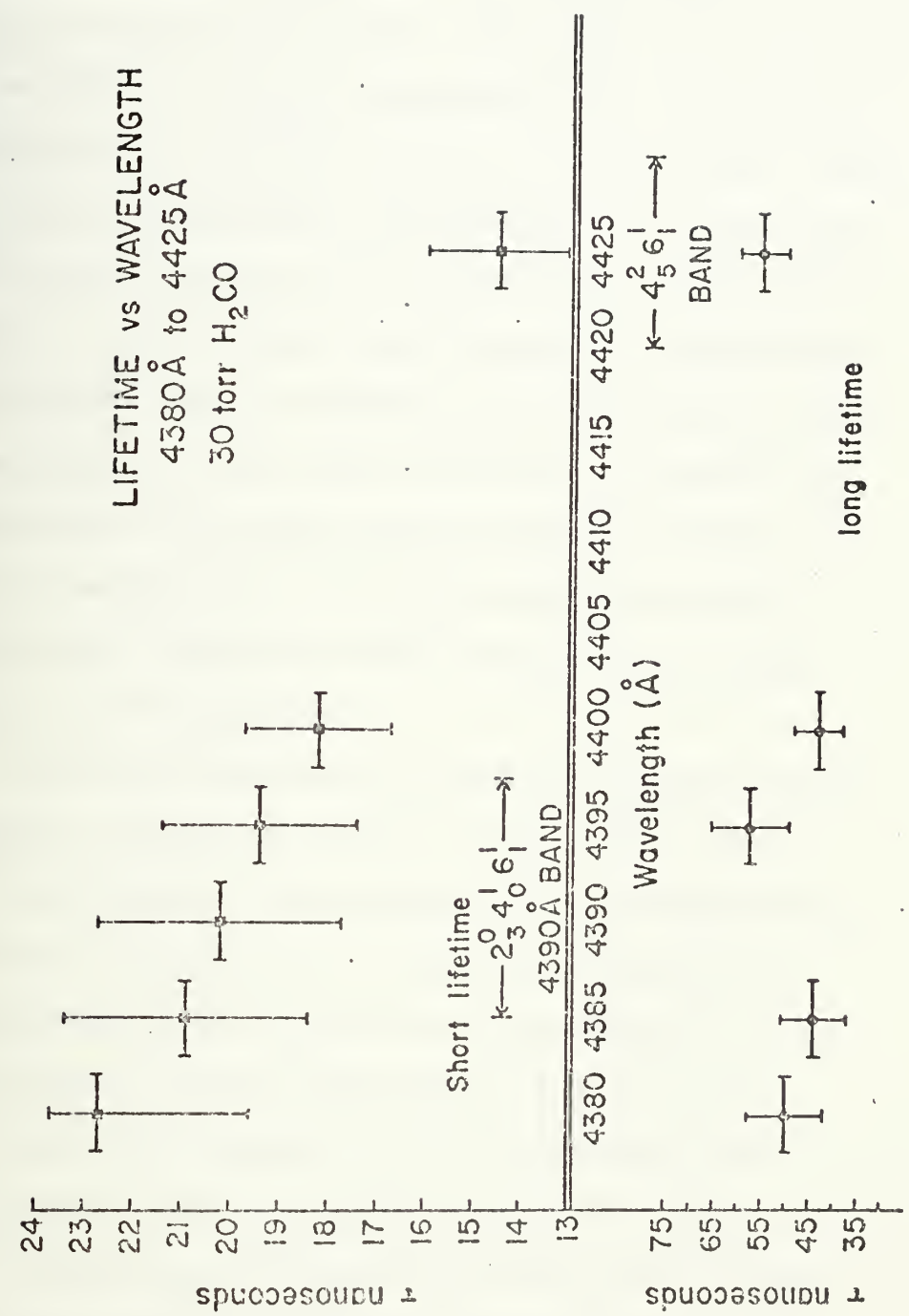
LIFETIME vs WAVELENGTH
4380Å to 4425Å
30 torr H_2CO
Short lifetime
$2_3^0 4_0^1 6_1^1$
4390Å BAND
long lifetime
$4_5^2 6_1^1$
BAND
Wavelength (Å)
4380 4385 4390 4395 4400 4405 4410 4415 4420 4425
τ nanoseconds
24 23 22 21 20 19 18 17 16 15 14 13
75 65 55 45 35

The Stern-Volmer plot of decay rate ($1/\tau$) as a function of pressure provides a convenient way to display the quantitative change of lifetime with pressure. Figure (30) shows such a plot for the 4505Å band. The most striking feature of the figure is the abrupt change in slope of the $1/\tau_S$ vs. pressure plot. Since this slope is proportional to the quenching cross section, this change implies that the cross section decreases sharply at about 60 torr, to a value close or equal to zero. The long lifetimes do not show any change in quenching cross section with pressure. For convenience, a short lifetime measured at a pressure above the threshold for the slope change is labeled τ_S' and the high pressure quenching cross section for the short lifetime is designated σ_S'. Following Freed[37], I shall call the change from σ_S to $\sigma_S' \sim 0$ "saturation."

Figure (31) illustrates the change of N_2 laser excited formaldehyde lifetime as a function of the partial pressure of an argon buffer gas. The pressure of H_2CO was held constant at 30 torr. The same qualitative behavior as observed for self-quenching is seen. Although the least square fit to the high pressure τ_S' points in figure (31) gives σ_S' somewhat greater than zero, a glance at the error bars shows that a cross section of zero is quite compatible with the data.

The qualitative behavior illustrated above is found in the decay curves and Stern-Volmer plots for the other low

FIGURE (30): Stern-Volmer Plot 4505Å Band, Self Quenching. Both the inverse of the short lifetime (τ_S) and that of the long lifetime (τ_L) are shown as a function of formaldehyde pressure. Representative error bars (about 10 to 15%) are shown. Different shaped points represent data taken on different days, in order to determine the reproducibility of the curve as well as to extend the plot to lower pressure. The solid lines represent a linear least square fit to the points and the error for the zero pressure lifetimes listed on the figure comes only from the deviation of the points from the fit. The error shown represents one standard deviation. Sources of error are discussed in section 3 and the best estimate of the accuracy of these values is given for all bands in table V.

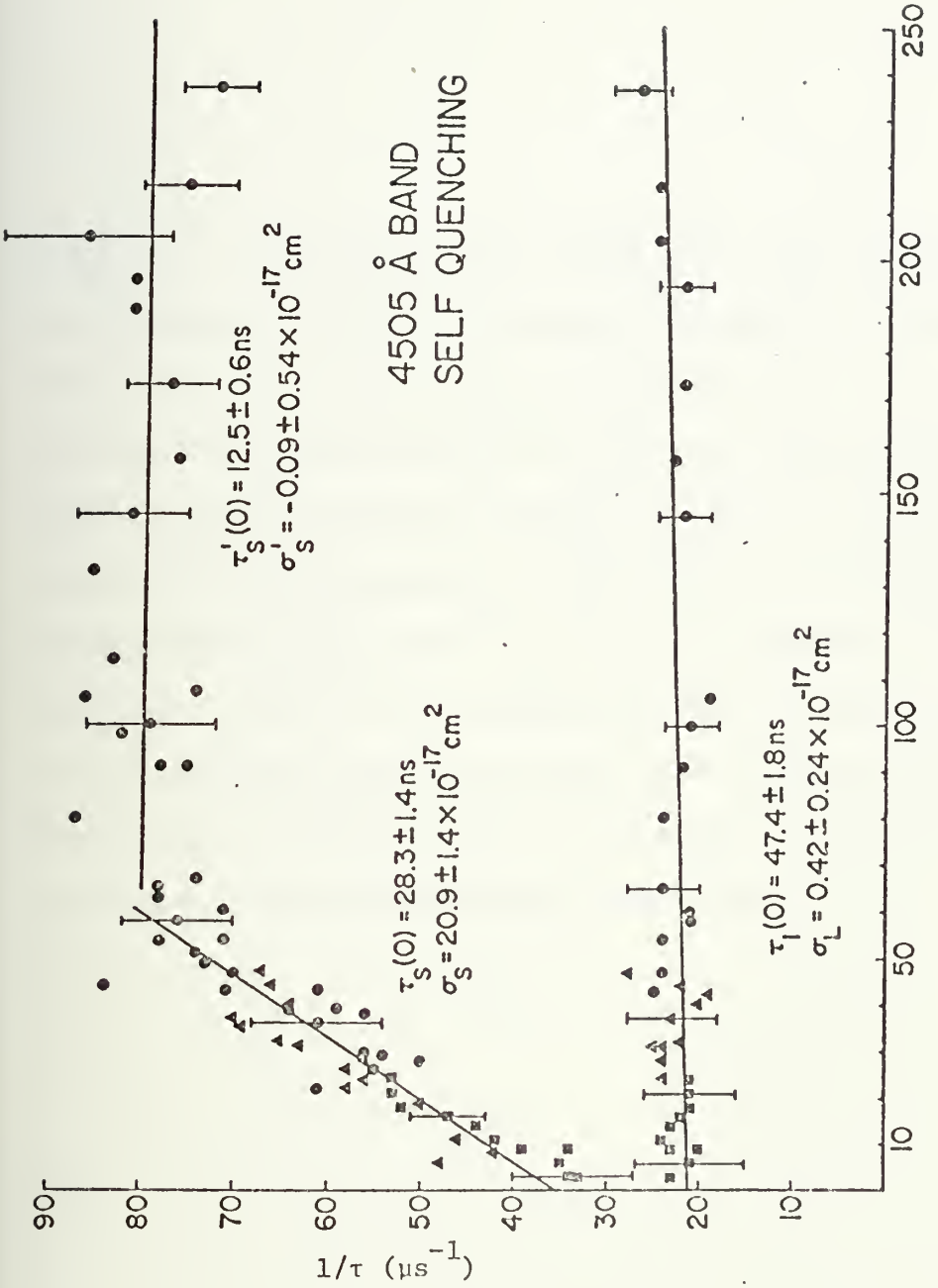
4505 Å BAND
SELF QUENCHING
$\tau_s'(0) = 12.5 \pm 0.6$ns
$\sigma_s' = -0.09 \pm 0.54 \times 10^{-17}$ cm^2
$\tau_s(0) = 28.3 \pm 1.4$ns
$\sigma_s = 20.9 \pm 1.4 \times 10^{-17}$ cm^2
$\tau_l(0) = 47.4 \pm 1.8$ns
$\sigma_L = 0.42 \pm 0.24 \times 10^{-17}$ cm^2
$1/\tau$ (μs^{-1})
H_2CO Partial Pressure (torr)

FIGURE (31): Stern-Volmer Plot, 4505Å Band, Argon Quenching.

The lifetime of the H_2CO fluorescence in this band was measured with a fixed 30 torr formaldehyde partial pressure. The pressure of an argon buffer gas was varied. The different symbols represent different days' data. There is a point off scale at 732 torr argon partial pressure for both the short lifetime ($1/\tau_S$ (734) = $96\mu s^{-1}$) and the long lifetime ($1/\tau_L'(734) = 18\mu s^{-1}$). All lines shown and the values for τ and σ represent linear least square fits to the data points. Notice that the pressure scale is compressed by a factor of two over that for self quenching in figure (30).

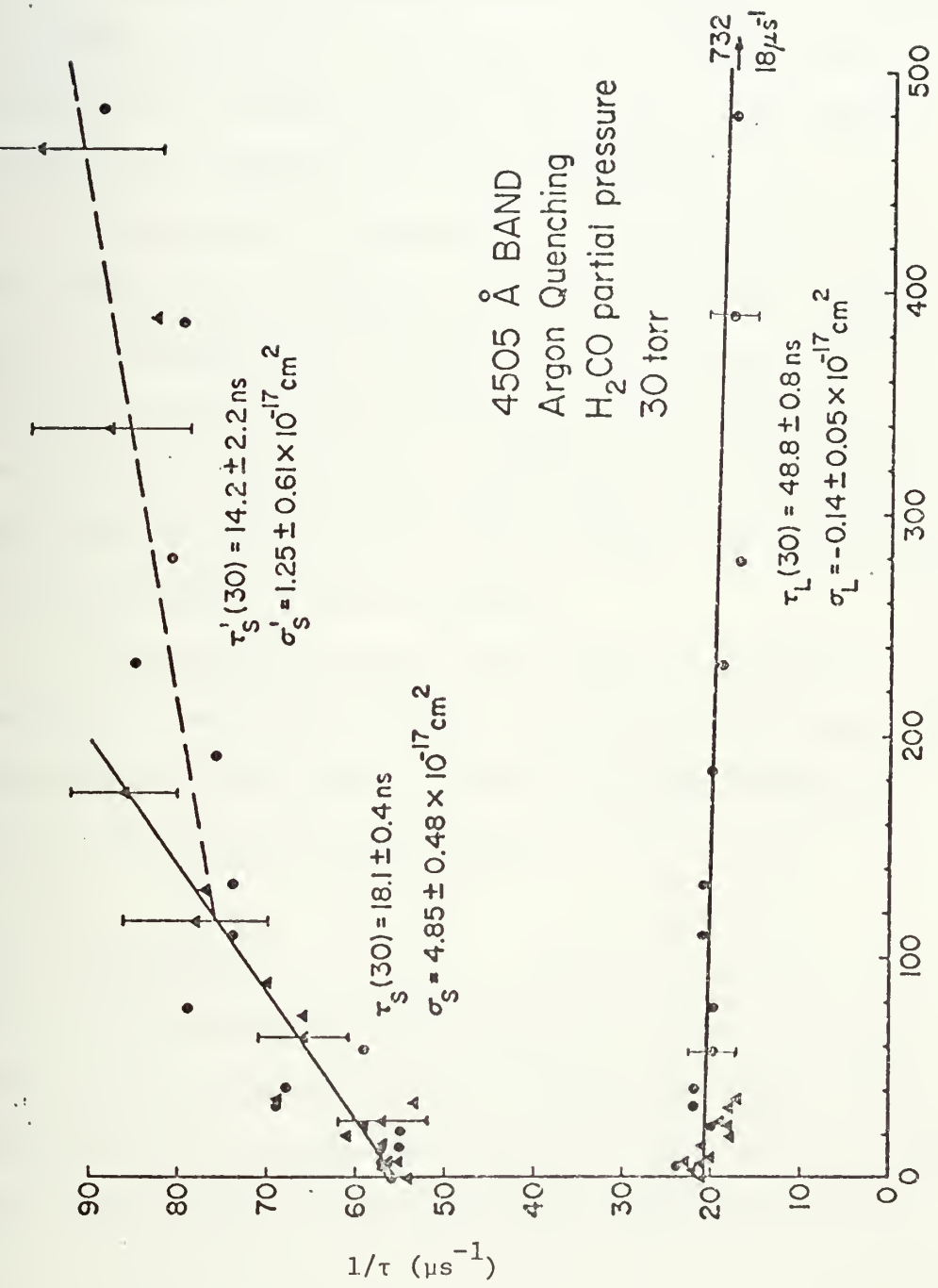
4505 Å BAND
Argon Quenching
H_2CO partial pressure
30 torr
$\tau_S'(30) = 14.2 \pm 2.2$ ns
$\sigma_S' = 1.25 \pm 0.61 \times 10^{-17}$ cm^2
$\tau_S(30) = 18.1 \pm 0.4$ ns
$\sigma_S = 4.85 \pm 0.48 \times 10^{-17}$ cm^2
$\tau_L(30) = 48.8 \pm 0.8$ ns
$\sigma_L = -0.14 \pm 0.05 \times 10^{-17}$ cm^2
732
18 μs^{-1}
$1/\tau$ (μs^{-1})
Argon partial pressure (torr)
0
10
20
30
40
50
60
70
80
90
100
200
300
400
500

pressure bands investigated. By way of contrast, the previously known bands originating from the 0^0 and 2^1 levels show only a single decay rate which varies slowly with pressure. Figure (32) illustrates this for two measured fluorescence curves for the 3860Å, $2_0^1 4_3^0$ band. The corresponding Stern-Volmer plot for this band is shown in figure (33). Figures (34) and (35) show the same information for the 3952Å, $2_1^0 4_1^0$ band.

Notice that the logarithm of the 31 torr decay curve for the 3952Å band in figure (34) only slowly approaches a straight line. It takes almost 75 nanoseconds after excitation for the log plot to become linear in this case. This corresponds to about twelve collision times. The 0^0 level is over 1000 cm^{-1} below the other bands measured here, so that a slow collisional population build up would be expected.

The lifetime and cross section data for all bands measured is summarized in table V. Stern-Volmer plots and representative decay curves for 4010Å, 4310Å and 4390Å bands are shown at the end of section three.

2. Discussion

This section will first compare the entries in Table V among themselves and with previous lifetime measurements. This discussion will be divided into two parts; the first will compare the 2^1 and 0^0 bands, and the second will address the new bands.

FIGURE (32): Decay Curves for 3860Å Band.

The upper curve is the logarithm of the decay curve measured by the electronics. The best estimate slope and the maximum and minimum slopes that were drawn on the chart can be seen in this figure.

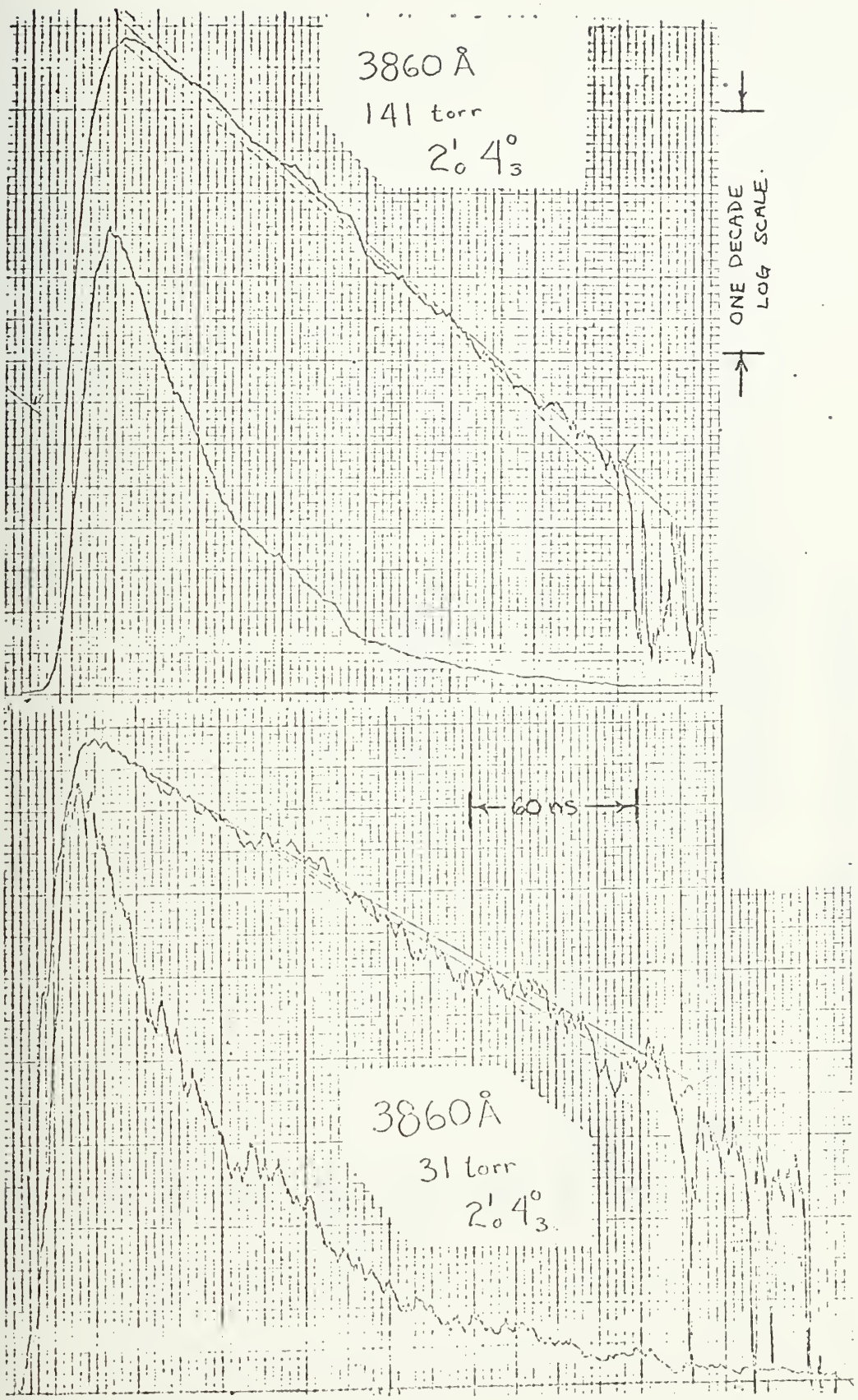
3860 Å
141 torr
$2_0^1 4_3^0$
ONE DECADE
LOG SCALE.
60 ns
3860 Å
31 torr
$2_0^1 4_3^0$

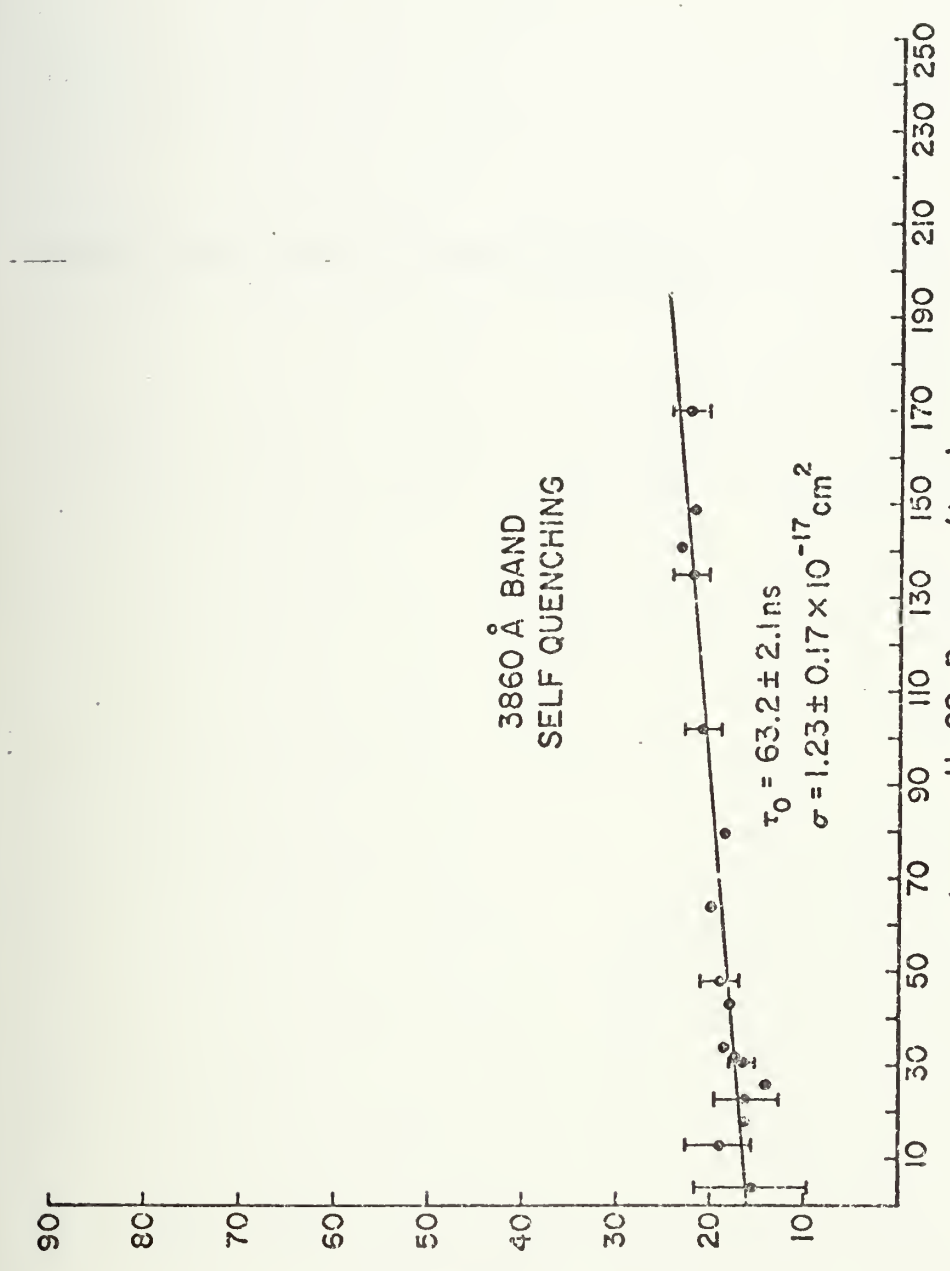

FIGURE (33): Stern-Volmer plot for 3860Å Band.

FIGURE (34): Decay Curves for 3952Å Band.

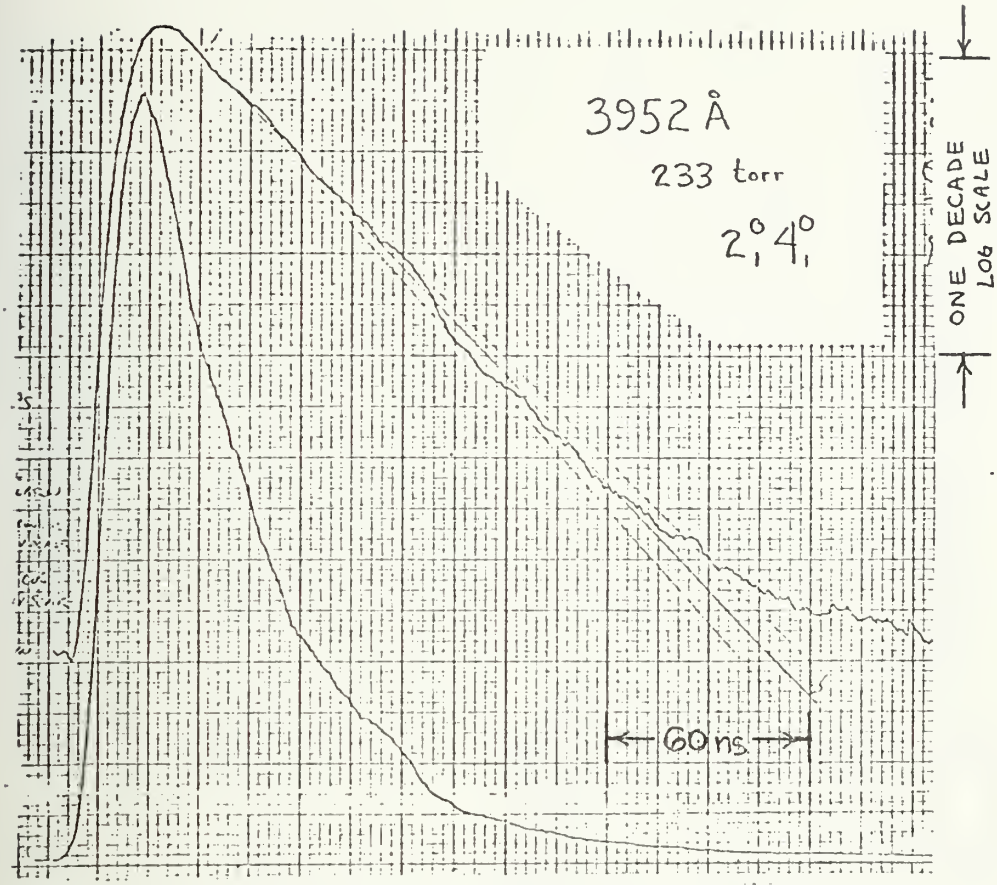
3952 Å
233 torr
2°, 4°
ONE DECADE
LOG SCALE
60 ns

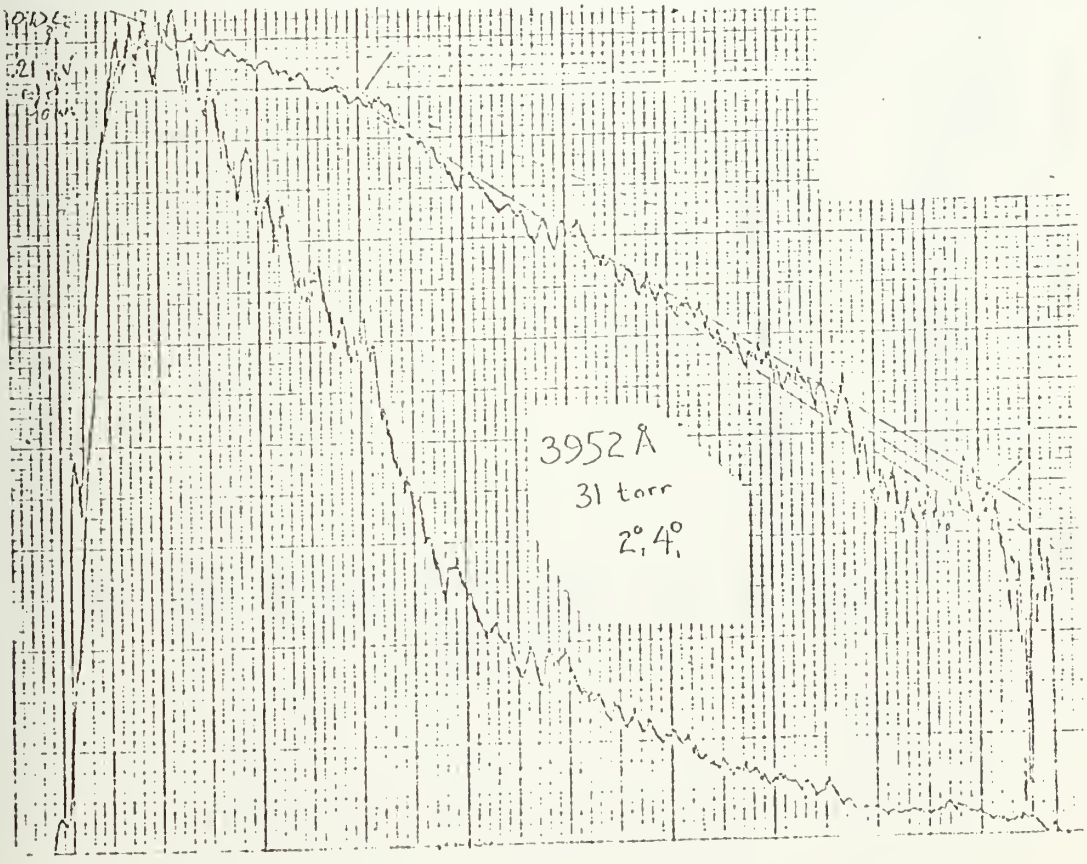
3952 Å
31 torr
2°, 4°

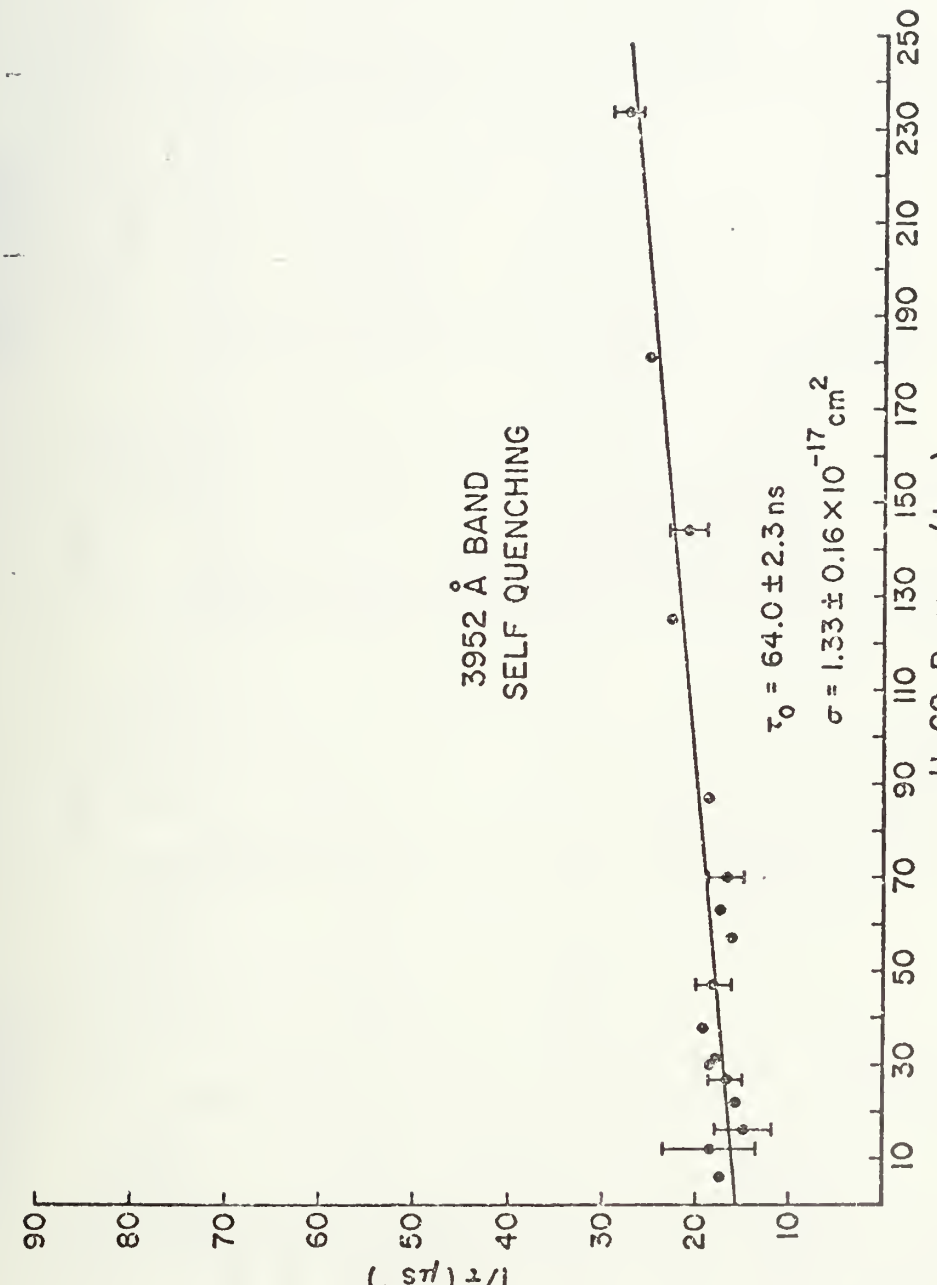

FIGURE (35): Stern-Volmer plot for 3952Å Band.

TABLE V: LIFETIME SUMMARY[a]

	TABLE SELF-QUENCHING			LIFETIME SUMMARY ARGON QUENCHING		
	$\tau_s(0)$ns $\sigma_s \times 10^{-17}$cm^2 $k_s \mu s^{-1}$torr^{-1}	$\tau_s'(0)$ns $\sigma_s' \times 10^{-17}$cm^2 $k_s' \mu s^{-1}$torr^{-1}	$\tau_L(0)$ns $\sigma_L \times 10^{-17}$cm^2 $k_L \mu s^{-1}$torr^{-1}	$\tau_s$ns $\sigma_s \times 10^{-17}$cm^2 $k_s \mu s^{-1}$torr^{-1}	τ_s'ns $\sigma_s' \times 10^{-17}$cm^2 $k_s' \mu s^{-1}$torr^{-1}	$\tau_L$ns $\sigma_L \times 10^{-17}$cm^2 $k_L \mu s^{-1}$torr^{-1}
3860 Å $2_0^1 4_3^0$	τ63.2±3.4 σ1.23±.17 k .044±.006					
3952 Å $2_1^0 4_1^0$	τ64.0±3.6 σ1.33±.16 k .048±.006					
4010 Å $4_3^2 6_1^1$	τ18.7±1.6 σ10.0±.7 k .36±.03 slope changes at 100 torr	(τ12.5±2.5) σ∿0 k∿0	τ45.4±3.9 σ-.04±.28 k-.001±.010	(τ(30)16.0±1.5) σ4.43±.65 k .16±.02 Slope changes at 130 Torr	(τ(30)13.1±1.8) σ1.2±.6 k .04±0.2	(τ(30)46.1±2.9) σ.17±.09 k .006±.003
4310 Å $2_1^0 4_3^2 6_1^1$	τ20.5±2.0 σ13.6±3.1 k .49±.14 slope changes at 60 torr	(τ∿15±4) σ∿0 k∿0	τ54.0±3.6 σ.76±.24 k .027±.008			

4390Å $2_3^0\ 4_0^1\ 6_1^1$	τ31.1±2.1 σ14.8±1.0 k .54±.04 slope changes at 70 torr	(τ18.5±2.2) σ1.3±1.1 k .047±.040	τ63±7 σ1.1±.5 k .040±.018	(τ(30)22.2±1.6) σ5.48±.42 k .198±.015 slope changes at 120 torr Argon	(τ(30)15.7±2.2) σ.87±.61 k .035±.022	(τ(30)52.3±3.3) σ-.09±.10 k-.003±.004
4505Å $2_2^0\ 4_2^1\ 6_1^1$	τ28.3±1.4 σ20.9±1.4 k .75±.05 slope changes at 60 torr	(τ12.5±1.6) σ-.09±.54 k-.003±.020	τ47.4±3.3 σ.42±.24 k .015±.008	(τ(30)18.1±1.6) σ4.85±.48 k 1.75±.017 slope changes at 120 torr Argon	(τ(30)14.2±2.7) σ1.25±.61 k .04±.02	(τ(30)48.8±2.8) σ-.14±.05 k-.005±.002
				(τ(50)16.7±1.6) σ5.74±6.0 k .207±.25		(τ(50)49.7±2.6) σ.77±.36 k .028±.013

(a) Errors are one standard deviation calculated from a least square fit to the Stern-Volmer plots. Extrapolated lifetime values have an additional estimated error due to possible baseline errors. See section 3.C.

This will be followed by a discussion of theories that may explain the two decay rates and the change in quenching rate with pressure that is characteristic of the new bands.

a) The 2^1 and 0^0 Bands, Comparisons.

The lifetimes and quenching rates in table V for the $2_0^1\ 4_3^0$ and $2_1^0\ 4_1^0$ bands are identical. Their decay curves below 30 torr differ as noted above: the $2_1^0\ 4_1^0$ band shows a much slower approach to an exponential decay than the $2_0^1\ 4_3^0$ band due to its greater energy separation from the laser excited state. It should also be noted that the 10Å bandwidth used for the lifetime measurements could not prevent some light from the overlapping 4_2^1 band from being observed with the $2_0^1\ 4_3^0$ band.

Although no other measurements have been made of the lifetime of the 2^1 level, Baronavski[8] has measured the lifetime of the 0^0 level using a more efficient excitation mechanism, for that level, than the nitrogen laser. He found a zero pressure lifetime of 336 nanoseconds by linear extrapolation of his data, all of which were for pressures below one torr. The quenching cross section he measured was 1.6×10^{-15} cm^2±20%. My data for the same level starts at 4 torr and goes to higher pressures (figure (35)). A linear extrapolation of this higher pressure data gives 64±4 nanoseconds as the zero pressure lifetime, and the slope yields a cross section of $1.3\pm2\times10^{-17}$ cm^2. For his measurements, Baronavski used adequate

signal averaging equipment and his results agree substantially with those of Jeunehomme and Duncan.[10] There can be little question about the accuracy of this zero-pressure lifetime.

The most satisfactory explanation for the discrepancy between the higher pressure 0^0 band data reported here and that taken at lower pressure by other observers is that a significant change in cross section occurs between one and four torr. This would be similar to the change seen directly in the data for other bands. Measurements made at 4 torr on a species with an unperturbed lifetime of 300 nanoseconds are certainly not collision free, and in view of the cross-sectional changes frequently observed here for other bands, as well as in Baronavski's H_2CO and D_2CO data, such a change in σ with pressure should not be ruled out.

Since linear extrapolation of the Stern-Volmer plot to zero is not valid for the long lifetime 0^0 state, such an extrapolation probably does not yield the true zero pressure lifetime for the 2^1 state either. Measurements of the 2^1 and 0^0 lifetimes between one and ten torr are needed to determine how the high and low pressure Stern-Volmer curves join. Nitrogen laser excitation is not an effective means for producing molecules in these states, since the levels are populated only by collisions after the laser pulse. Other excitation techniques should be used to make such measurements.

b) The $4^2\ 6^1$ and $4^1\ 6^1$ Bands, Comparisons.

The situation for the $4^1\ 6^1$ and the $4^2\ 6^1$ bands is more complicated (figures (30, 39-41)). The decay curves show two rates, τ_S and τ_L, and the quenching cross section for the faster rate saturates at about 60 torr. In addition, there is data here for argon quenching on three of these bands. Finally, comparison with other nitrogen laser excited lifetime measurements is difficult because of the wide bandwidths used for previous observations.

Some general comments about the data shown in table V should be made. The bands which were identified, by wavelength and the pressure dependence of the band intensity, as originating in the $4^2\ 6^1$ state show the same zero pressure lifetime and low pressure quenching cross sections (19±2 ns., $11\pm2\ 10^{-17}$ cm^2). By contrast, the bands originating in the $4^1\ 6^1$ level show $\tau_S(0)$ of 29±2 nanoseconds, but two different quenching cross section: $21\pm2\times10^{-17}$ cm^2 for the 4505Å band, and $15\pm1\times10^{-17}$ cm^2 for the 4390Å band. The difference in σ_S between the two $4^1\ 6^1$ bands may be due to the partial overlapping of the 4390Å band by both high and low pressure bands. The data for the 4010Å, $4_3^2\ 6_1^1$, and the 4505Å, $2_2^0\ 4_2^1\ 6_1^1$, bands are probably the most reliable since these bands are the strongest, most isolated ones in the low pressure spectrum.

For all but the short lifetime, τ_S and its lower pressure self quenching cross section σ_S, the entries in table V are essentially the same for both $4^2\ 6^1$ and $4^1\ 6^1$ bands, if the extrapolated values in parentheses are not considered. The short lifetime does not change with pressure above about 60 torr for self quenching, and changes only slightly, if at all, above 120 torr for argon quenching. The long lifetime τ_L is about 50 nanoseconds and σ_L, although it shows some scatter, is compatible with about 0.5×10^{-17} cm^2 for these four bands. σ_L for argon quenching is compatible with zero.

The key factor which characterizes those measurements which differ between the $4^1\ 6^1$ and $4^2\ 6^1$ bands and those which do not is the number of collisions to which the excited molecules have been subjected before the measurement was made. τ_S and σ_S characterize the relatively unperturbed molecule while τ_L, τ_S' and σ_S' do not. The second decay rate $(1/\tau_L)$ does not appear until a minimum of ten mean collision times have passed since the beginning of the laser pulse. The change from σ_S to σ_S' occurs at a pressure where the logarithm of the decay curve does not become linear until at least seven mean collision times have passed since the excitation began. The significance of the numberof collisions will be discussed later.

The minimum bandwidth of any previous measurement of nitrogen laser excited formaldehyde lifetimes was 200Å. The

data presented here show that this is far too broad a bandwidth even for pressures as low as one torr. The lifetime given by Aoki et al.[12] of 18±1 nanoseconds is compatible with that of the $4^2\ 6^1$ bands, while that of Sakurai et al.[11], 27±2 nanoseconds, matches that of the $4^1\ 6^1$ bands, but both of these experiments used bandwidths in excess of 800Å. The different range of their pass-bands may be the cause of the difference in their measurements.

Baronavski's N_2 laser excited fluorescence lifetime measurements were also made without knowledge of the low pressure spectrum discovered here. His 200Å (FWHM) bandwidth, between 4300 and 4500Å, covered what I have shown to be a good sample of both $4^1\ 6^1$ and $4^2\ 6^1$ bands. His measurements between 0.1 and 2 torr resulted in a zero pressure lifetime of 46 nanoseconds ±10%, and a cross section of 2.5×10^{-15} cm^2±20%. With his bandwidth, this represents a kind of average between the $4^2\ 6^1$ and $4^1\ 6^1$ band lifetimes. As noted in II.C., the lack of signal averaging equipment capable of resolving the rapid decay rates <u>may</u> have introduced a systematic error in Baronavski's results. This would have tended to make measured lifetimes for this part of his data longer than the actual ones. Correction for such a possible error would bring his measurements and mine closer together. It is interesting to note that the extrapolated zero-pressure <u>long</u> lifetime reported here $\tau_L(0)$,

is the same as the only lifetime seen by Baronavski. The significance of this, if any, is not clear.

As with the 0^0 band, Baronavski's highest pressure measurement for nitrogen laser excited lifetimes is several torr below my lowest pressure measurement. Unfortunately the non-linear extrapolation suggested for the 0^0 band is not a satisfying explanation here, since the Stern-Volmer plot already has one break evident for the $4^2\ 6^1$ and $4^1\ 6^1$ bands. Although I can find no theoretical justification for two changes in σ_S, such a condition would not be inconsistent with the lowest pressure values on the Stern-Volmer plots shown in this chapter (e.g. Figure (30)). In addition figure (27) illustrates that band intensity is not a linear function of pressure in the region in question. For these bands, too, new experiments are needed to unambiguously join Baronovski's lower pressure, poor resolution, lifetime values to those reported here.

c) Models

The lifetime data collected here for the low pressure bands is far too complicated to be described by the Stern-Volmer Equation(eq. 10). Two major problems are the existence of two decay rates, τ_S and τ_L, and the change in quenching cross section from σ_S at lower pressure to σ_S' at higher pressure.

This section discusses essentially qualitative models that can account for the two phenomena. There are still too many unknowns to make meaningful quantitative calculations using the models presented.

The 10Å bandwidth greatly reduced the probability that much fluorescence was observed from bands other than the one intended; however, since such a bandwidth covers many rotational lines and a few k sub-bands, it might be possible to construct an ad hoc model for a particular band which could explain the existence of both τ_L and σ_S'. This would require postulating different lifetime and different quenching parameters for different but closely spaced rotational levels. Such differences would not be unexpected since the lifetime of a single ro-vibrational level in formaldehyde is strongly dependent upon the energy separation between it and the levels of the predissociative intermediate state. That separation should vary almost randomly within some range. The individual ro-vibronic lifetimes of the 4^1 level measured by Baronavski did vary by a factor of almost two.

Although a theory which postulated the direct excitation of two rotational levels with different quenching rates and different lifetimes might thus plausibly explain the two-τ and two-σ phenomena, a new and ad hoc set of parameters must be hypothesized for each band that exhibits these characteristics.

This includes not only bands in H_2CO but in D_2CO and HDCO as well. A more universal explanation is desirable. Reasonable qualitatiave models of both phenomena can be found in two papers by Freed. The "step-ladder" model of Freed and Heller[36] can satisfactorily account for the slow lifetime τ_S, while Freed's theory of collision-induced intersystem crossing[31] presents the best explanation I have found for the saturation of quenching rates.

The step ladder model was developed for molecules larger than H_2CO where a series of closely spaced vibrational levels are present in the excited electronic state. If one of the levels were to be excited, collisions would cause the excitation to move stepwise down through the ladder of vibrational levels. Although this situation does not exactly obtain for formaldehyde, the theory can be qualitatively generalized to involve, for example, the various k sub-levels within a vibrational band.

The important feature of the step-ladder model for this discussion is that, given a sufficient number of collisions, the excited molecular system will reach a statistical equilibrium among the strongly coupled levels in the step-ladder. These levels might, in this case, be either a subset of the S_1 vibrational manifold, or the k structure of one or several vibrational modes. After equilibrium is achieved the lifetime

for all the coupled levels will be the same, and equal to an average, weighted over the Boltzman distribution, of all the collisionally coupled states' lifetimes. Since the general trend with decreasing energy in formaldehyde is toward longer lifetimes, and since the Boltzman distribution gives greater populations to the lowest energy levels, the equilibrium lifetime should be longer than that of the originally excited state, if that state is coupled to a lower set of levels. The equilibrated lifetimes will remain constant, independent of pressure unless some other, much weaker, collisional coupling can transfer energy to additional levels.

The qualitative features strongly suggest that τ_L is an equilibrium lifetime of the kind discussed by Freed and Heller.[36] There is evidence for strong collisional coupling between the $4^2\ 6^1$ and $4^1\ 6^1$ levels. There may be other couplings to the $3^1 4^2$ and 4^4 levels which are less than 17 cm^{-1} distant from the $4^2\ 6^1$ state. In addition there are $4^2\ 6^1$ k sub-levels within 10 cm^{-1} of the sub-level, or levels, excited by the nitrogen laser. Finally, a much weaker coupling between the $4^2\ 6^1$ and 4^1 and 0^0 levels is in evidence.

The quantitative discussion in the Freed-Heller paper was based upon "a simple model (used) to elucidate some of these qualitative effects"[36] (their italics). In particular the model assumed a single harmonic oscillator and therefore equally

spaced levels. The non-radiative lifetime was assumed to decrease linearly with increasing vibrational energy. It also assumed that each collision could change the molecular energy by only one quantum. Unfortunately the situation here is rather different. It is not known which states are actually coupled by the collisions, but regardless of whether they are J, K, or vibrational modes they are certainly not evenly spaced. In addition the lowest strongly coupled level is not known, thus the ground level of the effective oscillator in the model is not known. My efforts to apply the quantitative theory of the Freed-Heller paper despite these problems have yielded ambiguous results. More information concerning the collisional coupling would be needed.

Another, but perhaps less applicable, collisional model which can produce decay curves with two apparent rates is the quantum mechanical analog to the Stern-Volmer Equation developed by Nitzan, Jortner, Kommandeur, and Drent.[40] This shows that under certain conditions quantum beating between the S_1 levels and the densely packed levels of the intermediate state (I) involved in predissociation could produce a smooth two-rate decay without the oscillations usually associated with quantum beats.* This theory requires more special assumptions than the step-ladder model to mimic a two-rate behavior and is therefore

*See in particular curve IV in figure 3 of reference 40.

less likely to contain the desired universal explanation for the phenomena.

The following paragraphs discuss Freed's intersystem crossing theory[37] as a potential explanation for the abrupt change of quenching cross-section at pressures around 60 torr. His theory considers the case of a molecule that may radiate from an excited state or may be converted via collisions to another state or set of states which do not radiate. Collisions are described using the impact approximation. Instead of the Green's function approach used by Langhoff and Robinson in reference 41, Freed uses the more difficult density matrix approach because "The existing Green's function theories of electronic relaxation cannot readily be genaralized to incorporate the description of the randomly occurring collision induced transitions." In his formalism, then, the effect of collisions becomes a time independent part of the description of the system. If collisions broaden the (I) levels until they overlap to form a quasi-continuum, energy transfer to the (I) levels becomes irreversable; while for every S_1 energy level there will be a corresponding (I) level, almost all of the quasi-continuum of (I) states will not overlap an S_1 state. Thus a molecule in an S_1 state can cross to the (I) continuum but few (I) state molecules can cross back. In time the (I) state molecules dissociate.

The important point of the model, in this context, is that once that portion of the system density matrix which represents the (I) manifold becomes a continuum, an increase in the collision rate has little effect upon it, and the pressure dependence levels off. Freed[31] gives a broad condition for the appearance of this "saturation." In units where h does not equal one it is:

$$Z(\text{sec}^{-1}) \gtrsim [(.1 \rightarrow .01) \times 2\pi C)]/\rho(\text{levels/cm}^{-1}). \qquad (12)$$

Z is the inelastic collision rate and ρ in our case is the level density for the (I) state. Assuming that (I) is really composed of high-lying S_0 vibrations and using the theoretical level density ($10/\text{cm}^{-1}$) given by Houston and Moore[2] for S_0 near the S_1 origin, I calculate

$$Z \gtrsim (1.9 \rightarrow .19) \times 10^9 \text{ sec}^{-1}. \qquad (13)$$

For the geometric cross section at 400°K, equation (13) yields the pressure range in which the saturation should occur:

$$P \gtrsim 30 \rightarrow 300 \text{ torr}. \qquad (14)$$

This correlates quite well with the 60 torr where the short lifetimes become independent of pressure in the self quenching experiments. Therefore, not only does Freed's theory of collision induced intersystem crossing qualitatively reproduce the observed

deviations from Stern-Volmer behavior, but the observations are compatible with the theoretical level spacing of the S_0 manifold at those energies. This lends some support to the notion that the predissociation intermediate state is indeed a part of the high energy range of the ground (S_0) electronic manifold, since the triplet spacing is much wider and would therefore yield a much higher pressure for the change to σ_S'.

Freed's theory also predicts anomalous behavior of the fluorescence in a magnetic field. A properly designed experiment using this properly may be able to independently confirm whether this mechanism is operating in formaldehyde.

3. Measurement and Error Considerations

Discussion of my measuring techniques and error estimates for lifetime measurements is given below. First, several miscellaneous points are made, mainly to support the fact that the saturation in σ_S is real and not instrumental. This is followed by a description of the method used to correct for dispersion introduced by the delay cable between the pre-amplifier and the boxcar integrator. Finally, the significance of possible baseline errors in the decay curves is mentioned.

a) Miscellaneous

The significant deviations from normal Stern-Volmer behavior in my data must be proven to be real and not a function of the experimental apparatus. Strong confirming evidence is the presence of this type of behavior in the measurements made by C.B. Moore's group[8] on different bands in H_2CO and in D_2CO and HDCO. Those observations were made using different excitation mechanisms and were made on longer lived, and therefore more easily measured, states.

The change in the slope of the Stern-Volmer plots is not due to a speed limitation of the measuring electronics used here. When tracing the shape of the nitrogen laser pulse itself, the circuitry was able to respond well to a signal dropping at a rate three times faster than that at which the measured fluorescence decay rate maximized. If the decay rate had continued to increase with pressure, such an increase would thus have been detected.

Radiation trapping, which can have strong effects upon the apparent lifetimes of atomic states, is not important here since all observed transitions from S_1 are to excited vibrational levels of the ground state which are virtually unpopulated. Diffusion of molecules in or out of the volume of gas excited by the laser is also unimportant since even a collision-free molecule would move less than 5×10^{-3} cm in 100 nanoseconds;

i.e., less than the smallest dimension of the focused laser beam.

A glance at the decay curves will show that there is a significant increase in the noise on the logarithmic plot for lower intensity signals. This is a natural result of taking the logarithm. A small linear change when added to a strong signal will be insignificant when the logarithm is taken, but it may amount to a decade or more change when added to a weak signal. Consequently the error of individual long lifetime measurements is over 20% while the short lifetimes, where the fluorescence intensity is greater, have about 10% precision.

One reason commonly encountered for double decays is that there are two states initially excited and it is the sum of the fluorescence from both states that is actually measured. Reasons why this is probably not the case here have already been discussed, the primary one being Baronavski's single line excitation of the 4^1 state in H_2CO: double decays occurred even when the excitation bandwidth was narrow enough to insure that only a single ro-vibronic state was excited. The possibility that the nitrogen laser excites two or more levels with different lifetimes cannot, however, be completely ruled out. Analysis of the data using that assumption requires digitizing the decay curves for each pressure and band. The result of such an analysis would be to greatly increase the decay rate for the higher pressure measurements. This would not, however,

eliminate the distinct change between σ_S and σ_S'.

The two-state type of analysis was made for several decay curves and it was found that the measured transition between the curves represented by τ_S and τ_L was somewhat too sharp to be modeled in that way. For all the above reasons the slopes ($1/\tau_S$ and $1/\tau_L$) measured directly off the logarithmic decay curves were assumed to represent the actual lifetimes, after they had been corrected for the cable dispersion.

b) Correction for Cable Dispersion

The most important systematic error in the raw data is due to the use of a ∿100 ft. coaxial cable to delay the photomultiplier signal before it was processed by the boxcar integrator. The integrator could not accept signals less than 100 nanoseconds after it was triggered. (It should be noted, however, that because its timing circuits are stable to better than 100 picoseconds, there is no loss in timing accurace due to this delay.) In addition to delaying the signal, the cable causes dispersion. Figure (36) shows the effect of this upon a measurements of the nitrogen laser pulse. The impulse response for the measuring system can be derived by comparing the measurements illustrated by figure (36), which were made using a fast oscilloscope (Tektronix 7603), and those of the nitrogen laser pulse made using the Ortec preamplifier, 100 feet of cable, and

FIGURE (36): Effect of Cable Dispersion on a Measurement of the N_2 Laser Pulse. The two curves are tracings from oscilloscope photographs: (a) shows the signal that was presented to the boxcar integrator, having been delayed by 100 feet of RG-58U cable, (b) shows the photomultiplier signal without the cable delay.

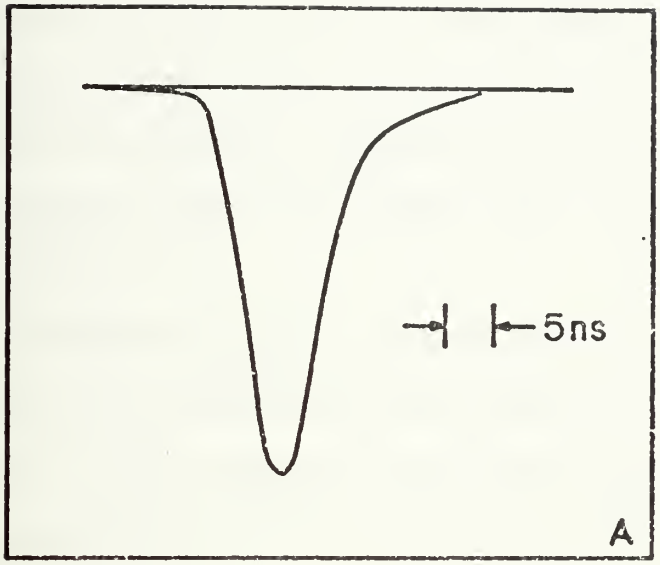

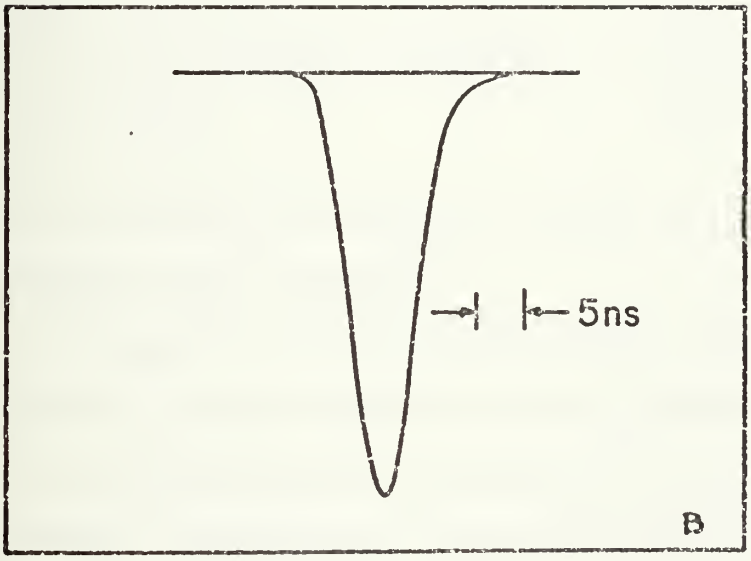

FIGURE (36)

the boxcar integrator. This response can be approximated by a time constant of 4.4 nanoseconds. The actual impulse response is not a simple function, but the first decade of the electronically measured rise and decay of a nitrogen laser pulse can be satisfactorily modeled using an exponential impulse response. This will be shown later and illustrated by figure (37).

The observed decay curves are a convolution of the actual decay curves with the impulse response of the measuring electronics. If the laser excitation were impulsive the measured fluorescence signal should be proportional to the convolution integral,

$$h(t) = \int_0^t e^{-(u/\tau_f)} e^{-(1/\tau_e)(t-u)} du = \frac{e^{-t/\tau_f} - e^{-t/\tau_e}}{1/\tau_e - 1/\tau_f} \qquad (15)$$

where τ_f is the actual fluorescence lifetime and τ_e is the time constant of the electronics.*

From equation (16) it can be seen that a measurement will yield the true fluorescence rate if it is made at a time after the excitation which is long compared to the electronic time constant. Unfortunately, it was not possible to wait

---

*This dispersion induced time constant should not be confused with the exponential averaging time constant set on the boxcar mainframe, which should not cause a distortion of the signal.

that long due to the weakness of the fluorescence and the emergence of the second radiative lifetime about 30 nanoseconds after the excitation. Therefore, the short lifetime had to be measured when the electronic time constant was still affecting that measurement. An additional complication was caused by the fact that fluorescence was not excited by an impulse, but by an eight nanosecond (FWHM) laser pulse.

A numerical model of the measurement process was constructed and evaluated using a Hewlett Packard 65 programmable calculator. The laser pulse was approximated by a triangle function with the same width as the actual pulse. It was found that a triangle function was sufficient to match the observed response to a laser pulse over a decade of intensity around the peak (figure (37)).

The calculation proceeded according to the following algorithm: the time for which the model fluorescence intensity was to be calculated was fixed. Then the convolution integral was evaluated for each point of the triangle function and weighted by the assumed laser intensity for that point. All the values of h were summed and the natural logarithm was taken. This result (up to an additive constant) yielded the logarithm of the modeled fluorescence intensity at the fixed time. The logarithmic decay curve is the locus of such values for different times.

FIGURE (37): Model Prediction of Nitrogen Laser Pulse Measurement. The laser pulse was assumed to be a triangle function with an 8 nanosecond full width at half maximum. It was convoluted with an exponential approximation to the instrumental impulse response function. The model matches the actual measurements well, for over a decade in intensity. This figure is shown to demonstrate the ability of the model to account for intensity changes more rapid than any encountered in the fluorescence decay curves.

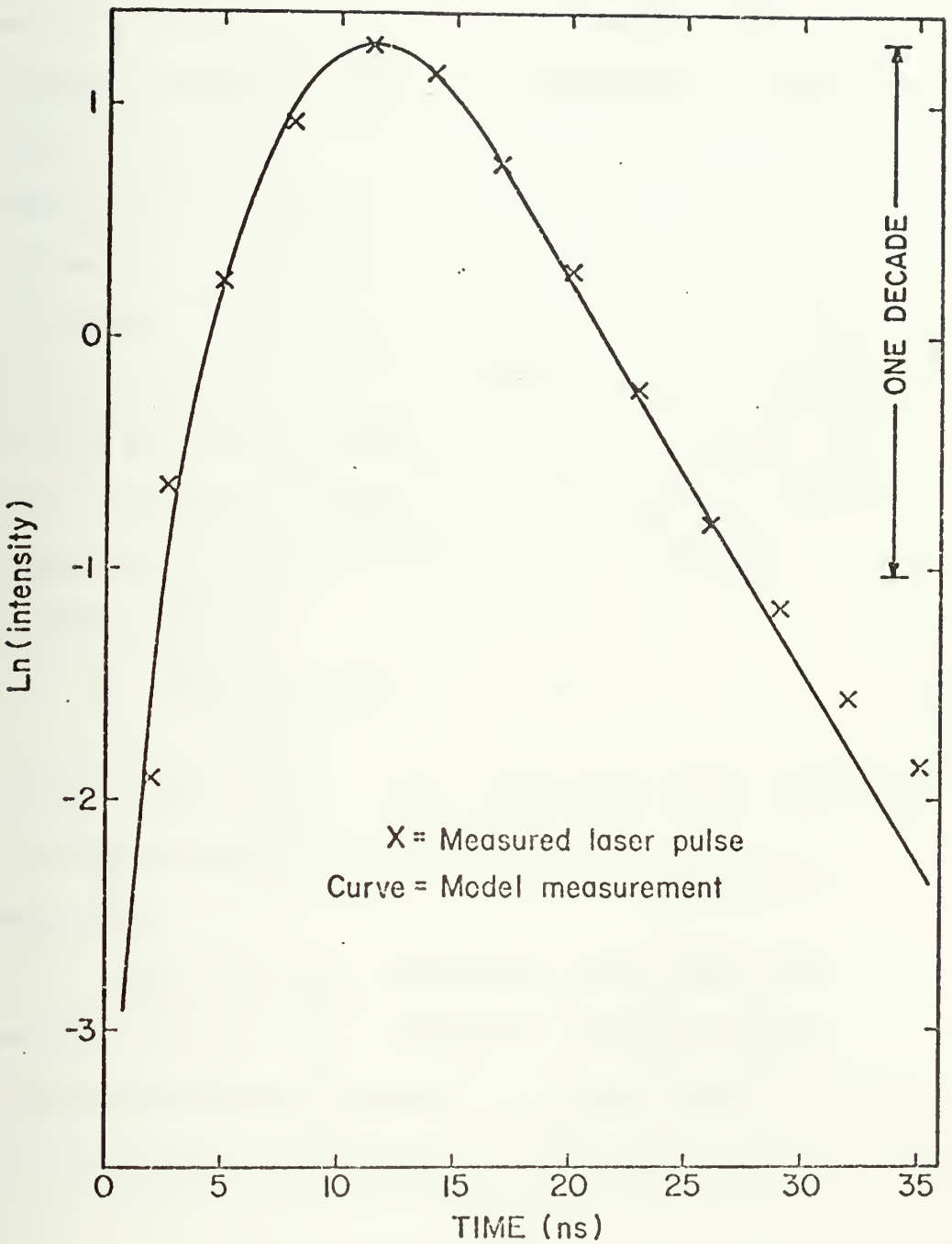
Ln (intensity)
1
0
-1
-2
-3
0
5
10
15
20
25
30
35
TIME (ns)
ONE DECADE
X = Measured laser pulse
Curve = Model measurement

FIGURE (37)

Having satisfactorily modeled the detection systems's response, the next step was to find a means of adequately correcting the data to remove cable dispersion. For this purpose, a number of model decay curves were calculated and compared to actual measurements which had similar τ_f. One of the curves is shown in figure (38). The apparent decay rate of the model curves was then read off for the same time period in which the actual measurements had been made. The apparent rate for all cases was (within one percent) the same as that value calculated by adding τ_f and τ_e in quadrature. For this reason I have corrected all lifetime values using the following equation:

$$\tau_f = \sqrt{\tau^2_{\text{measured}} - \tau^2_e} \; ; \quad \tau_e = 4.4 \text{ ns} \; . \tag{16}$$

This correction amounts to about nine percent for a lifetime of 10 nanoseconds and less than one percent for one of 30 nanoseconds.

The model is very insensitive to the form of the excitation function. For example the difference between modeled measurements calculated for a single impulse excitation and those using a triangle function excitation is only one percent.

FIGURE (38): Modeled Lifetime Measurement.

This displays the logarithm of a modeled fluorescence curve measurement calculated by the algorithm given in the text. The log of the exciting triangle function is also shown. The assumed ("true") fluorescence lifetime was 20 nanoseconds and the instrumental time constant was 4.4 nanoseconds. For real measurements with a similar τ_s the short lifetime was determinable only between about 28 to 58 nanoseconds after the initial rise of the fluorescence curve. A least square fit to the model points between these times (arrows) yields a measured lifetime of 20.47 nanoseconds. The sum, in quadrature, of true fluorescence and instrumental time constants gives 20.48 nanoseconds.

The time scale here is greatly expanded relative to that of the fluorescence curves shown, for example, in figure (30).

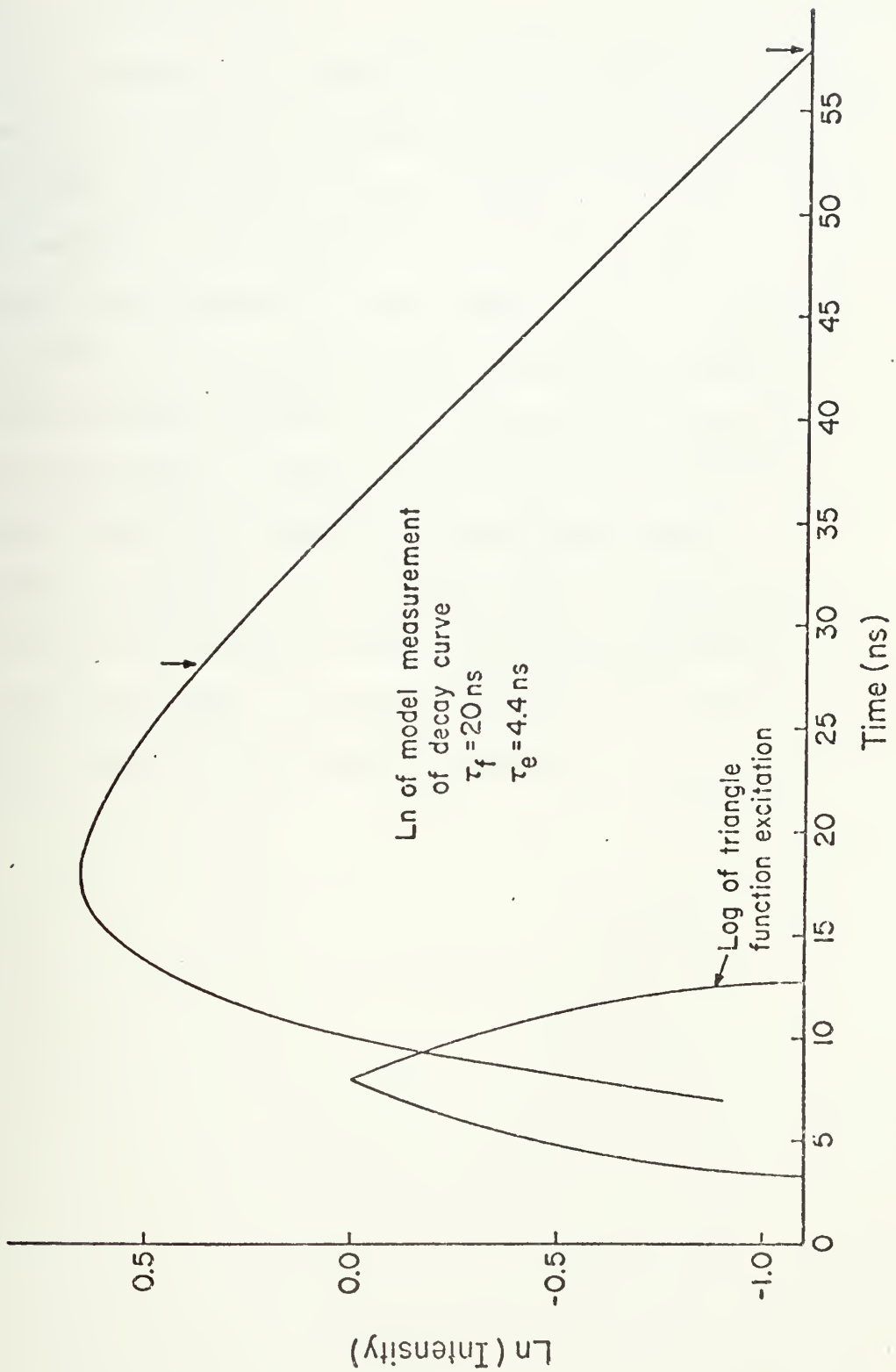
Ln (Intensity)
0.5
0.0
-0.5
-1.0
0
5
10
15
20
25
30
35
40
45
50
55
Time (ns)
Ln of model measurement
of decay curve
τ_f=20 ns
τ_e=4.4 ns
Log of triangle
function excitation

c) Baseline Error

Another form of error in the lifetime measurements was caused by the problem of establishing the proper baseline for the decay curves. Small errors in setting the baseline of the log amp input are the principle reasons for the scatter of points in Stern-Volmer plots shown here. Because of the small possibility of a systematic error in baseline setting, a maximum possible deviation of 1.5 nanoseconds for τ_S and 3.0 nanoseconds for τ_L has been added in quadrature to the standard deviations listed on the Stern-Volmer plots to produce the probable errors listed in table V. This value was arrived at by noting the worst case error encountered in early data taking. No baseline correction is required for the errors in cross section measurements.

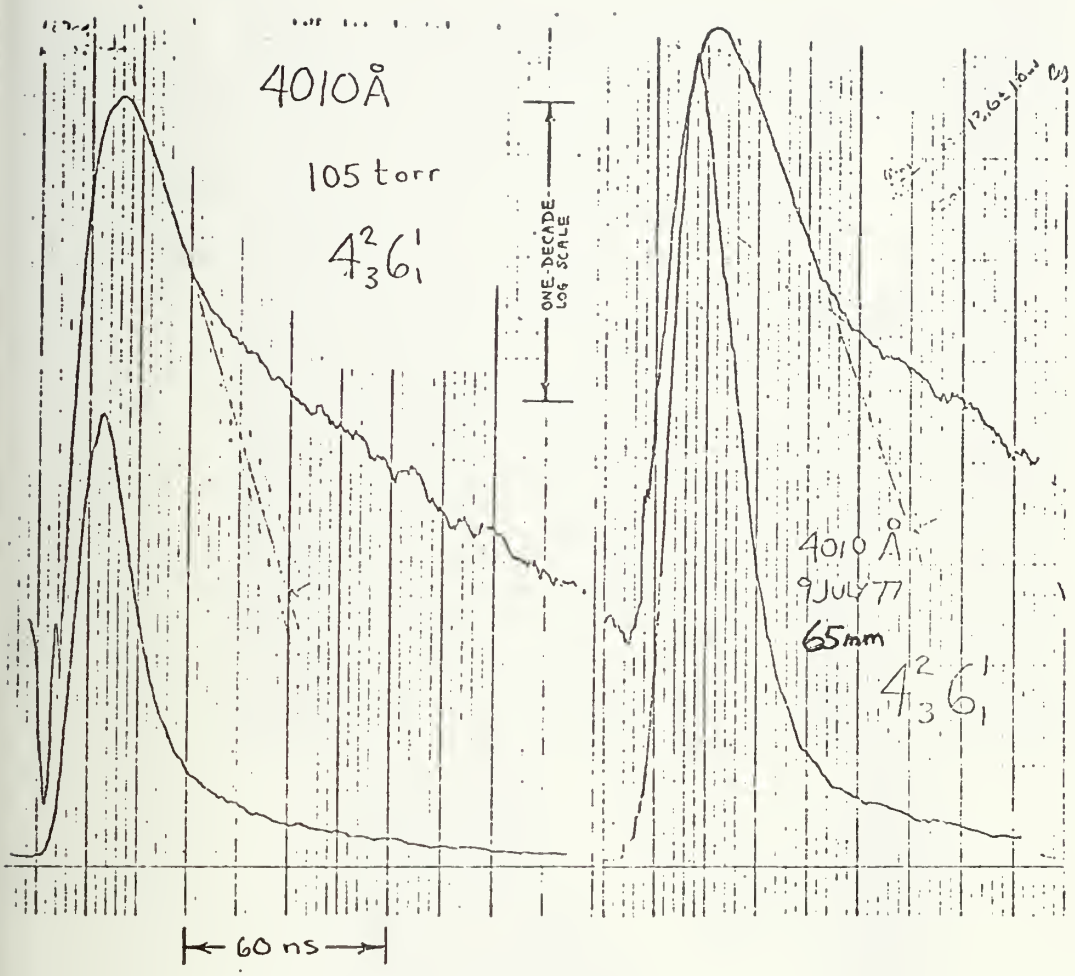

FIGURE (39): Decay Curves for 4010Å Band.

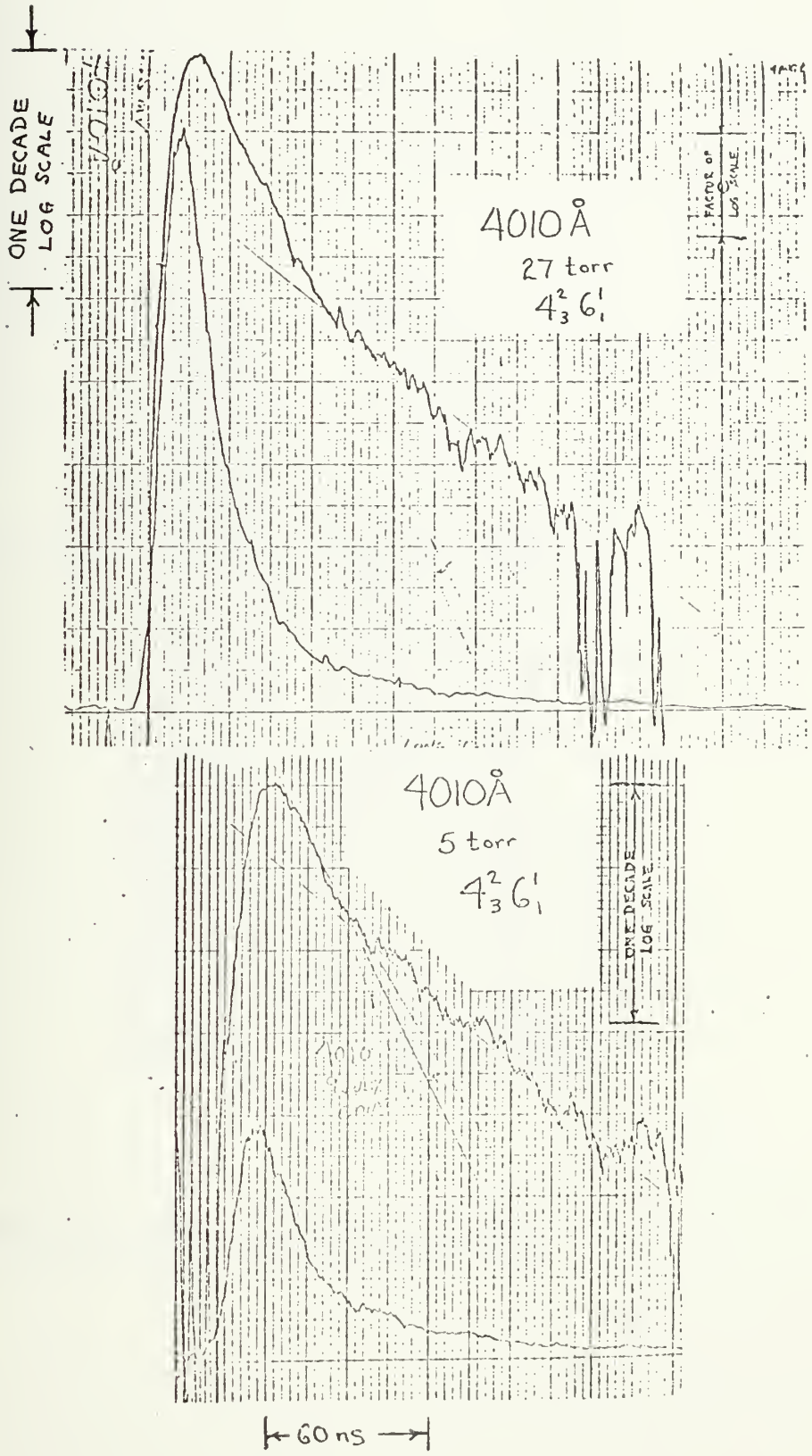

FIGURE (39): continued

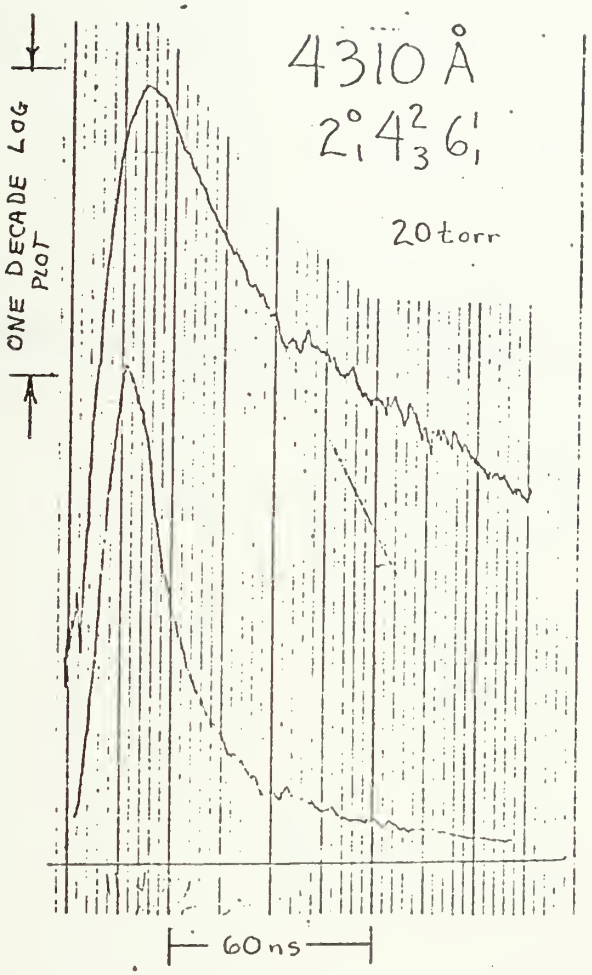

FIGURE (40): Decay Curve for 4310Å Band.

FIGURE (41): Decay Curve for 4390Å Band.

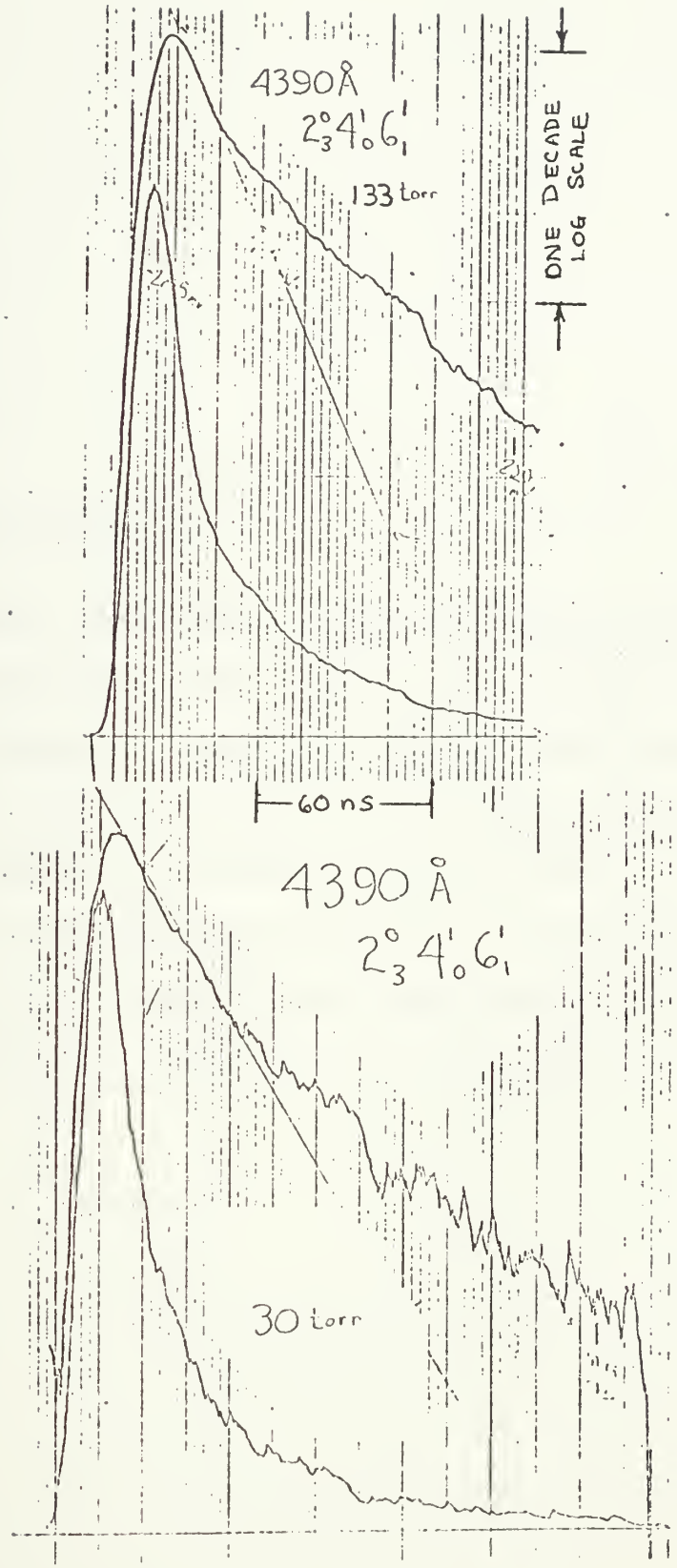
4390Å
$2_3^{\circ}4_0^{\prime}6_1^{\prime}$
133 torr
ONE DECADE
LOG SCALE
60 ns
4390 Å
$2_3^{\circ}4_0^{\prime}6_1$
30 torr

FIGURES (42) through (47):

The figures that follow show the plots from which the data in Table V was abstracted. The points have been corrected for the cable dispersion. Solid lines represent least square fits to the points. The error limits listed are one standard deviation calculated only from the scatter of the fit. Other factors have been considered in the final error estimates listed in Table V. The pressure scale for argon quenching plots is compressed relative to that for self-quenching ones.

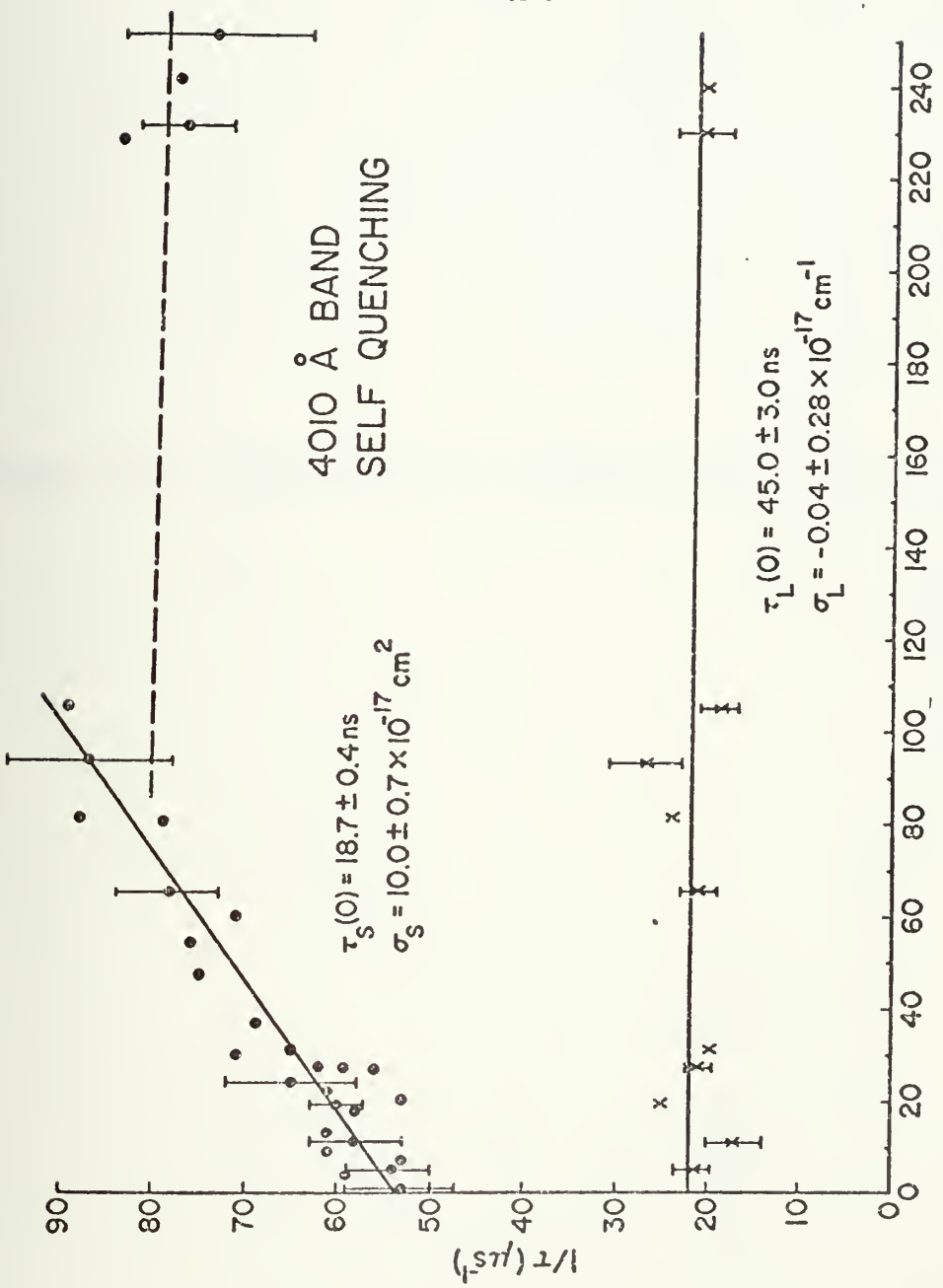

FIGURE (42): Stern-Volmer Plot; 4010Å Band Self Quenching

FIGURE (43): Stern-Volmer Plot; 4010Å Band Argon Quenching

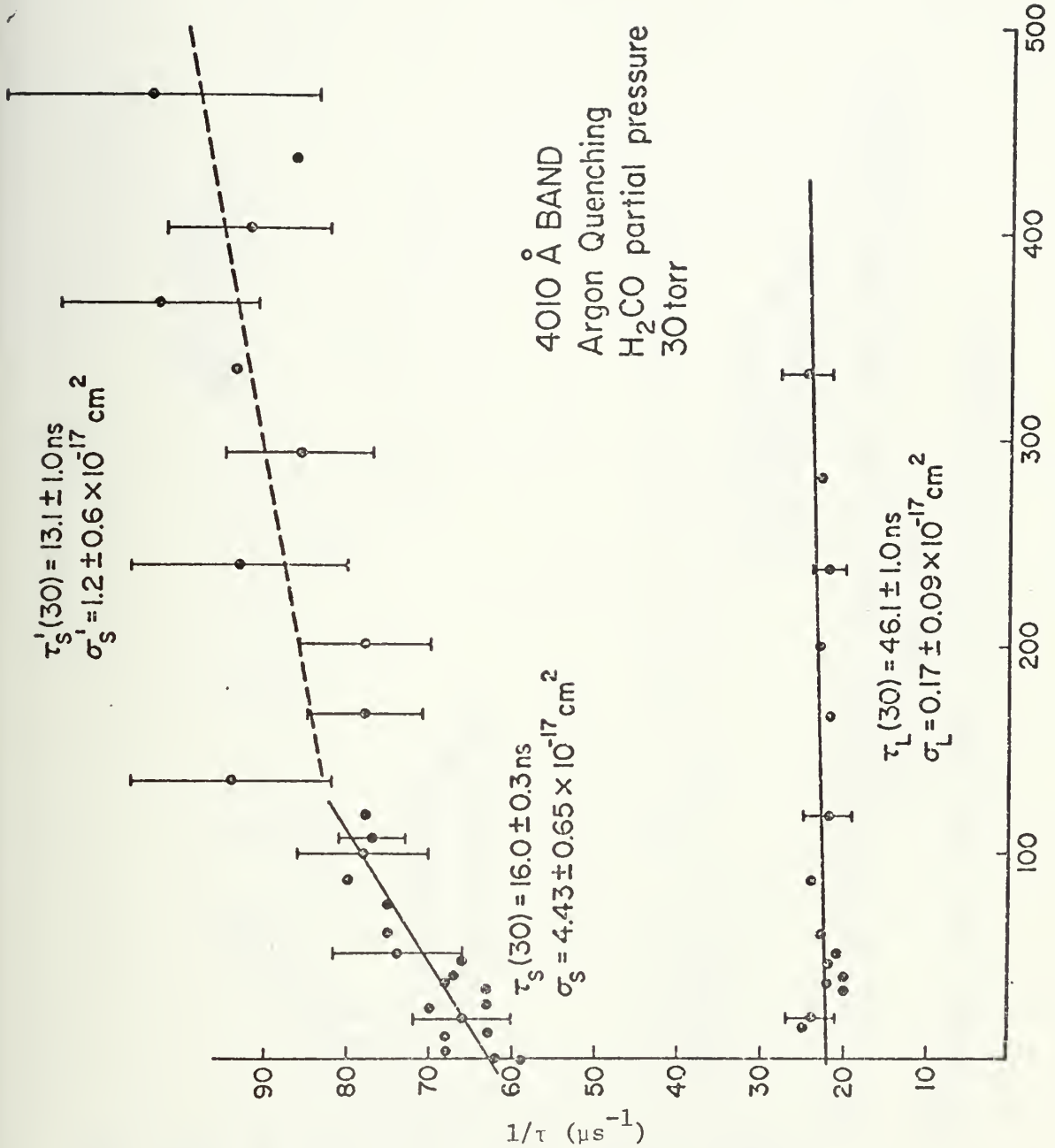
4010 Å BAND
Argon Quenching
H_2CO partial pressure
30 torr
$\tau_s'(30) = 13.1 \pm 1.0$ ns
$\sigma_s' = 1.2 \pm 0.6 \times 10^{-17}$ cm^2
$\tau_s(30) = 16.0 \pm 0.3$ ns
$\sigma_s = 4.43 \pm 0.65 \times 10^{-17}$ cm^2
$\tau_L(30) = 46.1 \pm 1.0$ ns
$\sigma_L = 0.17 \pm 0.09 \times 10^{-17}$ cm^2
$1/\tau$ (μs^{-1})
Argon Partial Pressure (torr)

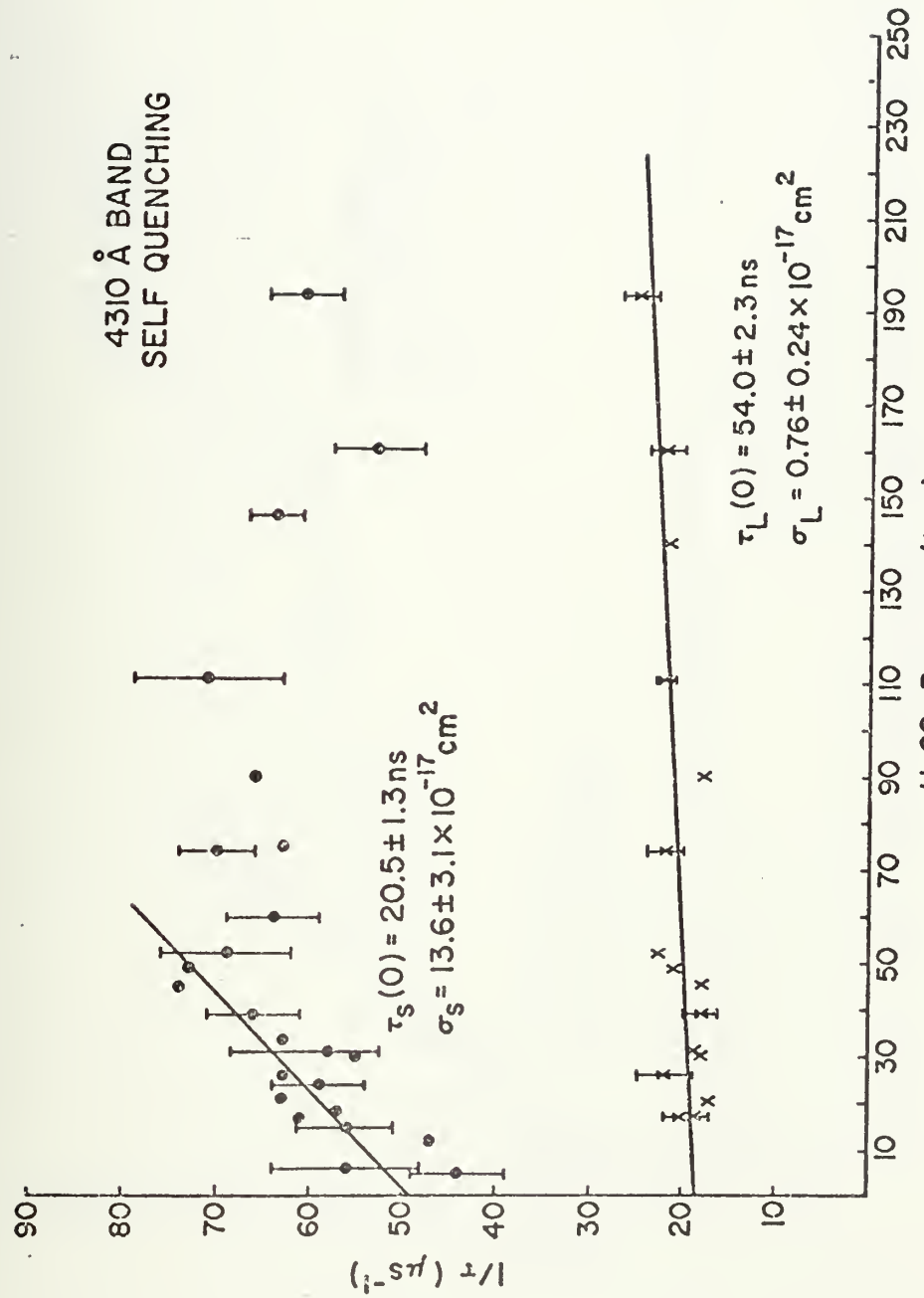

FIGURE (44): Stern-Volmer Plot; 4310Å Band Self Quenching

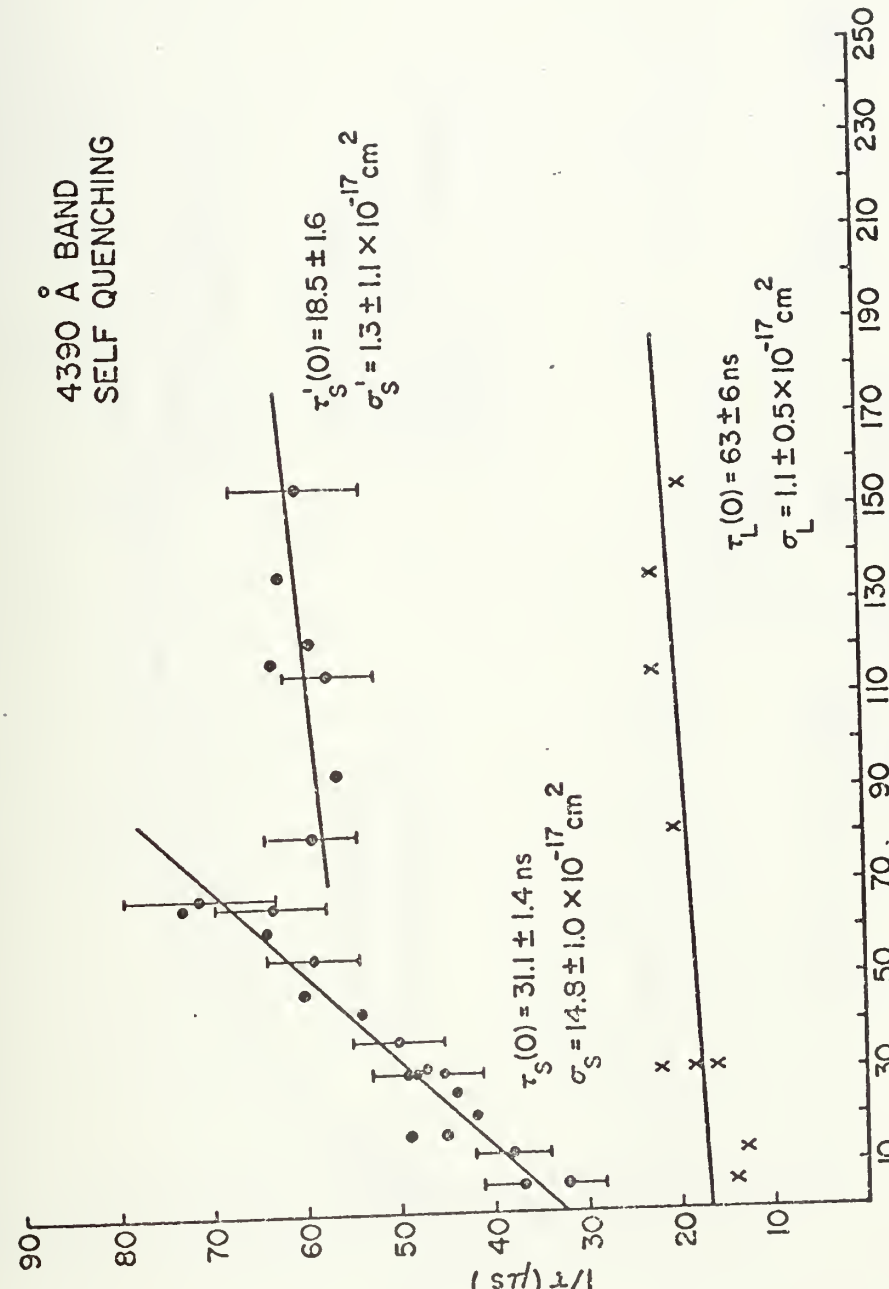

FIGURE (45): Stern-Volmer Plot; 4390Å Band Self Quenching.

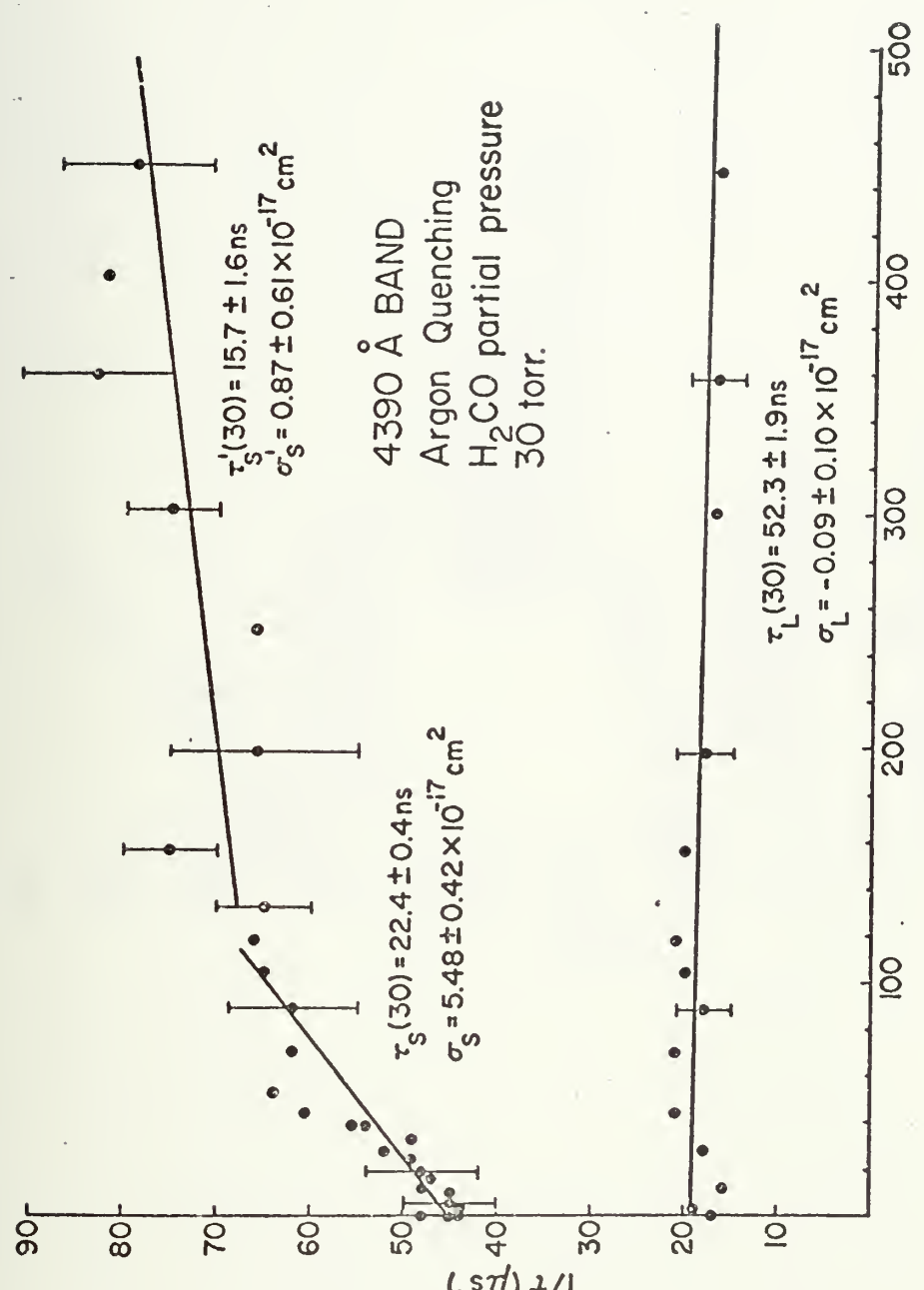

FIGURE (46): Stern-Volmer Plot; 4390Å Band Argon Quenching, 30 Torr H_2CO

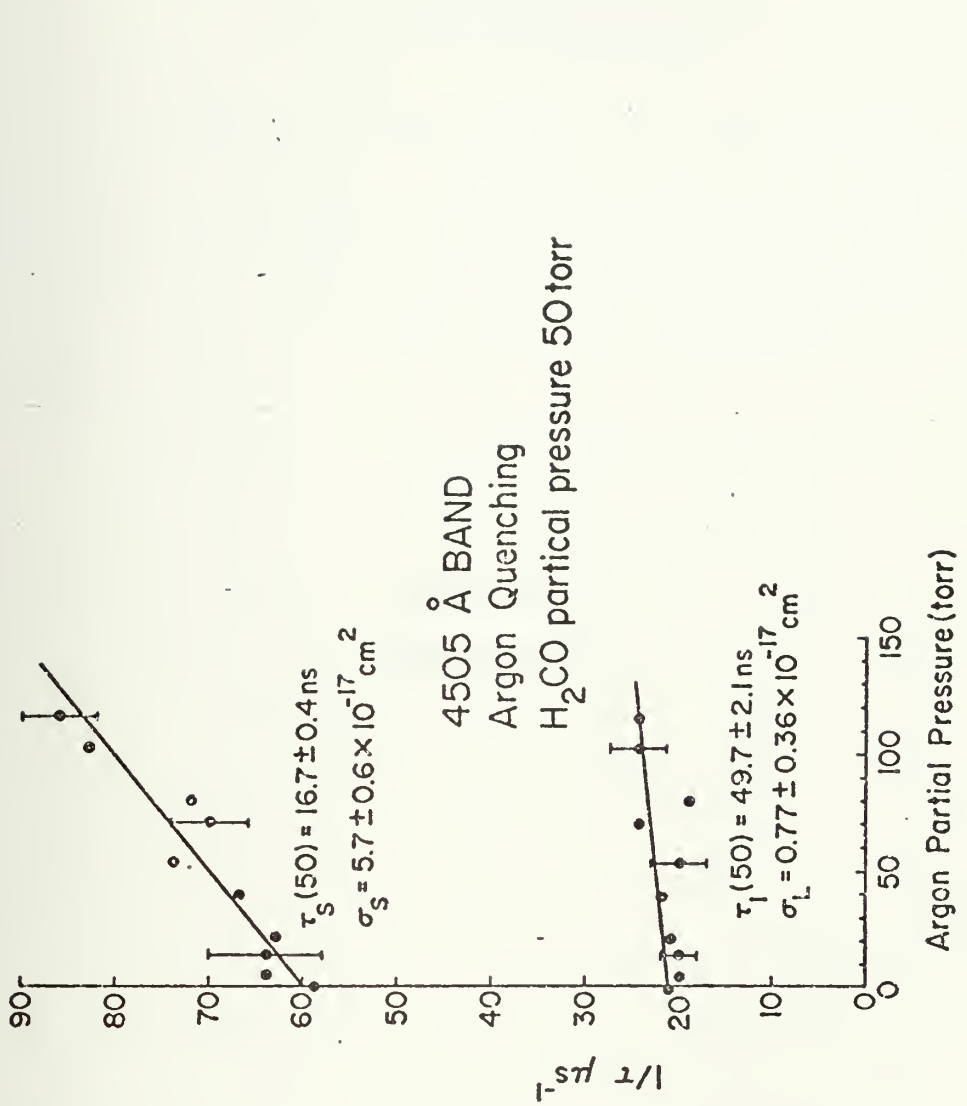

FIGURE (47): Stern-Volmer Plot; 4505Å Band, Argon Quenching

CHAPTER V

CONCLUSIONS

V.A. APPARATUS IMPROVEMENTS

The experiments reported here can be improved and extended given significant changes in the apparatus. Improvements are possible both in the laser power and in the data collection system. These and attendant improvements are discussed below.

100 kilowatts of laser power does not come close to saturating the formaldehyde absorption, and more power will provide more fluorescence. In view of the faint images which appeared on the 127-04 photographic plate, an increase of fluorescence intensity by a factor of five should provide enough light to obtain photographic spectra of some of the high pressure bands beyond 5000Å. Increased power would allow better resolution of the low pressure bands which would assist in their identification. More power would also allow extension of the Stern-Volmer plots to lower pressures, and improve the signal to noise of the individual decay curves. In addition it would make more attractive the idea of using a Fabry-Perot cavity to provide single nitrogen laser line excitation.

Commercial nitrogen lasers, between five and ten times more intense than the home-built prototype used here, are available, but expensive. Unfortunately, however it may be obtained, higher power will compound the problem of sludge

formation on the windows where the laser beam enters and exits the cell.

The resolution of the photoelectric spectra could be greatly enhanced by digital collection methods. The analog exponential averaging system provided by the PAR 162 boxcar integrator requires continuous spectral scanning and is limited by the gain of its amplifiers. In contrast, a spectrometer with a stepping motor drive, combined with a photon counting system, or other digital storage schemes, can provide as much resolution as the experimentor has time for. Such a digitized system would also be capable of subtracting repetitive background signals caused by the laser radio-frequency firing noise. This could improve the signal to noise of the fluorescence decay curves taken at low pressure.

Any extension of the lifetime or spectral studies to lower pressure would require a number of modifications to the fluorescence cell. Methods to direct more of the fluorescence light emitted into the spectrometer would need to be devised, and a new pressure monitoring system would have to be developed.

The measurements reported here represent the best that can be accomplished with the present system. In addition to providing the information reported above, they were necessary to determine what further improvements in apparatus might be needed to extend such measurements.

V.B. SUMMARY

This dissertation has reported measurements made of the fluorescence resulting from nitrogen laser excitation of H_2CO vapor at pressures between one and 760 torr. The spectra observed at about 760 torr have been photographed and measured photoelectrically. These observations have supplemented Brand's measurements for emission bands originating in the 4^1 and 0^0 levels and extended the identification of these band systems beyond 5000Å. It has been shown that further extensions are possible and desirable.

Photoelectrically detected spectra of the fluorescence from formaldehyde at pressures below 100 torr revealed an entirely new band structure. Over 25 new bands have been observed and tentatively identified, all originating in either the $4^2\ 6^1$ or $4^1\ 6^1$ levels. The variation of the band intensity with pressure appears to indicate a strong collision-dependent coupling between these two levels.

Measurements of the fluorescence decay curves for several bands have been made using an observation bandwidth twenty times smaller than that of any previous measurements. The spectral studies reported here show that the 10Å used here is close to the maximum bandwidth that can unambiguously separate the $4^2\ 6^1$ and $4^1\ 6^1$ bands. Both levels exhibit two

decay rates and the more rapid rate becomes independent of pressure above about 60 torr.

Similar behavior is found when argon is introduced as a buffer gas and its partial pressure is changed. Possible explanations of these phenomena have been suggested but no quantitative model of this behavior can reasonably be constructed due to the large number of unknown parameters involved. Finally, the lifetime versus pressure data reported here cannot be joined smoothly to that taken by Baronavski at lower pressure but with a much larger bandwidth. New spectrally resolved measurements of nitrogen laser excited fluorescence lifetimes are needed between 0.5 and 10 torr, as well as a determination of which ro-vibronic state (or states) are excited by the nitrogen laser.

APPENDIX: NITROGEN LASER

APPENDIX

THE NITROGEN LASER

This appendix discusses the construction of the nitrogen laser used in these experiments. A brief introduction to the physics of the lasing action in nitrogen is followed by a description of the electrical and mechanical configuration of this laser. The advantages and drawbacks of the present design are discussed and a number of references are provided.

Electron impact with nitrogen molecules can preferentially populate the $C^3\Pi_u$ electronic level relative to the $B^3\Pi_g$ level if the electron temperature is high enough. The radiative transition that subsequently occurs between the C and B levels has a lifetime of about 40 ns. Since the B level has a decay time of about six μs., the population in that state will rapidly build up and destroy the population inversion. This quenches the lasing. If lasing on the C→B transition is to occur at all, an extremely rapid excitation of the C state must be provided. This requires that the electric discharge circuit of the laser must have as low an inductance as possible. In order to provide a large number of high temperature electrons to generate the nitrogen excitation, high capacitance and high voltage are required as well.

FIGURE (48): Nitrogen Laser Cross Sectional View.

The laser and capacitors are completely immersed in transformer oil. The bandsaw blade electrodes are clamped in heavy aluminum bars which are attached to the high voltage plates of the capacitors. The $BaTiO_3$ slugs are clamped in a sandwich which includes, from top to bottom: a flat pressure plate, the 0.05 cm thick aluminum sheet that serves as the upper ground plane, one ceramic capacitor slug, a polished aluminum bar serving as the high voltage capacitor plate, a second slug, and the lower ground sheet. The clamps are "U" sections of aluminum extrusion which have been drilled and tapped for the clamping screws. Mylar strips were punched and forced over the slugs to prevent the formation of carbonized particle-trails on the sides of the slugs which would provide a conductive path for arcing. Nitrogen enters the discharge region from the upper plenum and is evacuated through the lower one to provide transverse gas flow.

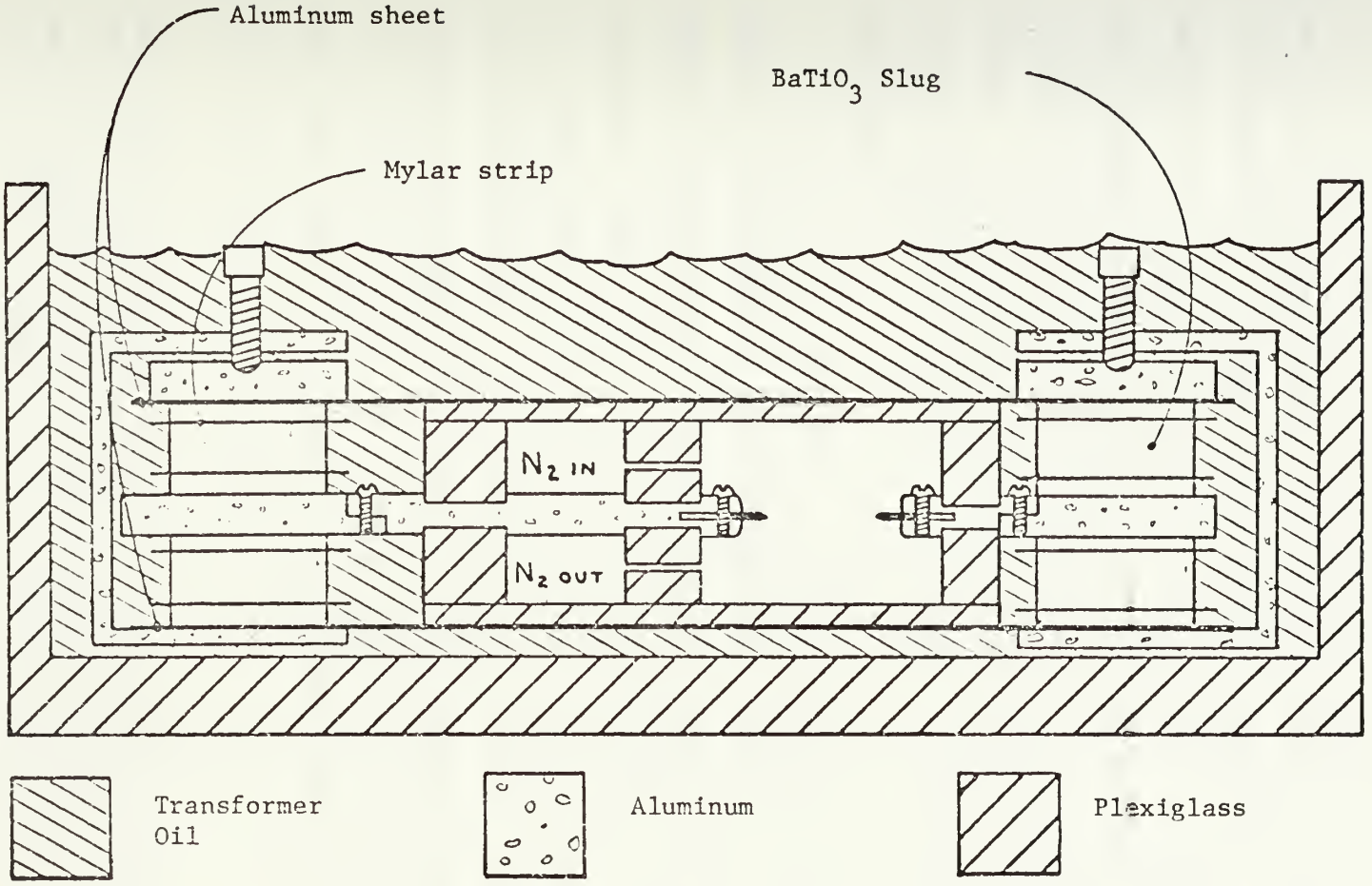
Aluminum sheet
$BaTiO_3$ Slug
Mylar strip
N_2 IN
N_2 OUT
Transformer Oil
Aluminum
Plexiglass

In 1973 Nagata and Kimura[59] showed that the use of barium titanate capacitors would significantly reduce the size of a Blumlein type nitrogen laser without decreasing the energy storage capacity or speed. The capacitors as commercially packaged however, have very narrow connectors which contribute unnecessarily to the inductance of the discharge circuit. The prototype laser used for the experiments related in this dissertation was built in an attempt to reduce this inductance.*

Bare, unencapsulated barium titanate cylinders were obtained from Sprague Electric Corporation. They were clamped between aluminum plates to form the energy storage capacitance as shown in figure (48). The laser has 92 such $BaTiO_3$ cylinders, 1.5 cm high and 2.5 cm in diameter, spaced along both sides of the laser channel. The channel length was 100 cm. Each cylinder has a nominal capacitance of 650 picofarads; however, when placed in the laser the measured capacitance per cylinder was greater than 1000 picofarads. Figure (49) illustrates the circuit diagram of the laser.

---

*This laser was initially constructed for use as a dye laser pump and has performed satisfactorily in that role. It has been used to pump a cresyl violet-rhodamine B dye mixture in a laser which produced a 200 watt, 0.01Å bandwidth, 6400Å wavelength output. This was used to measure the oscillator strength (2×10^{-12}) of a single ro-vibronic transition between the 0 and 5 ν_3 ground state vibrational levels of acetlyene.

FIGURE (49): Laser Circuit Diagram.

This is the standard Blumlein circuit with the addition of a second set of capacitors placed above the laser tube. Both the left and right electrodes (arrow heads) are initially charged to high voltage. Firing the thyratron grounds the right-hand electrode while the impedance of the inductor holds the left-hand electrode at high potential. The resulting breakdown of the nitrogen gas in the laser channel causes a population inversion and lasing. The upper capacitors and ground plane serve to decrease the discharging inductance by producing symmetric current flow, increase the capacitance per unit length, provide electrical safety by reducing access to the high voltage portions of the circuit, and reduce radio frequency noise emitted by the discharge

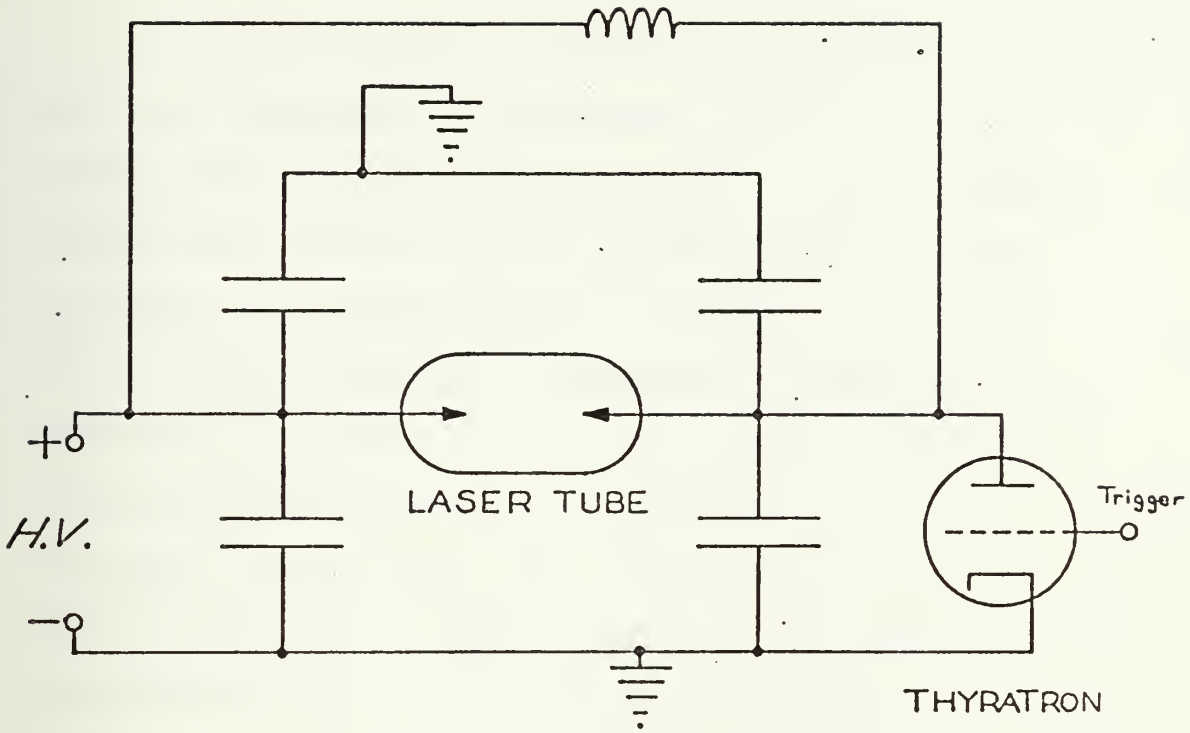
+
H.V.
−
LASER TUBE
Trigger
THYRATRON

An air gap between the ground and high voltage electrodes of 1.5 cm (that required by the capacitor size) is not sufficient to stand the high voltage necessary to provide high power nitrogen laser operation, so that additional insulation had to be provided. After exploring several methods, a decision was made to completely immerse the laser channel and capacitor structure in transformer oil. Even so, considerable difficulty was experienced with arcing across the capacitor slugs after a few hours of running time. This was traced to the formation of tiny carbon particles made by microscopic arcs between the $BaTiO_3$ slugs and the contacting electrode surfaces. These particles would migrate in the oil along the field gradient on the capacitor surfaces until a conducting path was was built up and a major short circuiting arc developed. The problem was cured by the use of thin mylar guards to prevent the migration of the carbonized particles next to the capacitors. To effect this, the cylinders were forced through holes punched in mylar strips, placed near the tops and bottoms of the slugs. (See figure (48)).

Test sections of this type of capacitor configuration have been subjected to over 10^6 pulses at 20 KV with no sign of deterioration. The laser itself has operated for 590 hours at a voltage averaging about 14 KV and at 15 pulses per second. This amounts to a total of 3×10^7 pulses on each of the 92

ceramic slugs without a single capacitor failure. An added advantage to the discrete unencapsulated ceramic capacitors is that if a failure occurs, the individual cylinder can be sand-blasted to remove the surface conduction path and then it can be reused.

After this laser was completed, a paper was published by C.L. Sam[60] involving a similar design inspired by the work of Nagata and Kimura. This article discusses several design features independently discovered during the construction of the laser reported here, including the advantage of using a low-reflectance output coupling mirror. Sam's design involves the use of silicone potting compound around the capacitor slugs, and this has apparently proven to be more subject to arcing than transformer oil in the long run.[61] The reader is referred to reference 60 for further details on the design of ceramic capacitor lasers.

A serious safety problem present with the Blumlein design is that the N_2 gas is in essence <u>always</u> exposed to high voltage, not just when the discharge takes place. If the gas pressure is inadvertantly lowered, it is possible that current can flow through the low pressure nitrogen down the input and output gas lines, thus creating an extreme shock hazard. Very long gas hoses and careful attention to grounding them can reduce this danger.

It is interesting to notice that this laser which is 100 cm long could produce, under the best conditions, only a little more than three times the power of the 10 cm laser reported by Sam.[60] (500 KW peak vs. 170 KW.) Part of the better performance of the smaller laser may be due to an improved thyratron and more care in matching the thyratron impedance to that of the circuit, but there is a general trend in the literature which indicates that longer nitrogen lasers do not perform as well as simple linear scaling might suggest.

Intermittent, extremely intense pulses at very low N_2 flow rates suggest that a preionization scheme similar to that reported by Levatter and Lin[62] might increase the output of this laser by over a factor of two.* Investigation of the cause of the occasional giant pulses was delayed in order to conduct the experiments reported in this dissertation. Provisions have been made in the laser design to allow preionization experiments but they have yet to be conducted. The anomalous pulses did not occur at the laser pressure and flow rate used in the formaldehyde experiments.

As an entry into the literature, the best review, that I have encountered of nitrogen laser theory and construction can be found in a paper by Fitzsimmons, Anderson, Riedhauser,

---

*This paper is also of interest because of its comments concerning the lack of traveling wave excitation in nitrogen lasers of the Blumlein design.

and Vrtilek of the University of Wisconsin.[63] Additional useful articles on nitrogen lasers are listed as references 64 through 74.

REFERENCES

1. Yeung, E.S., Moore, C. Bradley, J. Chem. Phys., 58, 3988 (1973).

2. Houston, P.L., Moore, C. Bradley, Lawrence Berkeley Lab - 4913 preprint (1976).

3. Clark, J.H., Haas, Y., Houston, P.L., Moore, C.B., Chem. Phys. Lett. 35, 82 (1975).

4. Houston, P.L., Optical Engineering, 13, 489 (1974).

5. Koren, G., Oppenheim, U.P., Tal, D., Okon, M., Weil, R. Appl. Phys. Lett. 29, 40 (1976).

6. Allegrini, M., Johns, J.W.C., McKellar, A.R.W., Herzberg Institute of Astrophysics, preprint (1977).

7. Rank, D.M., Townes, C.H., and Welch, W.J., Science 174, 1083 (1971).

8. Baronavski, A.P., Dissertation U.C. Berkeley (1976), University Microfilm order number 77 4371.

9. Baronavski, A.P., Hartford, A., Moore, C.B., J. Mol. Spect. 60, 111 (1976).

10. Jeunehomme, M., Duncan, A.B.F., J. Chem. Phys., 41, 1692 (1964).

11. Sakurai, K., Capelle, G., Broida, H.P., J. Chem. Phys. 54, 1412 (1971).

12. Aoki, T., Morikawa, T., Sakurai, K., J. Chem. Phys. 59, 1543 (1973).

13. Andreyev, S.V., Antonov, V.S., Knyazev, I.N., Letokhov, V.S., Chem. Phys. Lett. 45, 166 (1977).

14. Brand, J.D.C., Reed, R.I., J. Chem. Soc. (London) 1957, 2386 (1957).

15. Yeung, E.S., Moore, D.B ., J. Chem. Phys. 60, 2139 (1974).

16. Brand, J.C.D., Trans. of the Faraday Soc. 46, 805 (1950).

17. Brand, J.C.D., J. Chem. Phys. 19, 377 (1951).

18. Brand, J.C.D., J. Chem. Soc. (London), 1956, 858 (1956).

19. Robinson, G.W., DiGiorgio, Can. J. Chem. 36, 31 (1958).

20. Moule, D.C., Walsh, A.D., Chemical Reviews 75, 67 (1975).

21. Herzberg, G., Molecular Spectra and Molecular Structure Vol. III: Electronic Spectra of Polyatomic Molecules, (Van Nostrand Reinhold; New York) p.2, 518 (1966).

22. Levine, I.N., Molecular Spectroscopy (Wiley; New York) p. 53ff.

23. Herzberg, G., op. cit. p. 132.

24. Job, V.A., Sethuraman, V., Innes, K.K., J. Mol. Spect. 30, 365 (1969).

25. Herzberg, G., op. cit., see footnote page 519.

26. Dieke, G.H., and Kistiakowsky, G.B., Phys. Rev. 45, 4 (1934).

27. Levine, I.N., op. cit. p. 197-216.

28. Sethuraman, V., Job, V.A., Innes, K.K., J. Mol. Spect. 33, 189 (1970).

29. Ebers, E.S., Nielsen, H.H., J. Chem. Phys. 5, 822 (1937).

30. Callomon, J.H., and Innes, K.K., J. Mol. Spect. 10, 166 (1963).

31. Walsh, A.D., J. Chem. Soc. (London), 1953, 2306 (1953).

32. For a review of the history and literature on spectroscopic investigations of formaldehyde see Moule and Walsh, reference 20.

33. Robinson, G.W., Can. J. Phys. 34, 699 (1956).

34. Herzberg, G., Franz, K., Z. Phys. 76, 720 (1932).

35. Walsh, A.D., J. Chem. Soc. (London), 1953, 2306 (1953).

36. Freed, K.F., Heller, D.F., J. Chem. Phys. 61, 3942 (1974).

37. Freed, K.F., J. Chem. Phys. 64, 1604 (1976).

38. Busch, G.E., Rentzepis, P.M., Jortner, J., J. Chem. Phys. 56, 361 (1972).

39. Nitzan, A., Jortner, J., Rentzepis, P.M., Pro. Roy. Soc. Lond. A327, 367 (1972).

40. Nitzan, A., Jortner, J., Kommandeur, J., Drent, E., Chem. Phys. Lett. 9, 273 (1971).

41. Langhoff, C.A., Robinson, G.W., Molecular Physics 26, 249 (1973).

42. Park, J.H., Rao, D.R., Javan, A., Appl. Phys. Lett. 13, 142 (1968).

43. McQuigg, R.D., Calvert, J.G., J. Am. Chem. Soc. 91, 1590 (1970).

44. Stern, O., Volmer, M., Z. Physik 20, 183 (1919).

45. Cohen, A.D., Reid, C., J. Chem. Phys. 24, 85 (1956).

46. Pople, J.A., Sidman, J.W., J. Chem. Phys. 27, 1270 (1957).

47. Sidman, J.A., J. Chem. PHys. 29, 644 (1958).

48. House, E.H., Ph.D. Thesis, University of Rochester (1959). See references 10 and 47.

49. Crosswhite, Fe-Ni Hollow Cathode Tables, Johns Hopkins University 1965. Unpublished.

50. Chaffee, F.H. Jr., High-Resolution Atlas of The Thorium Spectrum Between 3060Å and 6000Å, Mt. Hopkins Observatory, Amado, Arizona (1976).

51. Spence, R., Wild, W., J. Chem. Soc., 338 (1953).

52. Texas Instruments Bulletin, No. DL-S 7311427, January 1971 Revised September 1973, Type SN56502, SN76502 Logarithmic Amplifiers.

53. Edlén, B., J. Opt. Soc. Am., 43, 339 (1953).

54. Vaidya, W.M., Pro. Roy. Soc. 147, 513 (1934),

55. Vaidya, W.M., Pro. Phys. Soc. 64A, 428 (1951).

56. Dyne, P.S., Style, D.W.G., Dis. Faraday Soc. 2, 159 (1947).

57. Herzberg, G., Molecular Spectra and Molecular Structure Vol. I: Spectra of Diatomic Molecules, 2nd ed. (Van Nostrand Reinhold; N.Y.) p.522 (1950).

58. Bass, A.M., Broida, H.P., N.B.S. Monograph 24, February 14, 1961.

59. Nagata, I., Kimura, Y., Journal of Physics E: Scientific Instruments, 6, 1193 (1973).

60. Sam, C.L., Appl. Phys. Lett., 29, 505 (1976).

61. Sam, C.L., private communication.

62. Levatter, J.I., Lin, Shao-Chi, Appl. Phys. Lett., 25, 703 (1974).

63. Fitzsimmons, W.A., Anderson, L.W., Riedhauser, C.E., and Vrtilek, J.M., IEEE J. Quantum Electronics, QE12, 624 (1976).

64. Leonard, D.A., Appl. Phys. Lett., 7, 4 (1965).

65. Gerry, E.T., Appl. Phys. Lett. 7, 6 (1965).

66. Ali, A.W., Kolb, A.C., Anderson, A.D., Appl. Optics, 6, 215 (1967).

67. Geller, M., Altman, D.E., DeTemple, T.A., Appl. Optics, 7, 2232 (1968).

68. Ali, A.W., Appl. Optics, 8, 993 (1969).

69. Targ, R., IEEE J. Quantum Elect., August, 726 (1972).

70. Basting, D., Schafter, F.P., Steyer, B., Opto-electronics, 4, 43 (1972).

71. Wang, C.P., Rev. Sci. Instrum., 47, 93 (1976).

72. Cubeddu, R., Curry, S.M., IEEE J. Quantum Elect.,April, 499 (1973).

73. Godard, B., IEEE J. Quantum Elect., QE-10 February, 147 (1974) (note that "power figures in this reference were later found to be optimistic by a factor of 3 due to errors in the calibration of photo diode measurement.")

74. Shenck, P., Metcalf, H., Appl. Optics, 12, 183 (1973).

Thesis
C409
c.1

Chatham
New investigation of nitrogen laser induced fluorescence in formaldehyde: Spectra and spectrally resolved lifetimes.

179199